Chapter 2. Synthesis and Characterizations of Various Titanium Oxide Nanostructures Produced by Wet Chemistry in Base Solution (NaOH-TiO_2)

2.1. Introduction

Different from the nanofibers of potassium titanate with the rigid tunnel structure[14-17] (see Section 3.6.), the nanostructures of sodium hydroxo titanates which crystallize as layer structures can be prepared from titanium dioxide precursors in sodium oxide solution with various morphologies, with various forms but same composition. We have observed various shapes with different ratio of their three dimensions such as nanosheet, nano-semitube, nanotube, nanoribbon, micro-stick...etc.

These titanate nanostructures can be transformed to titanium dioxides and retain their original morphologies after exchanged and calcinations in comparatively low temperature (<600° C) [1-3]. This phenomenon provides a good way to produce nanostructured TiO_2 with controllable and designable preferred orientations for improving efficiency of special surface and structural properties.

In this chapter, we study the relations between the synthesis conditions and various morphologies of products. Our goal is to find out the crucial condition for each special product, further to get a comprehension of morphologic control of titanium oxide nanostructures, and finally enable us to make every special structure tunable. These studies include preparing nanotitanates with various grain size precursors, basic or sodium concentrations, autoclaved temperatures and varying quantities of dissolved carbonate. We centre on the correlations between synthetic parameters and final product morphologies in the contents following. The characterizations of product morphologies and structures are carried out by SEM (Scanning Electron Microscopy), TEM (Transmission Electron Microscope) and

XRD (X-ray diffraction). The chemical compositions are characterized by EDX (X-ray Energy Dispersion Spectroscopy) and TGA-MS (ThermalGravimetric Analysis-Mass Spectroscopy). We also employ FT-IR (Fourier-Transform Infra-red Spectroscopy) with a universal attenuated total reflection (ATR) accessory (see characterization descriptions in Section 2.2) and FT-Raman (Fourier-Transform Raman Spectroscopy) to study the dangling or intercalated groups and structural information. In this section, you can see how the parameters we set (grain size and structure of precursors, basic or sodium concentration, temperature, carbonate effect…etc.) affect shape and structure of the final product.

We describe nature of precursors and experimental method in experimental section (Section 2.2). Then correlations of conditions and morphologies are gathered up in a table in the results section (Section 2.3). We discuss these parameters by selected necessary results (Section 2.4); all other results done are put into an "annex" section (Section 2.6) after conclusions of this chapter. The enhanced structural studies and possible growth mechanism will be completely discussed in the next chapter.

2.2. Experimental section

2.2.1. Reagents

Different commercial TiO_2 and synthetic amorphous TiO_2 hydrate were used as starting materials, and aqueous NaOH solution was selected as reagent and sodium source. The titanate nanostructures were synthesized by adding 1g of the precursor to 10ml of basic solution and heating in autoclave or reflux apparatus during 24-72 hours. The detail procedure and conditions are represented in following paragraphs.

A. Titanium sources

Table 2.1. Table of various titanium oxide precursors.

precursor name	structrure (or composition)	grain size	producer (or synthesis method)
$TiOCl_2$ solution (TC)	**$TiOCl_2$·1.4HCl·7H_2O**		Millénium
amorphous (am)	amorphous TiO_2 hydrate		**$TiOCl_2$** + excess **NH_4OH**, rinse by water and 70˚ C dry in air.
TiO_2 hydrate (TO)	amorphous TiO_2 hydrate + small anatase (10%)	< 5 nm	**"Titanium tetra(isopropoxide)"** (TTIP) + excess **H_2O**, rinse by water, and 70˚ C dry in air.
5nm anatase (5nm)	anatase	4~6 nm	Alfa Aesar
P25 TiO_2 (P25)	80% anatase + 20% rutile	30 nm	Degussa AG
RDH anatase (RDH)	anatase	100 nm~1 μm	Riedel-deHaën (Fluka)
Aldrich rutile (rut)	rutile + anatase (<10%)	0.1~3 μm	Aldrich

1. $TiOCl_2$ solution

The $TiOCl_2$ produced by "Millénium" is conserved in concentrated chlorhydric acid solution to avoid hydrolysis in the air. The concentration of $TiOCl_2$ in this solution is 5M in 2M $HCl_{(aq)}$. The totally composition can be interpreted as " $TiOCl_2$·1.4HCl·7H_2O".

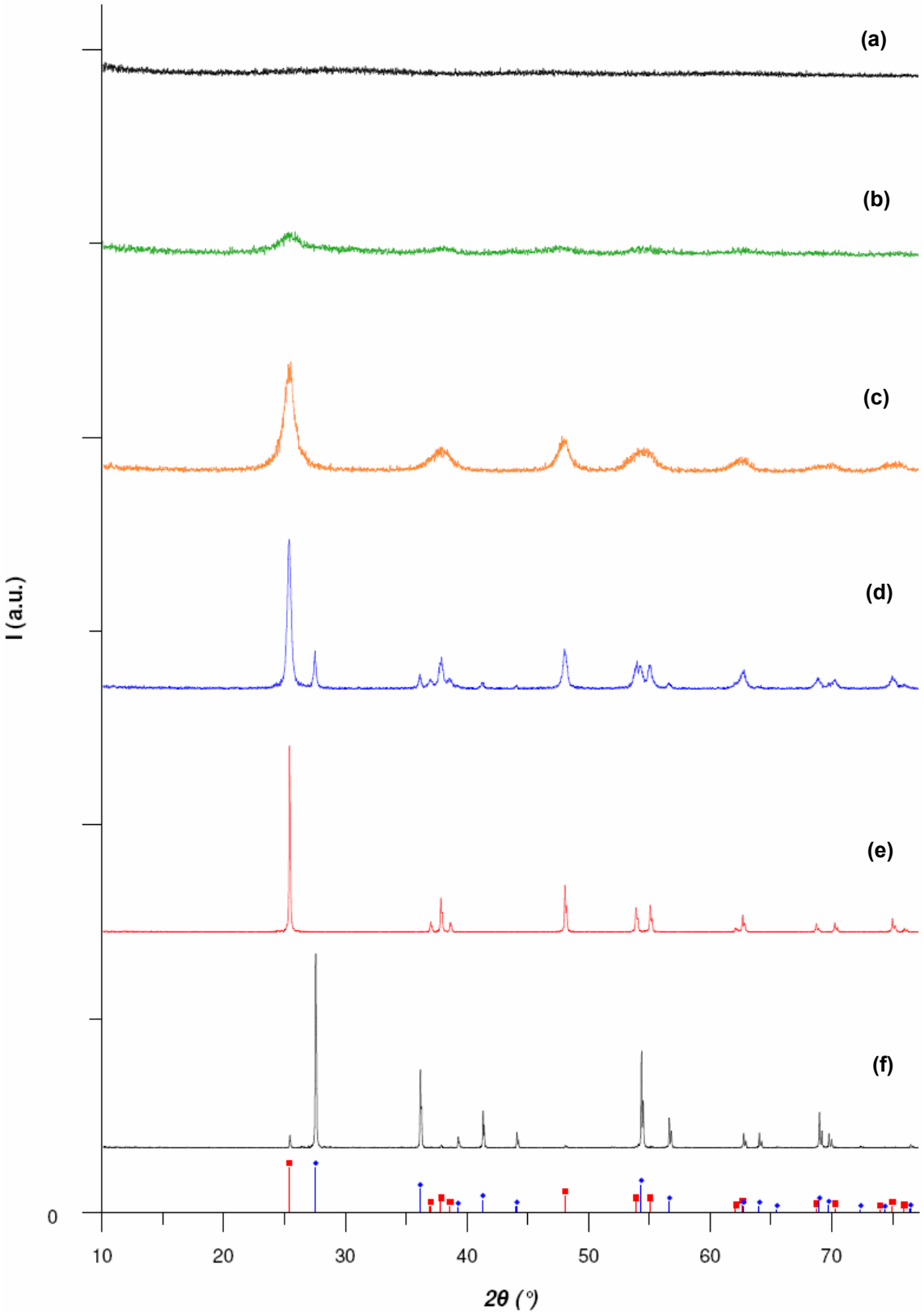

Figure 2.1. XRD diagrams of (a) amorphous TiO_2, hydrate from $TiOCl_2$; (b) TiO_2, hydrate from TTIP; (c) 5nm anatase; (d) Degussa P25; (e) RDH anatase and (f) Aldrich rutile. (■: peak positions of anatase and ◆: rutile phase TiO_2.)

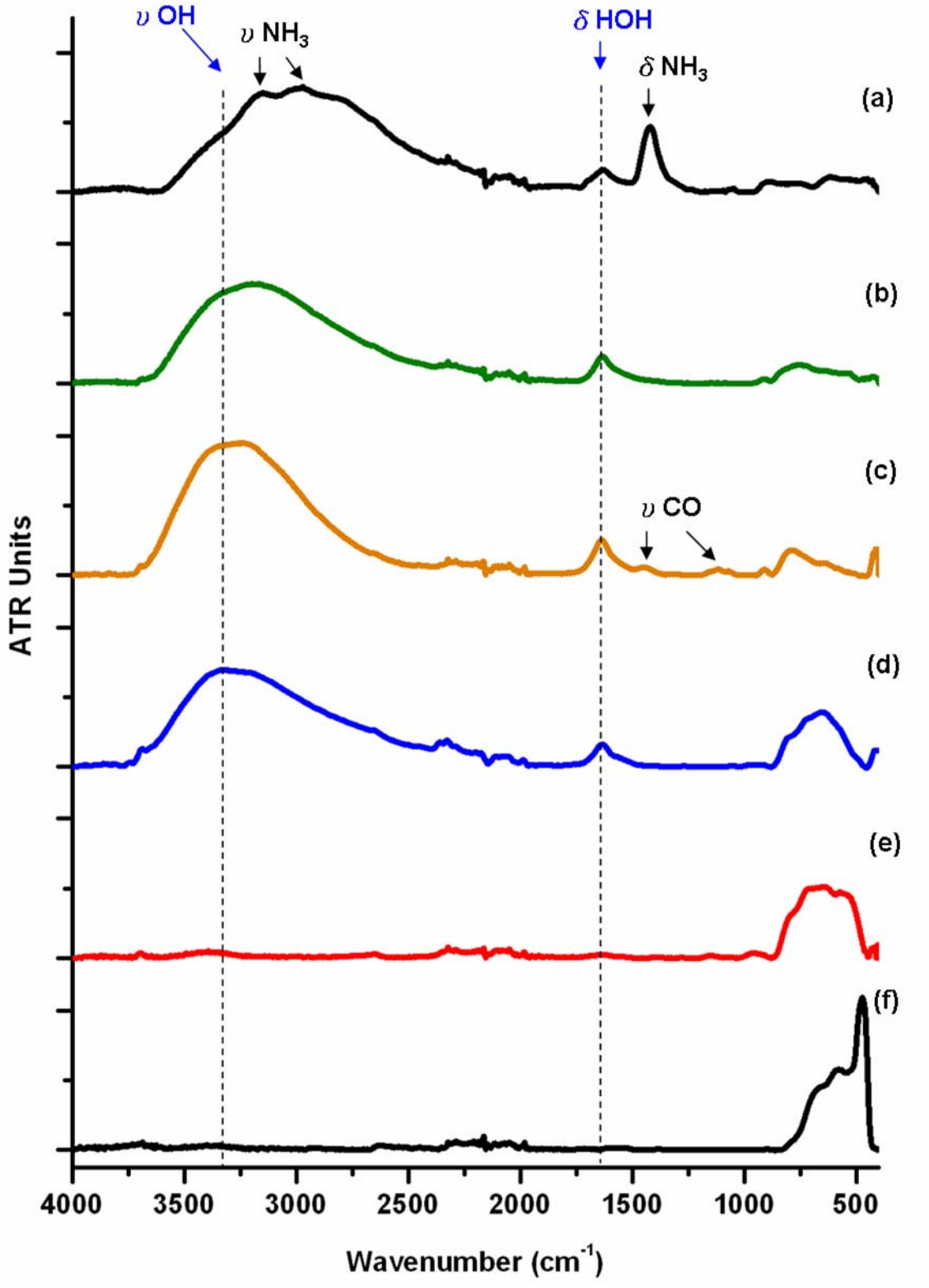

Figure 2.2. FT-IR ATR spectra of (a) amorphous TiO_2 hydrate from $TiOCl_2$; (b) TiO_2 hydrate from TTIP; (c) 5nm anatase; (d) Degussa P25; (e) RDH anatase and (f) Aldrich rutile.

2. amorphous TiO_2 hydrate from $TiOCl_2$

Amorphous TiO_2 hydrate (figure 2.1 should be put after this indication and not with the previous paragraph) is obtained by precipitation starting from *$TiOCl_2$ solution (see above description), and an excess of 25% wt. NH_4OH. We rinse the white precipitate product by de-ion water, it is filtered and then dried at 70° C in air. The final fine powder product is characterized as amorphous by XRD (without peak observed, see figure 2.1a). FT-IR spectrum reveals that there are obvious characteristic stretching band of dangling ammonium species from excess ammonium during hydrolysis process (see figure 2.2a). In the following TEM images, the sample presents a sheet-like structure at low magnification (figure 2.3a). A closer observation reveals that two types of morphology can be found: (b) amorphous particles (~5 nm in diameter); (c) amorphous larger sheets (~100 nm in diameter).

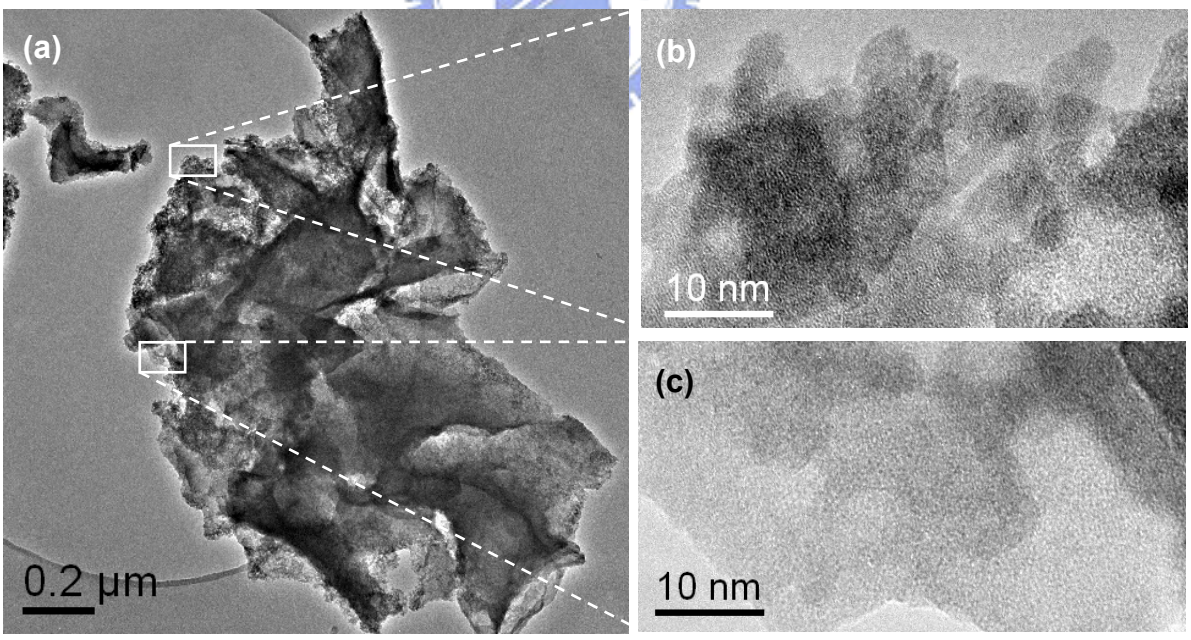

Figure 2.3. TEM image of (a) survey, (b) particle-like part and (c) plate-like part of amorphous TiO_2 hydrate from $TiOCl_2$.

3. TiO_2 hydrate from titanium tetra(isopropoxide)

Another TiO_2 hydrate is produced by hydrolysis of TTIP (titanium tetra-isopropoxide). Its morphology is different from the one obtained when starting with a "$TiOCl_2$" solution. The grain appears to be particles (figure 2.4a). Among them, parts are crystallized (figure 2.4b). On the X-ray diffraction, this gives rise to broad bumps located at the position of anatase peaks (see figure 2.1b).

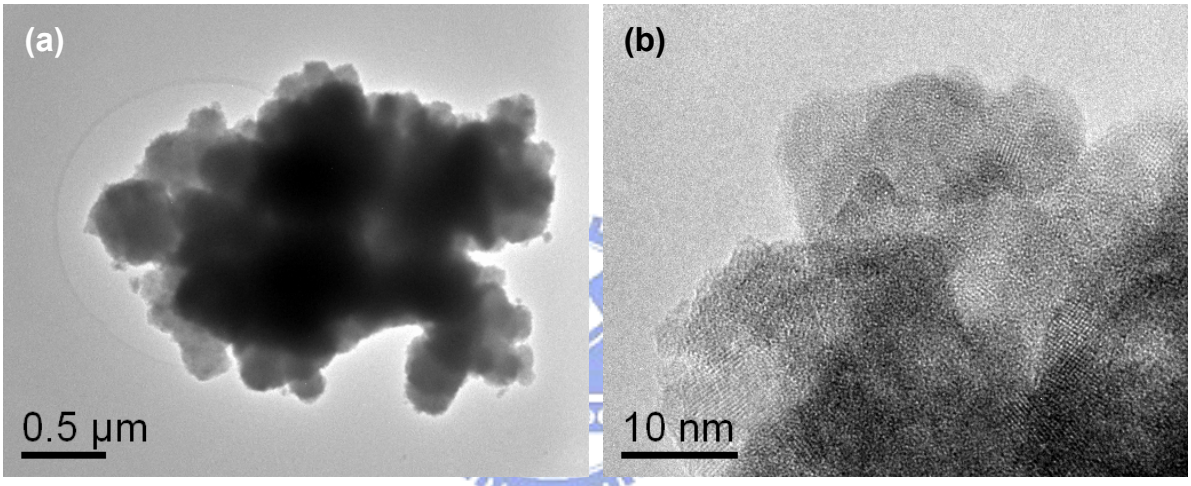

Figure 2.4. (a) low magnification and (b) high resolution TEM image of TiO_2 hydrate from hydralysis of TTIP.

4. Alfa 5nm anatase TiO_2

The 5nm anatase TiO_2 was purchased from Alfa Aesar Company. TEM observation confirms that this powder shows a very uniform and narrow size distribution: between 4~6nm (figure 3.5a). FT-IR spectroscopy (figure 2.2c) and TGA-MS reveal that some dangling carbonate groups are included in the sample. When not specially indicated, this powder is used as small crystallized titanium source.

5. Degussa P25 TiO_2

The P25 TiO_2 was purchased from Degussa Company. It is a mixture of anatase (~80%) and rutile phase (~20%) (see figure 2.1d and 2.5b). The grain size is about 30 nm (figure 2.5b).

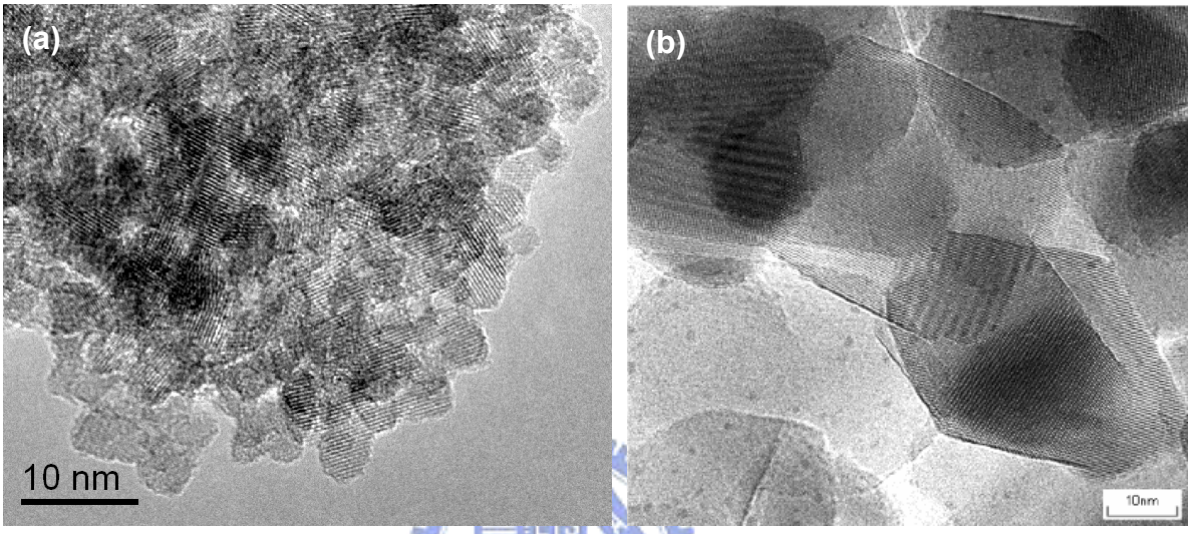

Figure 2.5. TEM image of (a) Alfa 5nm anatase and (b) Degussa p25 TiO_2.

6. RDH anatase TiO_2

RDH anatase which was purchased from Riedel-de-Haën (Fluka) Company is one of our main precursors used as big crystallized titanium source. The grain crystallize as anatase phase (figure 2.1e) and present a large size distribution 100~360 nm (figure 2.6a).

7. Aldrich rutile TiO_2

The rutile TiO_2 was purchased from Aldrich Company. Although this product is claimed to be rutile, a little bit (~5%) of anatase phase is involved (see figure 2.1f). The major (>80%) grain size is <1 μm (0.1~1μm, see figure 2.6b), but some big particle are easily detected since they are close to ~3μm.

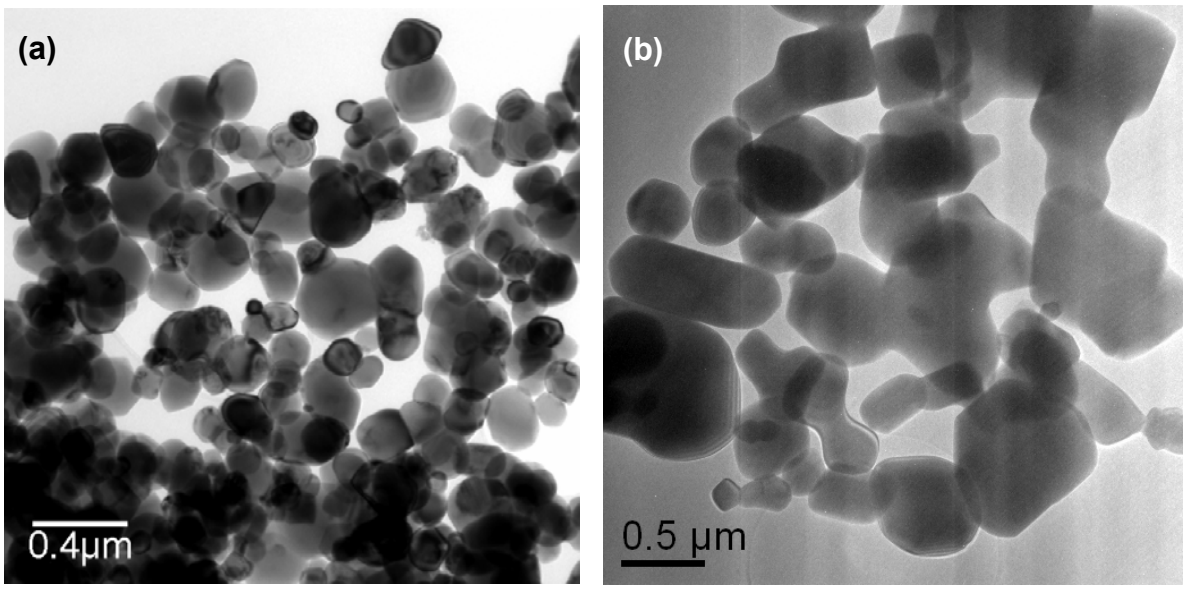

Figure 2.6. TEM image of (a) RDH anatase and (b) Aldrich rutile TiO_2.

B. Sodium sources and carbonates additives.

In our study, concentrated NaOH solution (1M, 5M, 10M and 15M) was used as sodium source and reagent. We prepared the basic solution by adding weighted sodium hydroxide pellets into calculated de-ion water (produced by Millipore system) in plastic (or teflon) cylinder then the mixture was stirred until the reactants become soluble. The effects of additional Na ion or carbonates have also been tested. We used NaCl, $NaHCO_3$ or Na_2CO_3 as additives. They all were weighted and added in the prepared aqueous NaOH solution.

Table 2.2. Table of various sodium sources or carbonate additives.

Reagent composition	purity	Molecular weight	form	producer
NaOH	97 %	40.00	Pellets pure	Merck
Na_2CO_3	99-100 %	106.00	powder	Prolabo (for analyse)
$NaHCO_3$	99.5 %	84.01	powder	Prolabo (for analyse)
NaCl	99 %	58.44	powder	Prolabo (Rectapur® crystallized)

2.2.2. Synthesis method

The synthesis method and conditions in this study is as the flow chart shown following. The product after rinsing by water is as principal one. After then, the titanate product was immersed in aqueous 0.1M HNO_3 solution to further exchange alkali ion by hydrogen ion. In the final step, the titanic acid type product was sintered at 400˚ C (or higher temperature when decomposition of intercalated carbonate group is necessary) during 4 hours to transform to TiO_2. The product in each stage has been characterized.

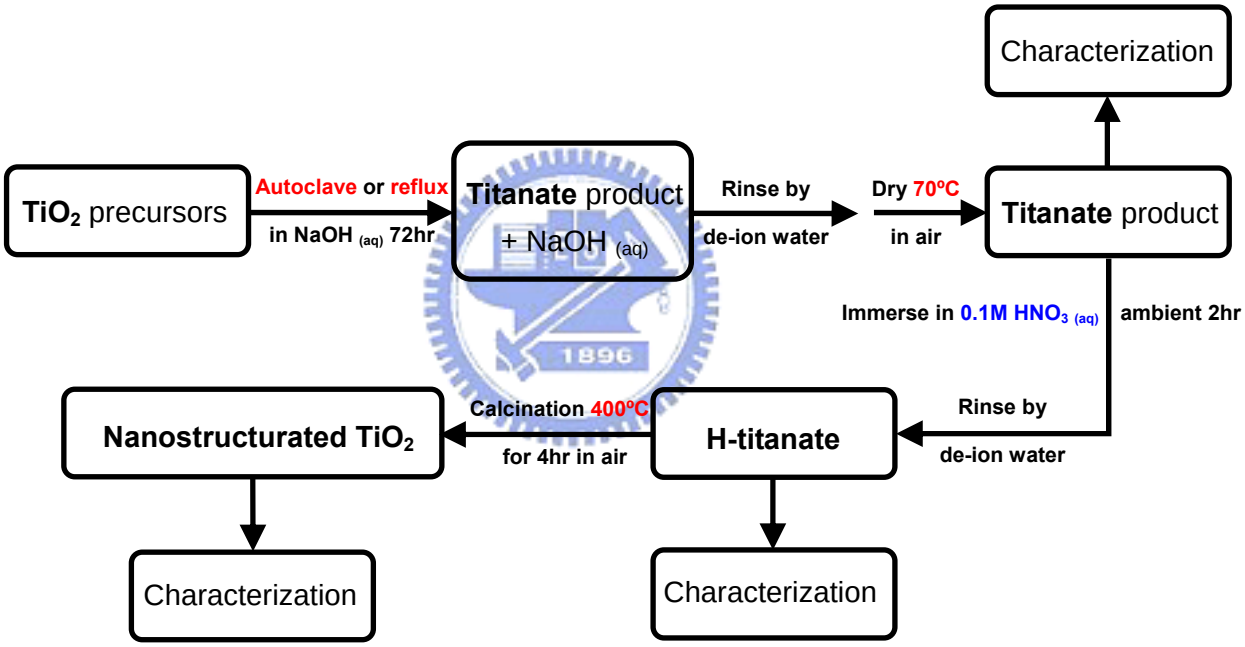

Scheme 2.1. Preparation procedure of nanostructured TiO_2 samples obtained by exchanged and calcination of titanate nanostructures from chimie-douce synthesis.

A. Autoclave

1 g of synthetic or commercial TiO_2 precursor was added to 10 ml different concentration aqueous NaOH solution (1M, 5M, 10M or 15M) and the mixture was kept at

different temperature (120˚ C, 140˚ C, 180˚ C or 220˚ C) during 72 hours in the autoclave apparatus with a sealed 50 ml capacity Teflon tubular container. The products were later rinsed by de-ion water and collected by centrifuge repeatedly until pH<12, after then dried in oven at 70˚ C under air.

B. Reflux

10 g of synthetic or commercial TiO_2 precursor was added to 100 ml different concentration aqueous NaOH solution (5M, 10M or 15M) and the mixture was placed in the 300 ml capacity PTFE round-bottom flask equipped with a coil reflux condenser. Then, the flask was placed in silicon oil bath and heat up to 150˚ C (oil temperature) and kept magnetically stirring and reflux during 72 hours. The products were later rinsed by de-ion water and collected by centrifuge repeatedly until pH<12, after then dried in oven at 70˚ C under air.

C. Proton exchange and calcinations

For proton (H^+) exchange, 1g of products with sodium (Na/Ti ≈ 0.4-0.6) after only de-ion water rinsing was immersed in 50 ml 0.1M HNO_3 aqueous solution and magnetically stirred in ambient condition for 2 hours. In the following, it was rinsed by de-ion water and collected by centrifuge repeatedly until pH>6, then dried in oven at 70˚ C under air.

The dried H^+-changed samples were then sintered to 400˚ C (some of them were under 800˚ C to eliminate carbonate and transform to anatase completely) for dehydration and transformation to TiO_2 nano-crystallites.

2.2.3. Characterization

A. X-ray powder diffraction (XRD)

All the products in this study were structural characterized by X-ray powder diffraction (XRD) using a Siemens D5000 diffractometer with Cu Kα radiation in a Bragg-Brentano geometry. The sample was ground to fine powder by agate mortar, and then press onto plastic holder with round notch. The scan range of XRD is 3˚-90˚, scan size is 0.03˚, and the scan time per size is 1 second for normal case and 20 seconds for overnight case to enhance the ratio of signal/noise.

B. Transmission electron microscopy (TEM)

For microcosmic observation of sample's morphology and structure, the selected area electron diffraction pattern (SAED), conventional and high resolution (HR) transmission electron microscopy (TEM) images were performed by Hitachi HF2000 with field emission gun electron source operated at 200 keV. The TEM samples were prepared by grinding and ultrasonic treating to disperse in ethanol solution, and then drop on holey or lacey carbon film supported on copper grid. We dried the sample at ambient in the air before transferred into TEM column chamber.

C. Scanning electron microscopy (SEM)

Scanning electron microscopy (SEM) was carried out by JEOL 6400F with cold cathode field emission gun electron source operated at 10 keV for morphologic survey of products. The sample was prepared by sticking the powder-like product onto carbon scotch on copper basic holder and then metalizing with Pt vacuum sputter before transferred into SEM column.

D. X-ray energy dispersion spectroscopy (EDX)

X-ray energy dispersion spectroscopy (EDX) was performed by Kavex X-ray analysis probe depended on JEOL 5800LV SEM with conventional tungsten electron source operated at 15 keV for chemical composition study (Na/Ti). The sample powder was prepared as pastille stuck on copper base holder by silver glue and sputtered carbon on the surface before transferred into SEM column.

E. Thermalgravimetric analysis - mass spectroscopy (TGA-MS)

For completing the composition study of adsorbed and structural H_2O, OH^- and CO_2 in our product, thermalgravimetric analysis with mass spectroscopy (TGA-MS) was performed by SETARAM TG 92 system in 1° C -800° C range of temperature with rate of 5° C per minute under argon gas environment.

F. Fourier-transformation inferred spectroscopy (FT-IR)

The Fourier-transformation inferred spectroscopy was carried out by Bruker Vertex 70 equipped with a universal attenuated total reflection (ATR) accessory called Golden Gate™ Single Reflection Diamond ATR for observation the chemical dangling group such as OH^- and CO_3^{2-}. The accessory uses a 2mm x 2mm square diamond which brazed into a tungsten carbide disc. The active area of the diamond is 0.6mm x 0.6mm. The top clamp compression head is fitted with a flat sapphire anvil for compressing hard solid samples.[4] We prepared the sample as fine powder and then compressed by the sapphire head on diamond window to do FT-IR-ATR. The scan range is 400 cm^{-1}-4000 cm^{-1} and scan times is 100 times.

G. Fourier-transformation Raman spectroscopy (FT-Raman)

For further structural and chemical environment information, Fourier-transformation Raman spectroscopy was performed by Bruker RFS100 with 1064 nm inferred laser as incident light focus on the sample area diameter <1 mm. The scan range is -500 cm^{-1}-3500 cm^{-1} and scan times is 100 times.

H. Specific surface measurement (BET)

The specific surface was performed by N_2 adsorption at 77K (under liquid nitrogen) using the adsorption apparatus Micromeritics ASAP 2010. Surface area of the samples was determined from the Brunauer-Emmett-Teller equation (BET method). All the samples were preheated to 70° C under vacuum for degas.

2.3. Results

2.3.1. Correlations of reactive conditions and product structures

Because of too many result data, we express the results as a table (table 3.3) of correlation of reaction and product structures. We only show some necessary results (XRD, images, TGA, IR and Raman) in discussion section. The other images also interesting were put into annex section after.

Table 2.3. Table of various reactive conditions and product morphologies.

sample name[*1]	reaction condition[*2]				**morphology**[*3]	structure[*4]	dimensions[*5](nm) **w(or ø) / t / l**
	precursor	solution concentration	temperature (K)	reactor			
am0M120	amorphous	0M NaOH	393	autoclave	**particle**	**anatase**	**10-30 / 10-30 / 10-150**
am0.1M120	amorphous	0.1M NaOH	393	autoclave	**particle** particle	**anatase** brookite	**10-60 / 10-60 / 10-200** -
am0.5M120	amorphous	0.5M NaOH	393	autoclave	**lamellar** small lamellar	**lepidocrocite** lepidocrocite	**50-150 / 3-15 / 50-150** 10-20 / 10 / 10-50
am1M120	amorphous	1M NaOH	393	autoclave	**lamellar**	**lepidocrocite**	**100-500 / 3-8 / 100-500**
am5M120	amorphous	5M NaOH	393	autoclave	small lamellar lamellar **semi-tubular**	lepidocrocite lepidocrocite **lepidocrocite**	40 / 5 / 40 50 / 5 / 500 **50 / 5 / 200**
am10M120	amorphous	10M NaOH	393	autoclave	fibrillar **semi-tubular** lamellar	lepidocrocite **lepidocrocite** lepidocrocite	120 / 7 / 1000 **10 / 3 / 100** 20 / 3 / 20
am15M120	amorphous	15M NaOH	393	autoclave	**particle**	**amorphous**	-
TO5M120	TiO_2 hydrate	5M NaOH	393	autoclave	**lamellar** semi-tubular	**lepidocrocite** lepidocrocite	**40 / 5 / 100** 10 / 5 / 100
TO10M120	TiO_2 hydrate	10M NaOH	393	autoclave	**tubular**	**lepidocrocite**	**10 / 3 / 100**
5nm5M120	5nm anatase	5M NaOH	393	autoclave	**semi-tubular** anatase	**lepidocrocite** lepidocrocite	**30 / 10 / 50-700** 5
5nm10M120	5nm anatase	10M NaOH	393	autoclave	**lamellar**	**lepidocrocite**	**15 / 3-8 / 50**

5nm15M120	5nm anatase	15M NaOH	393	autoclave	**particle**	**amorphous**	-
P255M120	P25 TiO_2	5M NaOH	393	autoclave	**lamellar** semi-tubular	**lepidocrocite** lepidocrocite	**30 / 3 / 100** 10 / 3 / 100
P2510M120	P25 TiO_2	10M NaOH	393	autoclave	**semi-tubular**	**lepidocrocite**	**8.5 / 3 / 300**
P2515M120	P25 TiO_2	15M NaOH	393	autoclave	**particle**	**amorphous**	-
RDH5M120	RDH anatase	5M NaOH	393	autoclave	**particle**	**anatase**	**100-300**
RDH10M120	RDH anatase	10M NaOH	393	autoclave	**tubular**	**lepidocrocite**	**8.5 / 3 / 300**
RDH15M120	RDH anatase	15M NaOH	393	autoclave	**particle** particle	**amorphous** anatase	- -
rut5M120	Aldrich rutile	5M NaOH	393	autoclave	**particle**	**rutile**	**100-1000**
rut10M120	Aldrich rutile	10M NaOH	393	autoclave	**tubular**	**lepidocrocite**	**8.5 / 3 / 150**
rut15M120	Aldrich rutile	15M NaOH	393	autoclave	**particle** particle	**amorphous** rutile	- -
am10M140	amorphous	10M NaOH	413	autoclave	lamellar **tubular**	lepidocrocite **lepidocrocite**	20 / 3 / 50-150 **8-10 / 3 / 50-250**
am10M180	amorphous	10M NaOH	453	autoclave	**fibrillar**	**"$Cs_2Ti_6O_{13}$"**	**20-200 / 20 / 500-10^4**
am10M220	amorphous	10M NaOH	493	autoclave	fibrillar **stick-like**	"$Cs_2Ti_6O_{13}$" **lamellar ramsdellite**	20-200 / 20 / 500-2000 **150-400 / 50 / 1000-5000**
5nm10M140	5nm anatase	10M NaOH	413	autoclave	**lamellar**	**lepidocrocite**	**10-20 / 3 / 10-50**
5nm10M180	5nm anatase	10M NaOH	453	autoclave	**fibrillar**	**"$Cs_2Ti_6O_{13}$"**	**20-200 / 20 / 500-10^4**
5nm10M220	5nm anatase	10M NaOH	493	autoclave	**fibrillar**	**"$Cs_2Ti_6O_{13}$"**	**20-200 / 20 / 500-10^4**
P2510M140	P25 TiO_2	10M NaOH	413	autoclave	lamellar **semi-tubular** tubular	lepidocrocite **lepidocrocite** lepidocrocite	30 / 2 / 50-250 **10 / 5 / 50-250** 10 / 2.5 / 50-250

P2510M180	P25 TiO_2	10M NaOH	453	autoclave	**fibrillar**	**"$Cs_2Ti_6O_{13}$"**	**20-200 / 20 / 500-10^4**
P2510M220	P25 TiO_2	10M NaOH	493	autoclave	fibrillar **stick-like**	"$Cs_2Ti_6O_{13}$" **lamellar ramsdellite**	20-200 / 20 / 500-2000 **150-400 / 50 / 1000-5000**
RDH10M140	RDH anatase	10M NaOH	413	autoclave	**tubular**	**lepidocrocite**	**8 / 3 / 50-250**
RDH10M180	RDH anatase	10M NaOH	453	autoclave	**fibrillar**	**"$Cs_2Ti_6O_{13}$"**	**40-300 / 10-40 / 500-2000**
RDH10M220	RDH anatase	10M NaOH	493	autoclave	**fibrillar** stick-like	**"$Cs_2Ti_6O_{13}$"** lamellar ramsdellite	**20-200 / 5 / 300-2000** -
rut10M140	Aldrich rutile	10M NaOH	413	autoclave	**tubular**	**lepidocrocite**	**8 / 3 / 50-250**
rut10M180	Aldrich rutile	10M NaOH	453	autoclave	fibrillar **stick-like**	"$Cs_2Ti_6O_{13}$" **lamellar ramsdellite**	20-200 / 20 / 500-2000 **150-400 / 50 / 1000-5000**
rut10M220	Aldrich rutile	10M NaOH	493	autoclave	**stick-like**	**lamellar ramsdellite**	**150-400 / 50 / 1000-5000**
am10MR	amorphous	10M NaOH	423[*6]	reflux	**fibrillar**	**"$Cs_2Ti_6O_{13}$"**	**10-40 / 3-10 / 100-700**
TO5MR	TiO_2 hydrate	5M NaOH	423	reflux	**lamellar**	**lepidocrocite**	**6 / 6 / 100**
TO10MR	TiO_2 hydrate	10M NaOH	423	reflux	**fibrillar**	**"$Cs_2Ti_6O_{13}$"**	**20 / 7 / 100-500**
5nm5MR	5nm anatase	5M NaOH	423	reflux	**lamellar**	**lepidocrocite**	**20 / 10 / 500-1000**
5nm10MR	5nm anatase	10M NaOH	423	reflux	**lamellar**	**lepidocrocite**	**20 / 3 / 50-100**
P255MR	P25 TiO_2	5M NaOH	423	reflux	**lamellar** semi-tubular tubular	**lepidocrocite** lepidocrocite lepidocrocite	**30 / 3 / 150** 10 / 3 / 150 10 / 3 / 150
P2510MR	P25 TiO_2	10M NaOH	423	reflux	**semi-tubular**	**lepidocrocite**	**15 / 5 / 250**
RDH5MR	RDH anatase	5M NaOH	423	reflux	fibrillar **particle**	"$Cs_2Ti_6O_{13}$" **anatase**	20 / 20 / 1000-3000 **300**
RDH10MR	RDH anatase	10M NaOH	423	reflux	**tubular** fibrillar	**lepidocrocite** "$Cs_2Ti_6O_{13}$"	**8 / 2 / 100-300** 4-20 / 4-20 / 600

RDH15MR	RDH anatase	15M NaOH	423	reflux	particle **lamellar** particle	amorphous **lepidocrocite** anatase	- **100 / 3-8 / 150** 20
RDH15MR-B (the product rinsed then **boiling in water 48h**)	RDH anatase	15M NaOH	423	reflux	**lamellar** particle	**lepidocrocite** anatase	**150 / 3-8 / 300** -
rut5MR	Aldrich rutile	5M NaOH	423	reflux	fibrillar **particle**	"$Cs_2Ti_6O_{13}$" **rutile**	30 / 8 / 1000-3000 **300-500**
rut10MR	Aldrich rutile	10M NaOH	423	reflux	**semi-tubular** tubular	**lepidocrocite** lepidocrocite	**10 / 3 / 250** 10 / 3 /250
5nm5M120-0.5CO3[*7]	5nm anatase	5M NaOH + 0.006 mol Na_2CO_3	393	autoclave	**lamellar**	**lepidocrocite**	**50 / 2-9 / 100**
5nm5M120-0.8CO3	5nm anatase	5M NaOH + 0.01 mol Na_2CO_3	393	autoclave	**lamellar**	**lepidocrocite**	**20-150 / 1-8 / 150-250**
5nm5M120-1CO3	5nm anatase	5M NaOH + 0.013 mol Na_2CO_3	393	autoclave	**lamellar**	**lepidocrocite**	**20-150 / 1-8 / 150-250**
5nm5M120-2CO3	5nm anatase	5M NaOH + 0.05 mol Na_2CO_3	393	autoclave	**lamellar**	**lepidocrocite**	**20-150 / 1-8 / 150-250**
5nm5M120-4CO3	5nm anatase	5M NaOH + 0.1 mol Na_2CO_3	393	autoclave	**lamellar**	**lepidocrocite**	**20-150 / 1-8 / 150-250**
5nm5M120-0.8HCO3	5nm anatase	5M NaOH + 0.01 mol $NaHCO_3$	393	autoclave	**lamellar** semi-tubular	**lepidocrocite** lepidocrocite	**50-100 / 3-15 / 150-250** 10-20 / 3-6 / 150-250
5nm5M120-1.6HCO3	5nm anatase	5M NaOH + 0.02 mol $NaHCO_3$	393	autoclave	**lamellar**	**lepidocrocite**	**50-100 / 3-15 / 150-250**

5nm5M120-1.6NaCl	5nm anatase	5M NaOH + 0.02 mol NaCl	393	autoclave	small lamellar **lamellar**	lepidocrocite **lepidocrocite**	5-20 / 3-9 / 20-50 **20-100 / 3-9 / 150-250**
am5M120-0.8CO3	amorphous	5M NaOH + 0.01 mol Na_2CO_3	393	autoclave	small lamellar **lamellar** semi-tubular	lepidocrocite **lepidocrocite** lepidocrocite	5-20 / 3-9 / 20-50 **20-100 / 3-9 / 150-250** 10 / 3 / 100
am10M120-0.8CO3	amorphous	10M NaOH + 0.01 mol Na_2CO_3	393	autoclave	fibrillar **semi-tubular** lamellar	lepidocrocite **lepidocrocite** lepidocrocite	120 / 7 / 1000 **10 / 3 / 100** 20 / 3 / 20
am15M120-0.8CO3	amorphous	15M NaOH + 0.01 mol Na_2CO_3	393	autoclave	**particle**	**amorphous**	-
am10M140-0.8CO3	amorphous	10M NaOH + 0.01 mol Na_2CO_3	413	autoclave	lamellar **tubular**	lepidocrocite **lepidocrocite**	20 / 3 / 50 **8.5 / 3 / 100**
am10M180-0.8CO3	amorphous	10M NaOH + 0.01 mol Na_2CO_3	453	autoclave	**fibrillar**	**"$Cs_2Ti_6O_{13}$"**	**20-200 / 20 / 500-10^4**
am10M220-0.8CO3	amorphous	10M NaOH + 0.01 mol Na_2CO_3	493	autoclave	fibrillar **stick-like**	"$Cs_2Ti_6O_{13}$" **lamellar ramsdellite**	20-200 / 20 / 500-2000 **150-400 / 50 / 1000-5000**
RDH10M180-0.8CO3	RDH anatase	10M NaOH + 0.01 mol Na_2CO_3	453	autoclave	**fibrillar**	**"$Cs_2Ti_6O_{13}$"**	**40-300 / 10-40 / 500-2000**
RDH15M120-2CO3	RDH anatase	15M NaOH + 0.025 mol Na_2CO_3	393	autoclave	tubular **semi-tubular**	lepidocrocite **lepidocrocite**	8.5 / 3 / 300 **8.5 / 3 / 300**
RDH15M120-4CO3	RDH anatase	15M NaOH + 0.05 mol Na_2CO_3	393	autoclave	**particle**	**amorphous**	-
am1M120-3.2NaCl	amorphous	1M NaOH + 0.04 mol NaCl	393	autoclave	**lamellar**	**lepidocrocite**	**100-300 / 3-8 / 100-300**

am0M120-4NaCl	amorphous	10 ml water + 0.05 mol NaCl	393	autoclave	**particle** particle	**anatase** brookite	- -
RDH5M120-4NaCl	RDH anatase	5M NaOH + 0.05 mol NaCl	393	autoclave	lamellar **particle**	lepidocrocite **anatase**	- **100-350**
RDH10M120-4NaCl	RDH anatase	10M NaOH + 0.05 mol NaCl	393	autoclave	**tubular**	**lepidocrocite**	**8.5 / 3 / 300**
TC0Na180[*8]	$TiOCl_2$	0.034 mol NaOH	453	autoclave	**particle** particle	**rutile** anatase	15 / 15 /50 5-8
TC0.5Na180	$TiOCl_2$	0.039 mol NaOH	453	autoclave	**lamellar** particle particle	**lepidocrocite** rutile anatase	**20-50 / 1.5-3 / 150-250** 15 / 15 / 50 5-8
TC0.63Na180	$TiOCl_2$	0.040 mol NaOH	453	autoclave	**lamellar** semi-tubular	**lepidocrocite** lepidocrocite	**20-50 / 1.5-3 / 150-250** 8-10 / 1.5-3 / 150-250
TC1Na180	$TiOCl_2$	0.044 mol NaOH	453	autoclave	**lamellar** semi-tubular	**lepidocrocite** lepidocrocite	**20-50 / 1.5-3 / 150-250** 8-10 / 1.5-3 / 150-250
TC1.26Na180	$TiOCl_2$	0.047 mol NaOH	453	autoclave	lamellar **semi-tubular**	lepidocrocite **lepidocrocite**	20-50 / 1.5-3 / 150-250 **8-10 / 1.5-3 / 150-250**
TC1.5Na180	$TiOCl_2$	0.049 mol NaOH	453	autoclave	**semi-tubular**	**lepidocrocite**	**8-10 / 1.5-3 / 150-250**
TC2Na180	$TiOCl_2$	0.054 mol NaOH	453	autoclave	**semi-tubular**	**lepidocrocite**	**8-20 / 2-5 / 50-250**
TC2.5Na180	$TiOCl_2$	0.059 mol NaOH	453	autoclave	**lamellar** stick-like particle	**lepidocrocite** lamellar ramsdellite amorphous	20-50 / 1.5-4 / 150-250 **200-500 / 50 / 1000-6000** 20-100

TC3Na180	$TiOCl_2$	0.064 mol NaOH	453	autoclave	lamellar **stick-like** particle	lepidocrocite **lamellar ramsdellite** amorphous	20-50 / 1.5-4 / 150-250 **200-500 / 50 / 1000-6000** 20-100
TC3.5Na180	$TiOCl_2$	0.069 mol NaOH	453	autoclave	**stick-like** particle	**lamellar ramsdellite** amorphous	**200-500 / 50 / 1000-6000** 20-100
TC4Na180	$TiOCl_2$	0.074 mol NaOH	453	autoclave	**particle**	**amorphous**	**20-100**
TC5Na180	$TiOCl_2$	0.084 mol NaOH	453	autoclave	**particle**	**amorphous**	**20-100**
TC1K110	$TiOCl_2$	0.044 mol KOH	383	autoclave	**fibrillar**	**"$K_2Ti_8O_{17}$"**	**1-3 / 1-3 / 5-10**
TC1K120	$TiOCl_2$	0.044 mol KOH	393	autoclave	**fibrillar**	**"$K_2Ti_8O_{17}$"**	**1-3 / 1-3 / 5-20**
TC1K150	$TiOCl_2$	0.044 mol KOH	423	autoclave	**fibrillar**	**"$K_2Ti_8O_{17}$"**	**1-5 / 1-5 / 10-30**
TC1K180	$TiOCl_2$	0.044 mol KOH	453	autoclave	**fibrillar**	**"$K_2Ti_8O_{17}$"**	**3-5 / 3-5 / 20-100**
TC1K220	$TiOCl_2$	0.044 mol KOH	493	autoclave	**fibrillar**	**"$K_2Ti_8O_{17}$"**	**5-20 / 5-20 / 100-1000**

*1: The samples were named by their reaction conditions as the type "(precursor) (basic concentration) (temperature) - (additive)".

*2: We described the conditions by precursor, basic solution concentration and reaction temperature (in autoclave or reflux system) respectively.

*3: We differentiated the various morphologies as particle, lamellar (nanosheet), semi-tubular (semi-nanotube), tubular (nanotube), fibrillar (nanofiber or ribbon) and stick-like (submicro-stick). The morphology maybe not uniform in product we marked the major as bold type.

*4: We described the structures as mineral name of similar structure or the composition in brackets “ ”.

*5: We charactered the length of three dimensional axis of crystallite as width (or diameter for tubular form) / thickness / length (w / t / l = c / a / b for titanate layer structure).

*6: The reflux temperature is the temperature of oil bath.

*7: We use “CO3” to represent Na_2CO_3 as additives (“HCO3” for $NaHCO_3$; “NaCl” for NaCl), and the number before additive name is proportion to quantity of Ti in precursor.

*8: We use a reaction equation as “$TiOCl_2 \cdot 1.4HCl \cdot 7H_2O_{(l)} + (x+3.4)NaOH_{(s)} \rightarrow (NaOH)_xTiO_2 + 3.4NaCl + 9.4\ H_2O$” to describe this expriment, Na means NaOH, and the number before Na is the x in the equation.

2.3.2. The characterizations of principle morphologies

All the obtained titanate nanostructures can be sorted out as five main types (see table 2.3) by different shapes: *nanosheet* (lamellar), *semi-nanotube* (semi-tubular), *nanotube* (tubular), *nanoribbon* (fibrillar) and *submicro-stick* (stick-like). The further three have similar structure (figure 2.7) but different curvature along c axis direction of titanate layer (see Section 1.3 and scheme 2.2). The nanoribbon has also similar layer structure but much better crystallized and longer length along b axis (axis direction of these 1D materials) (Section 2.3.2d). The submicro-stick has larger diameter about several hundreds of nanometers, and its structure is very different with others (Section 2.3.2e). It seems like rutile type structure such as hollandite and ramdesllite (see Section 1.2). We will discuss this rutile derived phase more deeply in chapter 4. In this section, we show the results of XRD and EM for the five main morphologies, other data and properties, such as composition, density and specific surface area, are detailed in the contents. The results of composition characterization (EDX and TGA-Mass spectrum) were put into annex section after (Section 2.6.).

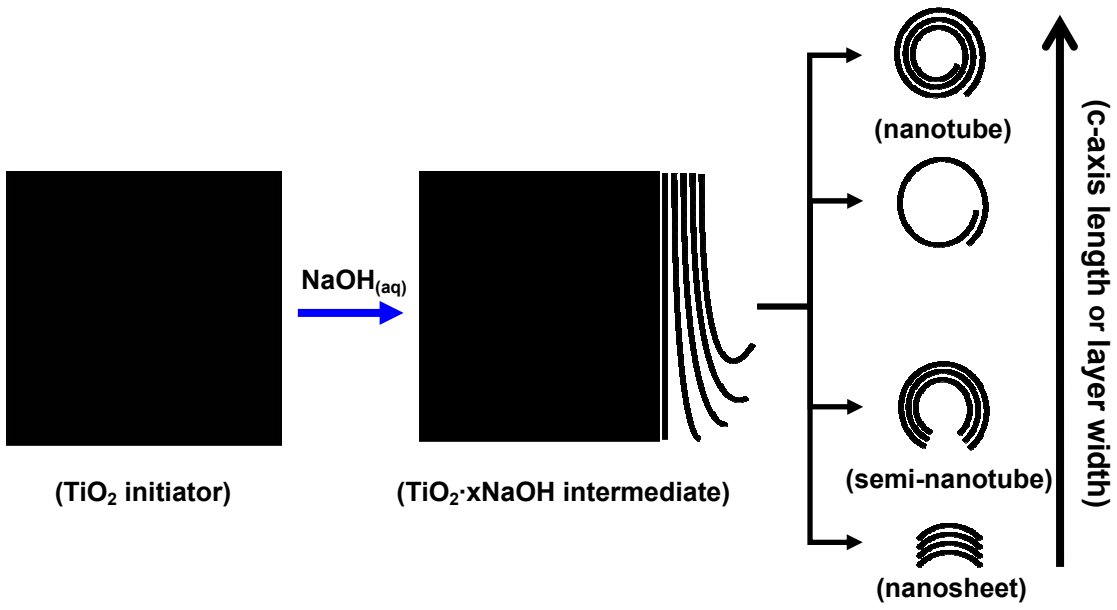

Scheme 2.2. Relation of titanate monolayer width and various product morphologies.

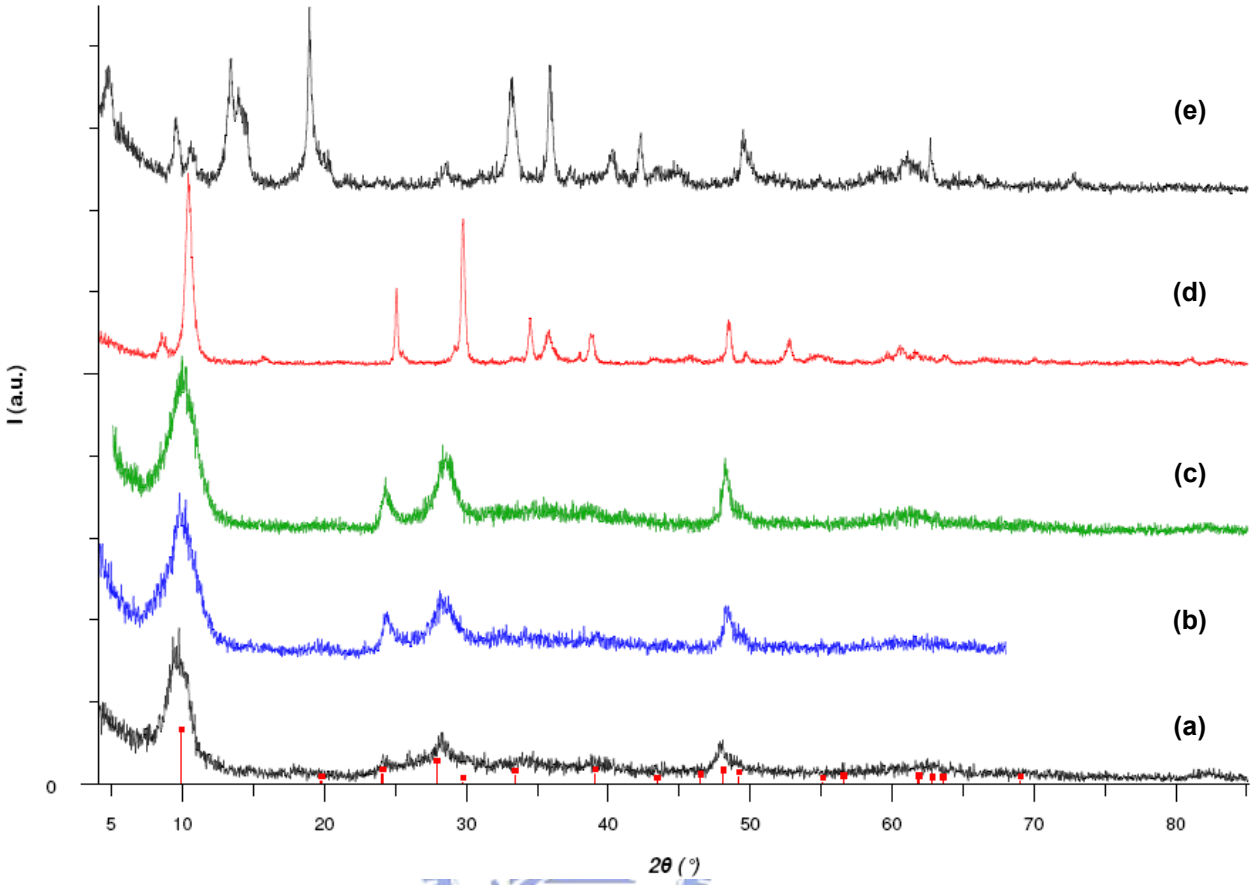

Figure 2.7. XRD diagrams of sodium hydroxo titanate (a) nanosheet (am1M120), (b) semi-nanotube* (rut10MR), (c) nanotube (RDH10M140), (d) nanoribbon (RDH10M180) and (e) submicrostick (rut10M220). (■: peak positions of lepidocrocite type titanic acid, $H_2Ti_2O_5 \cdot H_2O$, JCPDS 47-0124 [5]; *: rut10MR is a mixture of major semi-nanotubes and nanotubes.)

A. Nanosheets

The sheet-like product (figure 2.8 and 2.9) as show below can be observed in lower basic concentration condition (am0.5M120, am1M120…etc.), and a critical condition as grand anatase TiO_2 reflux in 15M NaOH (RDH15MR). It has width as 100-300 nm and constructed of 1-10 of titanate layers. Its composition calculated base on TGA and EDX can be expressed

as "0.33NaOH·0.67H_2O·TiO_2·0.02(CO + CO_2)·0.01CO_2" (RDH15MR-B, Section 2.6.1). The XRD pattern (figure 3.7a) reveals it has similar lattice parameters with lepidocrocite type titanic acid ($H_2Ti_2O_5·H_2O$, JCPDS 47-0124)[5]. After hydrogen exchanged and annealed to 400° C, it can retain sheet-like morphology, possess big specific area (287 $m^2·g^{-1}$) and good photo-catalytic property (see Chapter 4) comparing favorably with P25 (a commercial TiO_2 employed as standard photocatalyst).

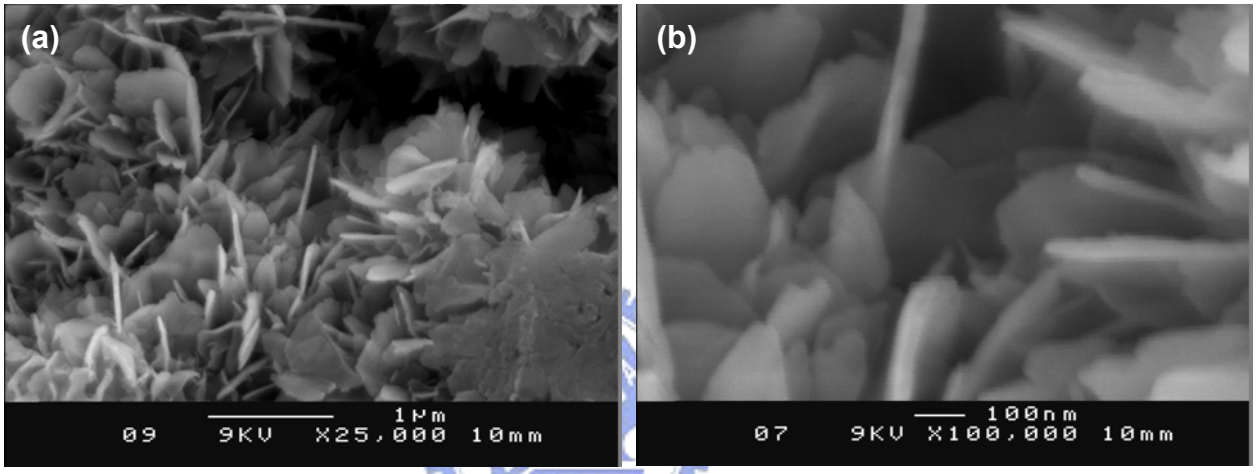

Figure 2.8. (a) The SEM image and (b) the magnified one of titanate nanosheets (am1M120).

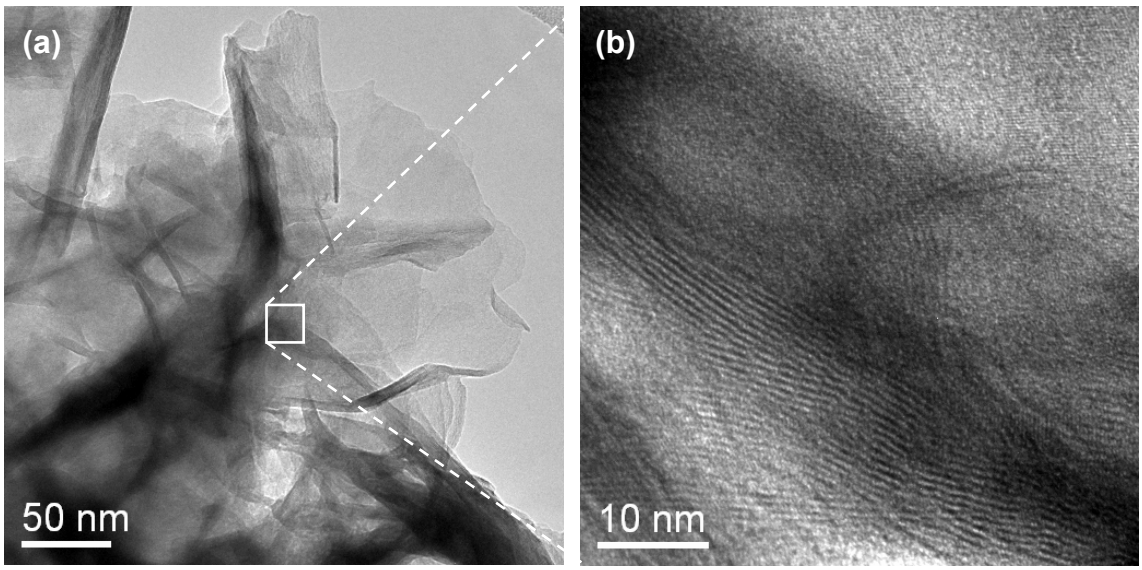

Figure 2.9. (a) The TEM image and (b) the magnified one of titanate nanosheets (RDH15MR).

B. Semi-nanotubes

We can observe semi-tubular structure not completely rolled up usually in small grain sized initiator and lower basic concentration cases (table 2.3). It can be regarded as intermediate between nanosheet and nanotube on their curvature. Its composition, curvature, diameter and length are very similar to tube (see following description of nanotube, Section 2.3.2C), but the width along c-axis is not enough to form a complete tube. Therefore, that is actually half of tube. It often mixes with nanotube and behaves the same characters on XRD, SEM or other macroscopic instruments. We can only distinguish them by TEM until now.

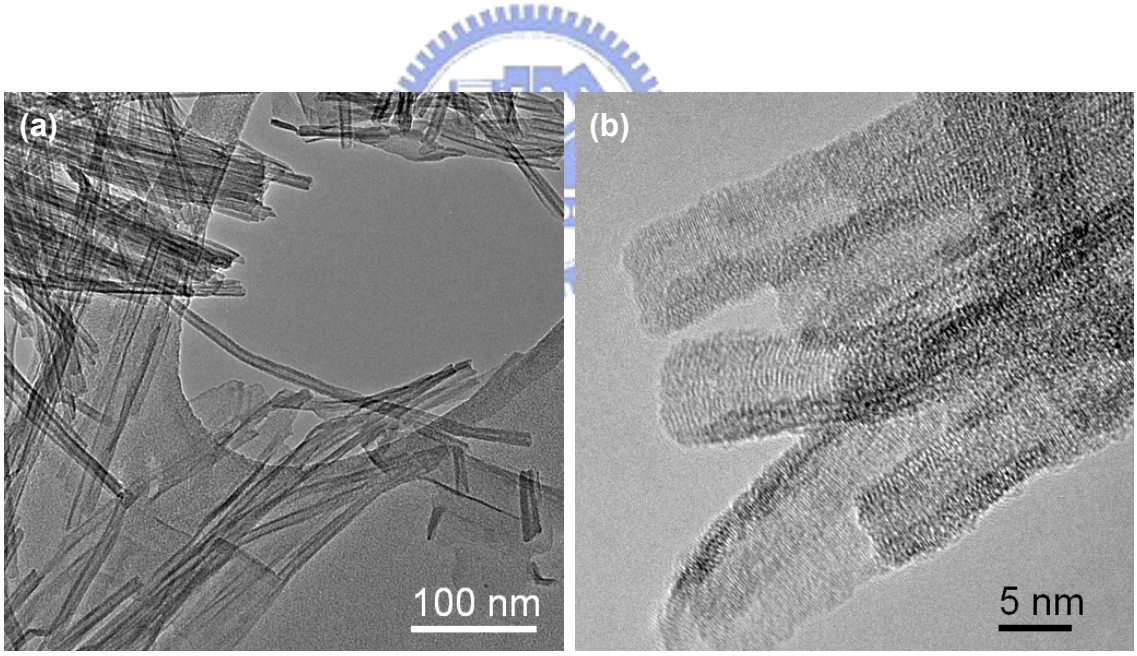

Figure 2.10. (a) The TEM image and (b) the magnified one of titanate semi-nanotubes (rut10MR).

C. Nanotubes

We can obtain tubular structure product with composition of "$0.38NaOH{\cdot}0.55H_2O{\cdot}TiO_2$" (without carbonate observed on TGA-MS and IR) (Section 2.6.1) in appropriate basic solution concentration as 10M NaOH at 100˚ C -150˚ C (by either autoclave or reflux method). This product is very uniform. By images of EM (figure 2.11 and 2.12), we observe that they are reel-like, 50nm-500nm as length, 8nm-10nm as diameter and usually rolled a monolayer up as 3~4 layers thickness (figure 2.12b). This titanate nanotube has very large specific surface (characterized by BET method, 2.2.3H) as 262 $m^2{\cdot}g^{-1}$ of raw material and 284 $m^2{\cdot}g^{-1}$ after proton-exchanging, even 323 $m^2{\cdot}g^{-1}$ after exchanging and annealing.

The nanotubes roll up along c axis of lepidocrocite type layer structure and the axis direction is along b (see chapter 3 and ref. 6). The further study about its special structure and properties will be deeply discussed in chapter 3 and 4.

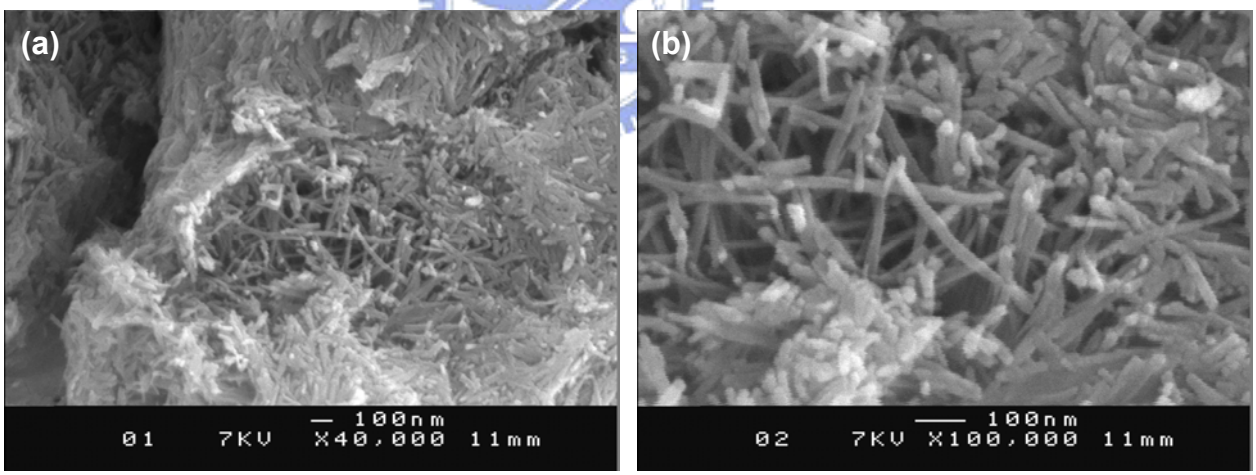

Figure 2.11. (a) The SEM image and (b) the magnified one of titanate nanotubes (RDH10M140).

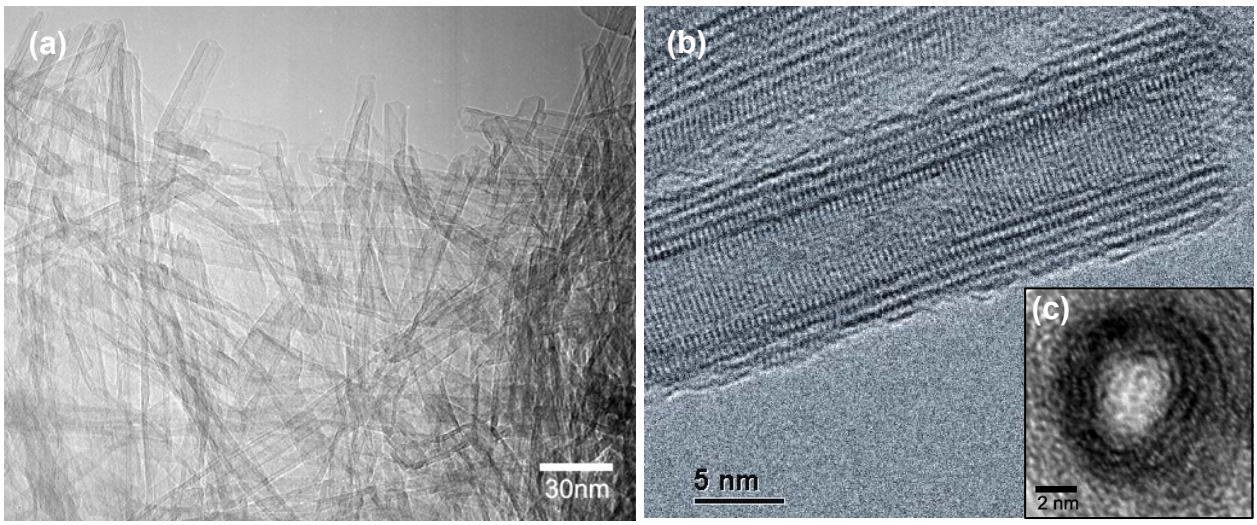

Figure 2.12. (a) The TEM, (b) HRTEM and cross-section images of titanate nanotubes (RDH10M140).

D. Nanoribbons

This product obtained in 180° C autoclave is formed of nanoribbons with 20nm-200nm thickness and 0.5μm -10μm length (figure 2.13 and 2.14). Its composition can be expressed as "$0.52NaOH{\cdot}0.30H_2O{\cdot}TiO_2{\cdot}0.02CO_2$" and has density about 3.17 $g{\cdot}cm^{-3}$ (RDH10M140). This nanoribbon can transform to TiO_2(B) nanoribbon which has the same size with titanate initiator after proton exchanging and calcinations. This TiO_2(B) phase can exist until 800° C and then transform to anatase phase. The TiO_2(B) nanoribbon has high capacity (150 mAh) and good reversibility of lithium ion intercalation. The anatase phase from nanoribbon has good photocatalytic efficiency (see Chapter 4). We can also obtain the same structure but much smaller nanofiber product (20nm thickness and 500nm length) in reflux condition (am10MR). The photocatalytic and lithium intercalation results manifested that the smaller one has even better efficiency than nanoribbon.

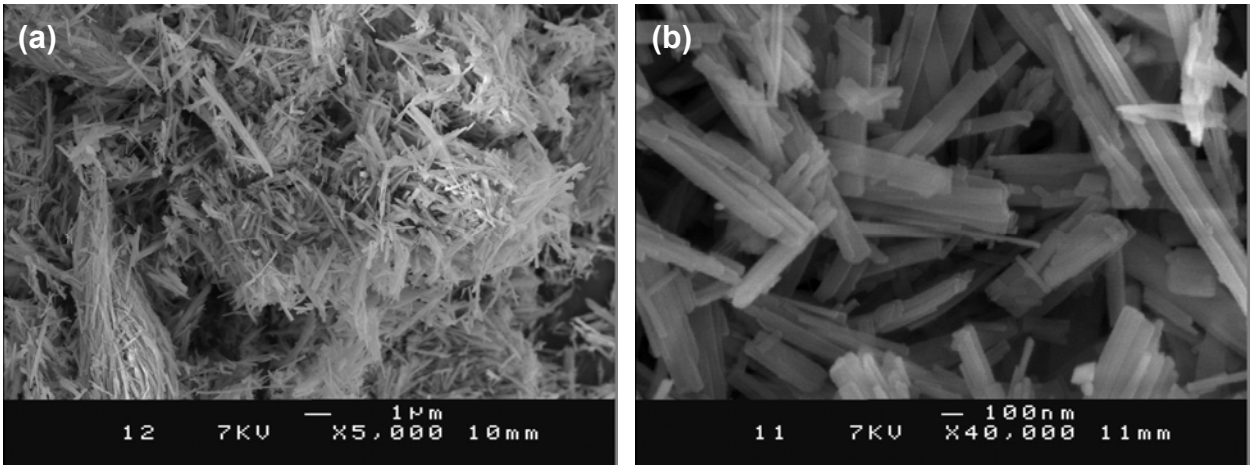

Figure 2.13. (a) The SEM image and (b) the magnified one of titanate nanoribbons (RDH10M180).

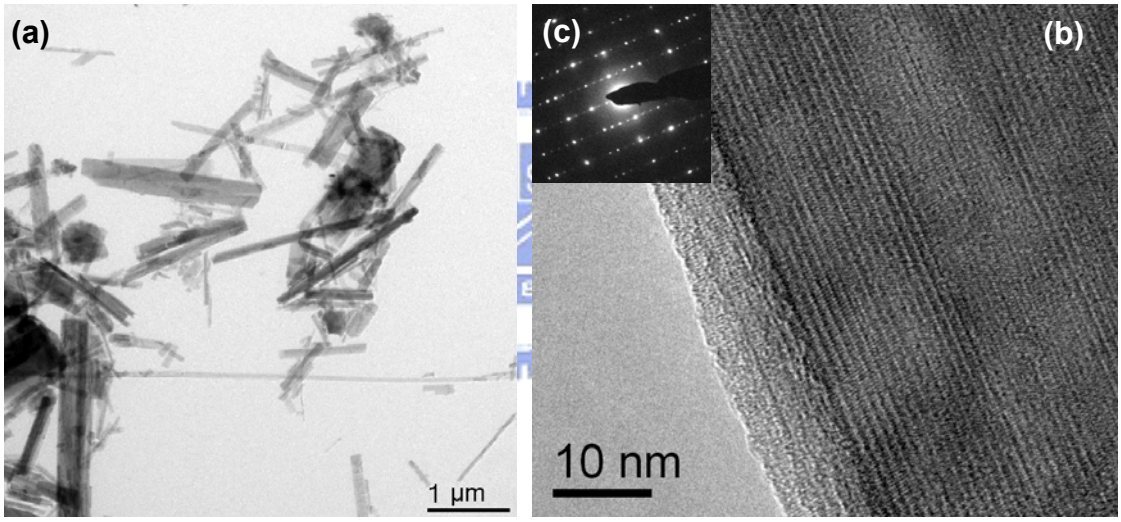

Figure 2.14. (a) The TEM, (b) HRTEM and (c) selected area electron diffraction pattern images of titanate nanoribbons (RDH10M180).

E. Submicro-sticks

We can observe a stick-like product in small grain-sized precursors autoclaved at 220° C, such as sample am10M220. Its composition can be described as "0.57NaOH·TiO_2" without surplus structural water as other sample. Its density is 3.22 g·cm^{-3} (am10M220). Its size is bigger as 200nm-600nm thick and 0.5μm-2μm long, therefore we name it "submicro" to

replace “nano” (figure 2.15 and 2.16). Uniquely, it will transform to rutile phase directly after proton exchanging and calcinations. Furthermore, we also observed that rutile TiO_2 can transform to this stick-like product at lower temperature (rut10M180). For these reasons, we infer that it is a rutile-type derivative. Further structural discussion is detailed into chapter 3.

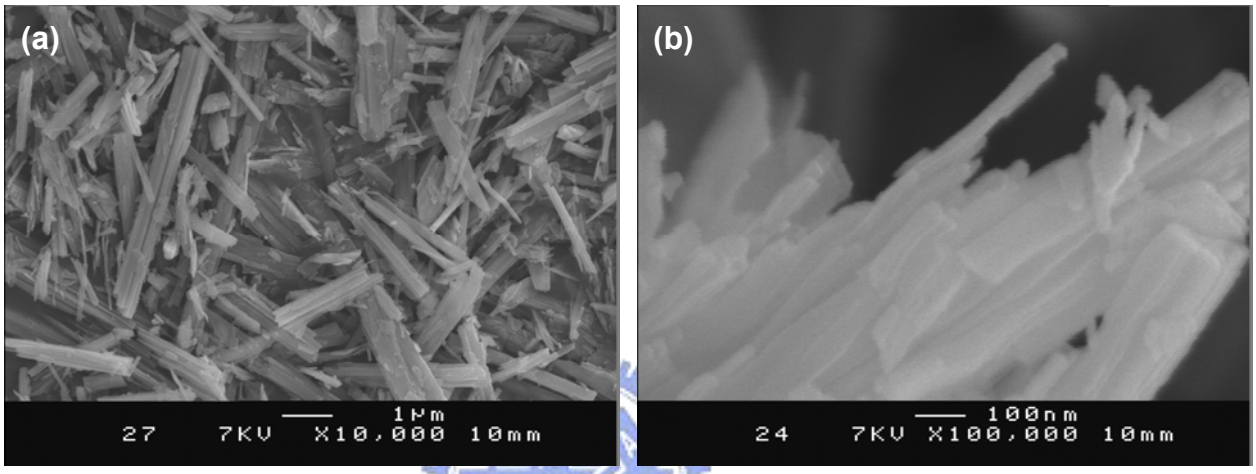

Figure 2.15. (a) The SEM image and (b) the magnified one of titanate submicro-sticks (am10M220).

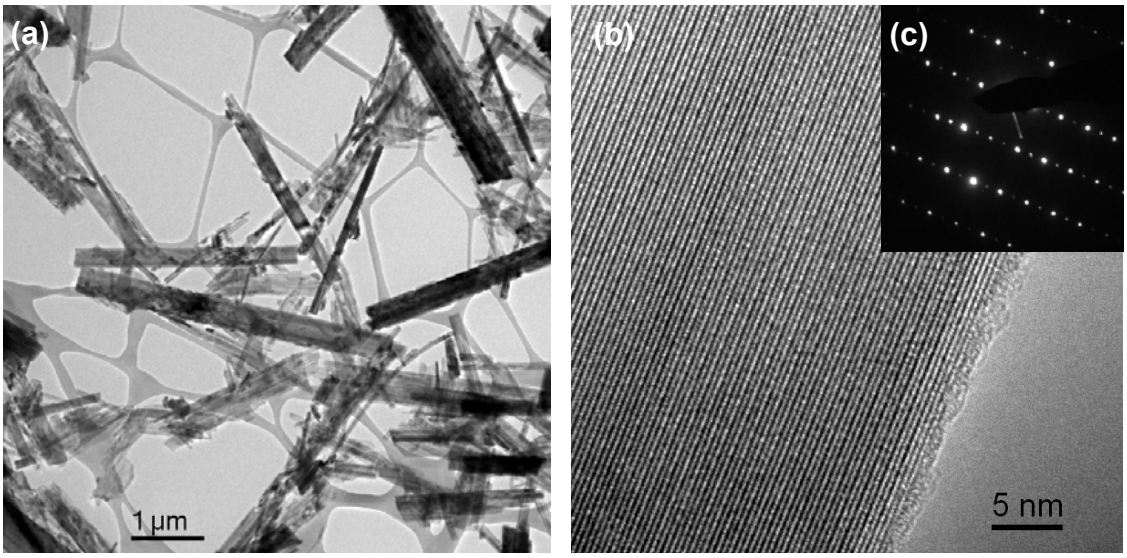

Figure 2.16. (a) The TEM, (b) HRTEM and (c) selected area electron diffraction pattern images of titanate submicro-sticks (am10M220).

2.4. Discussions

2.4.1. Influence of the nature of TiO_2 precursors

Although Tsai and Teng have already collected and compared the specific surface property of some titanate nanotubes from different titanium sources in their literature,[6] there is no report systematically comparing the morphologic differences of titanate nanostructure from various titanium sources until now. Every related report assumed nanotube structure as the product of course. However, we found that product morphologies sensitively depend on the nature of TiO_2 precursors in the same reaction condition by EM observation, even though they have no obvious difference in XRD (figure 2.17). In this section study, the discussion of the influence of initiator nature on the formation of nanotubes is lead stating on the results obtained from various precursors mentioned in experimental section (10M NaOH, 120° C autoclaved).

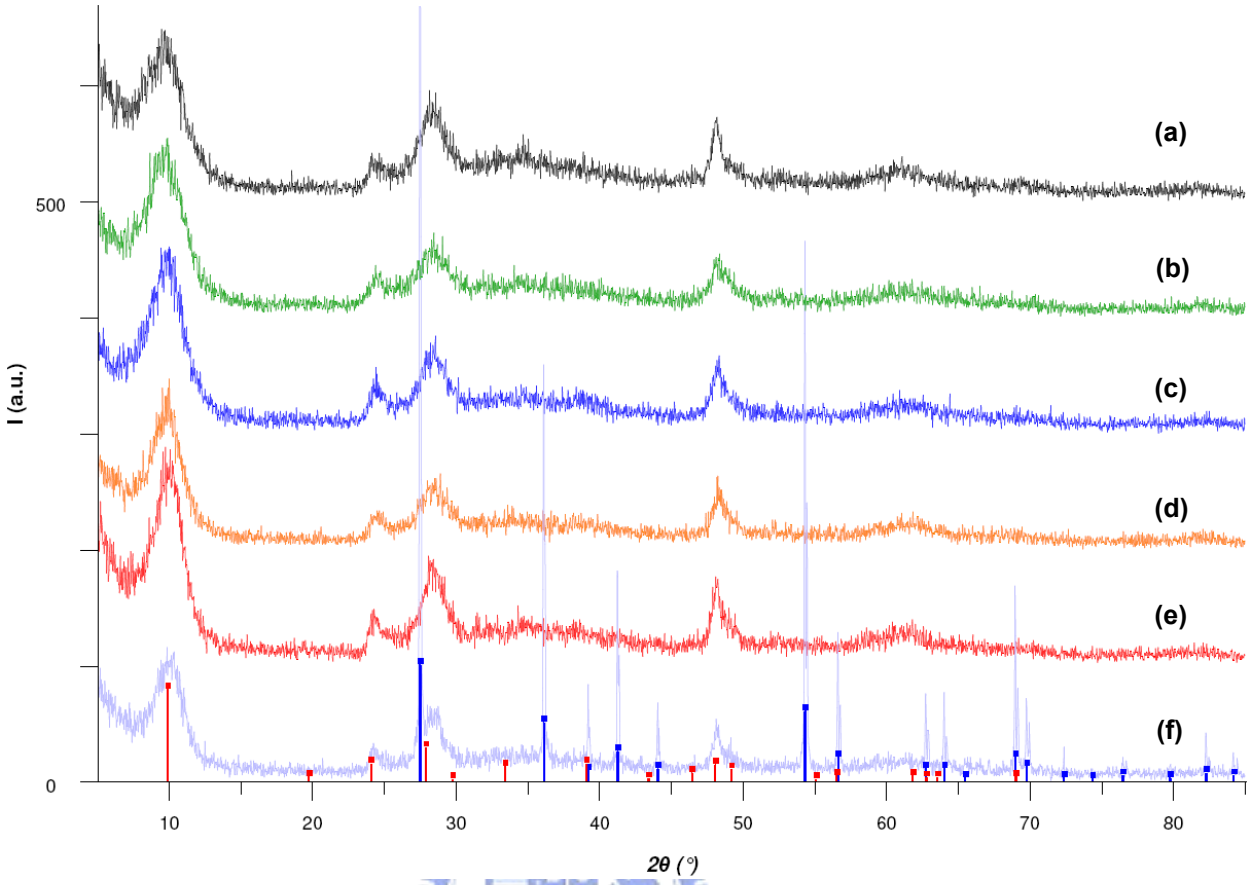

Figure 2.17. XRD diagrams of sodium hydroxo titanate from (a) amorphous (am10M120), (b) TiO_2 hydrate from TTIP (TO10M120), (c) 5nm (5nm10M120), (d) P25 (P2510M120), (e) RDH (RDH10M120) and (e) rutile (rut10M120) in 10M NaOH aqueous solution at 120° C during 72 hours. (■: peak positions of remained rutile in rut10M120, ■: of lepidocrocite type titanic acid, $H_2Ti_2O_5 \cdot H_2O$, JCPDS 47-0124 [5].)

By EM images (figure 2.18 and 2.19), we can observe the amorphous one is semi-nanotube (10nm diameter and 100nm length) as major product and small nanosheet (3nm thickness and 20nm width) as minor; the TiO_2 hydrate one is also semi-nanotube as major and small nanosheet as minor, but more curve than the amorphous one; the 5nm one is small nanosheet; the P25 one is semi-nanotube and nanosheet (50nm width and 200nm length); the RDH one is uniform nanotube (8nm diameter and 200nm-500nm length); the rutile product is nanotube and obvious remained rutile particle which can be observed in XRD

(figure 2.17e). According to these observations, we can induce that bigger grain size initiator (when considering a same phase) produces wider titanate layer structure (longer c-direction diameter) in lower temperature condition (scheme 2.2).

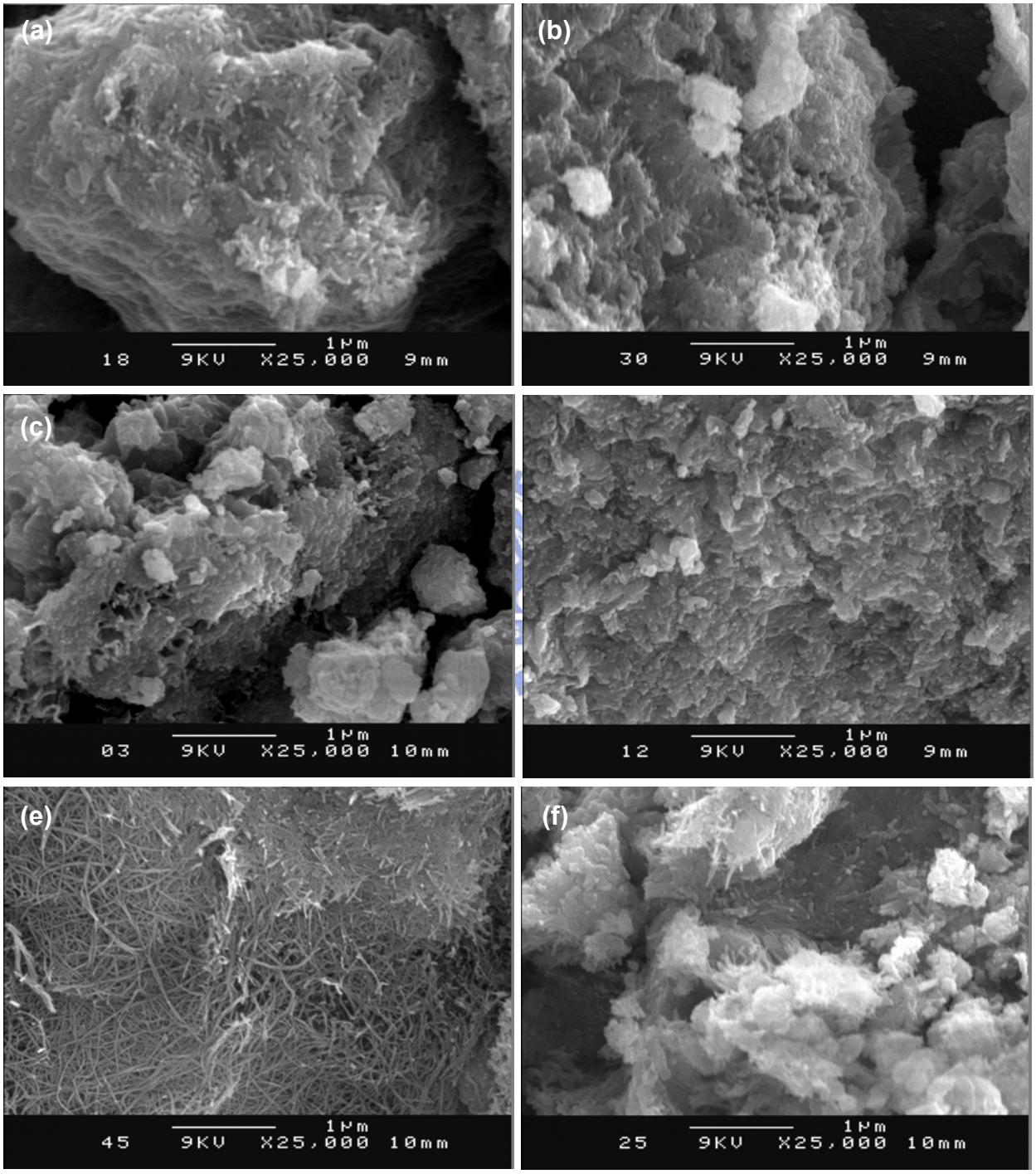

Figure 2.18. SEM images of sodium hydroxo titanate from (a) amorphous (am10M120), (b) TiO_2 hydrate (TO10M120), (c) 5nm (5nm10M120), (d) P25 (P2510M120), (e) RDH (RDH10M120) and (f) rutile (rut10M120).

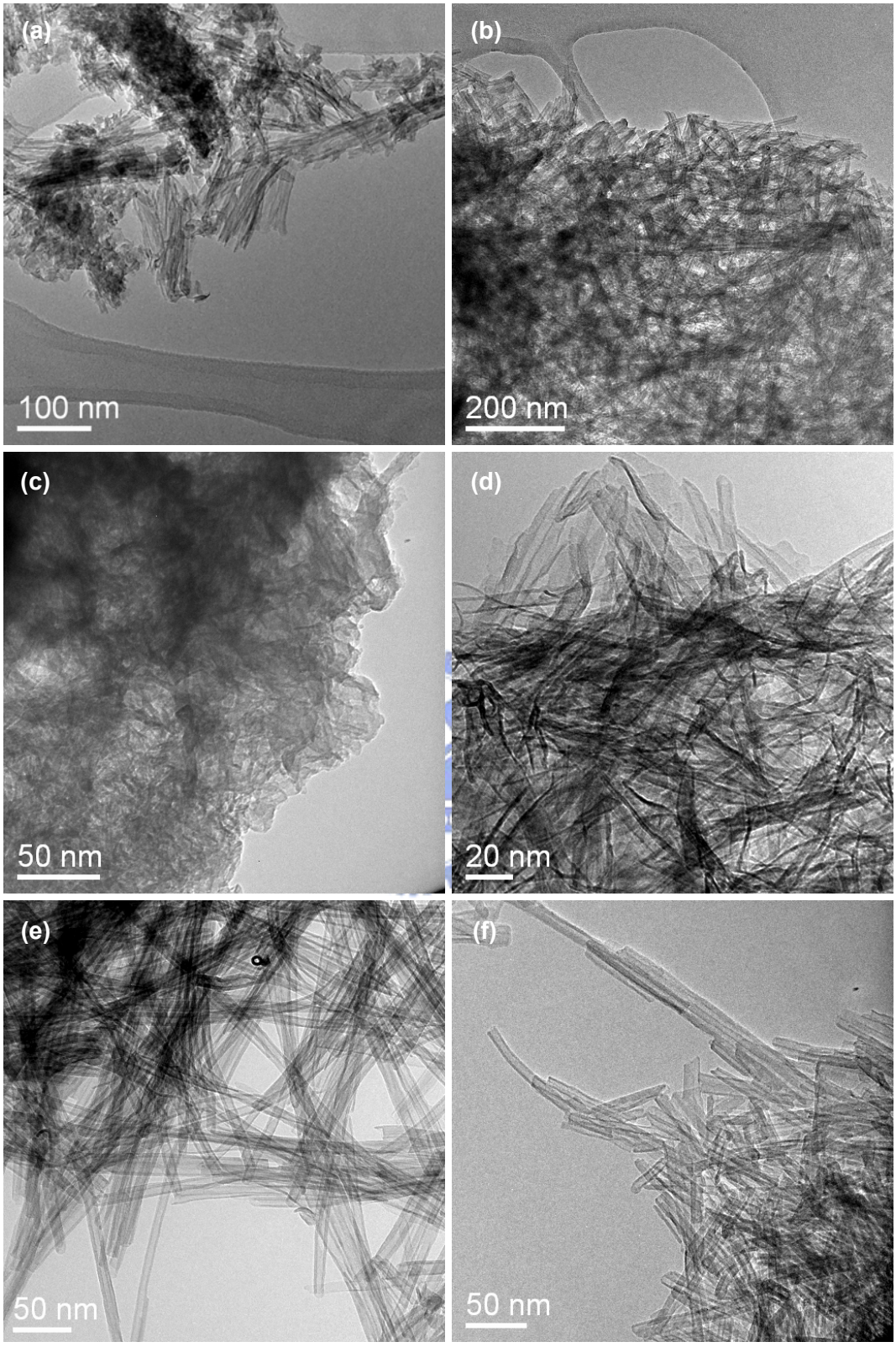

Figure 2.19. TEM images of sodium hydroxo titanate from (a) amorphous (am10M120), (b) TiO_2 hydrate (TO10M120), (c) 5nm (5nm10M120), (d) P25 (P2510M120), (e) RDH (RDH10M120) and (f) rutile (rut10M120).

At 140° C, which is the optimum temperature condition of nanotube formation, the XRD results still has no obvious difference among these various precursors (figure 2.20).

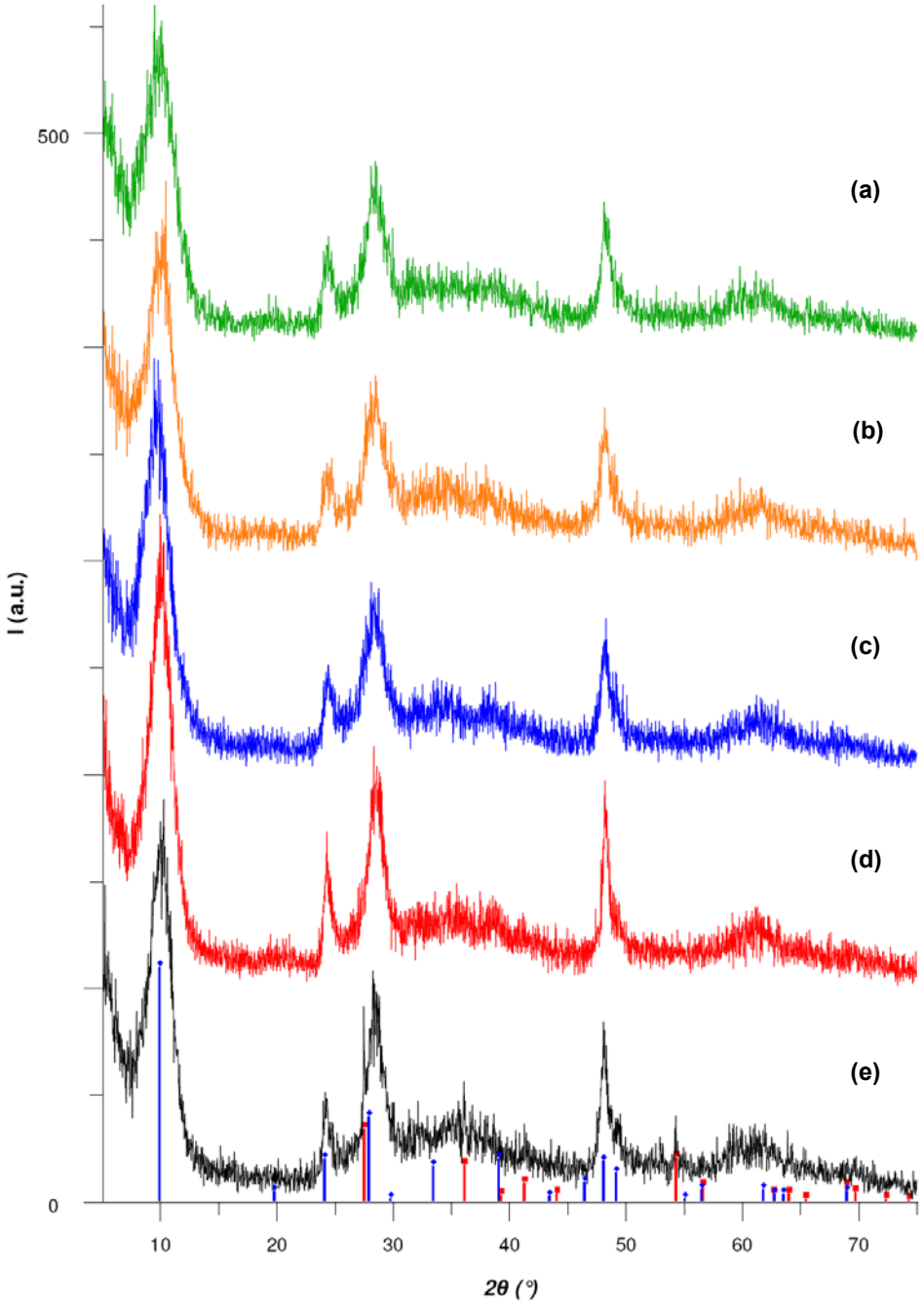

Figure 2.20. XRD diagrams of sodium hydroxo titanate from (a) amorphous (am10M140), (b) 5nm (5nm10M140), (c) P25 (P2510M140), (d) RDH (RDH10M140) and (e) rutile (rut10M140) in 10M NaOH aqueous solution at 140° C during 72 hours. (■: peak positions of remained rutile in rut10M120, ♦: of lepidocrocite type titanic acid, $H_2Ti_2O_5 \cdot H_2O$, JCPDS 47-0124 [5].)

However, by EM images (figure 2.21 and 2.22), we can observe the amorphous one is nanotube (8nm diameter and 200nm length) as major product and small nanosheet (3nm thickness and 20nm width) as minor; the 5nm one is small nanosheet; the P25 one is semi-nanotube and nanosheet (50nm width and 200nm length); the RDH one is uniform nanotube; the rutile product is nanotube and a little of remained rutile particle which can be observed in XRD (figure 2.20e) and SEM image as big rectangular block (figure 2.18e). These observations are well coincident with the 120° C ones; the bigger grain size initiator produces wider layer structure.

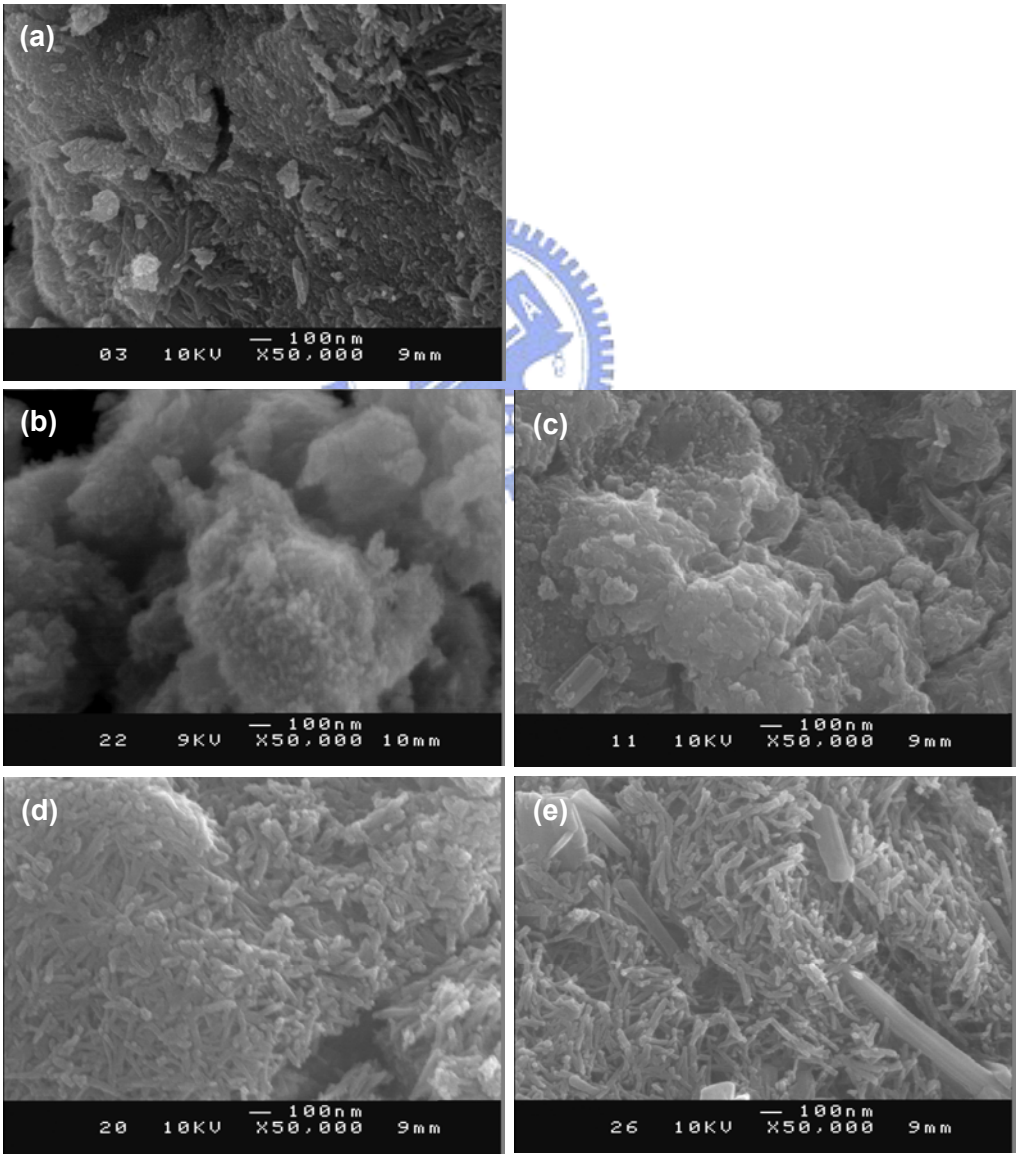

Figure 2.21. SEM images of the product from (a) amorphous (am10M140), (b) 5nm (5nm10M140), (c) P25 (P2510M140), (d) RDH (RDH10M140) and (e) rutile (rut10M140).

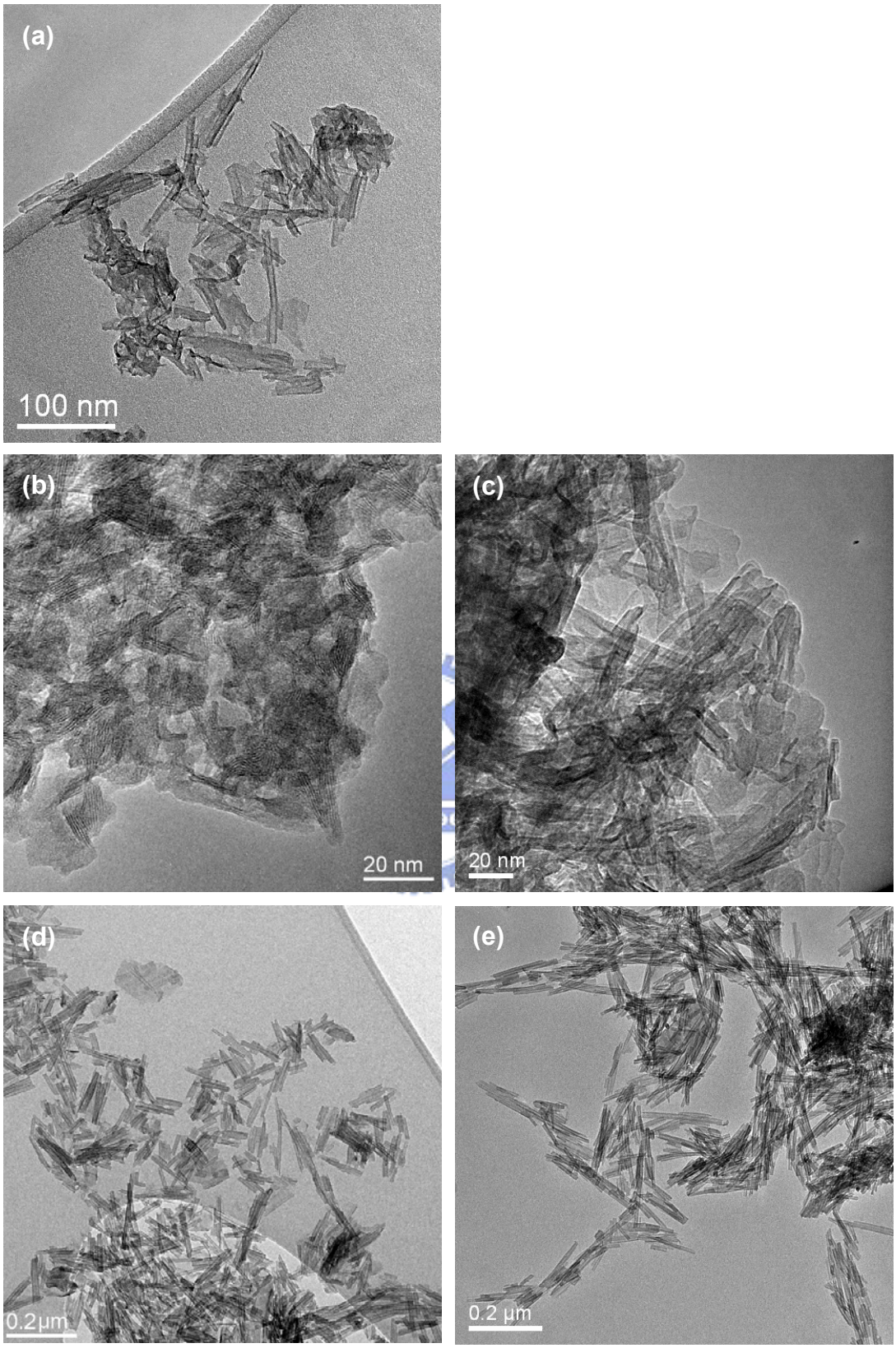

Figure 2.22. TEM images of sodium hydroxo titanate from (a) amorphous (am10M140), (b) 5nm (5nm10M140), (c) P25 (P2510M140), (d) RDH (RDH10M140) and (e) rutile (rut10M140).

According to above results, we concluded the c-direction growth of product is positive related to grain size of initiator. However, we also noticed that the behavior of amorphous and rutile one are not linear correlated with other three. The amorphous one has been nanotube yet, and the rutile one is almost the same sized nanotube as RDH. That infers the structural nature of precursor should be considerable. For studying the influence of precursor phase, we extracted and compared the samples from amorphous, RDH (anatase) and rutile at higher temperature (180˚ C and 220˚ C).

In XRD diagrams (figure 3.23), we are able to observe the amorphous and anatase both are lepidocrocite type titanate nanoribbon, and the rutile one has obvious rutile type phase peaks already at 180˚ C autoclaved environment. Although amorphous and RDH have the same structure but different diameter. By SEM images (figure 3.24), we observed that amorphous one diameter is thinner than RDH due to their grain size effect (the grain of amorphous is much smaller than RDH anatase).

At 220˚ C, the amorphous lead to rutile type as major product; the RDH mostly to lepidocrocite type; and the rutile one retains the pure rutile type phase. It is thus clear that the product morphologies also depend on the initiator structures, especially in higher reaction temperature. To sum up the results mentioned above, these evidences imply that the intermediate building block which construct titanate layer depend on the structural nature of precursor (grain size and structure). The bigger grain sized one of the same structure initiators produces bigger titanate crystallite. The rutile and small grain sized anatase can transform to rutile-type phase at high temperature. The possible intermediates are discussed in Chapter 3.

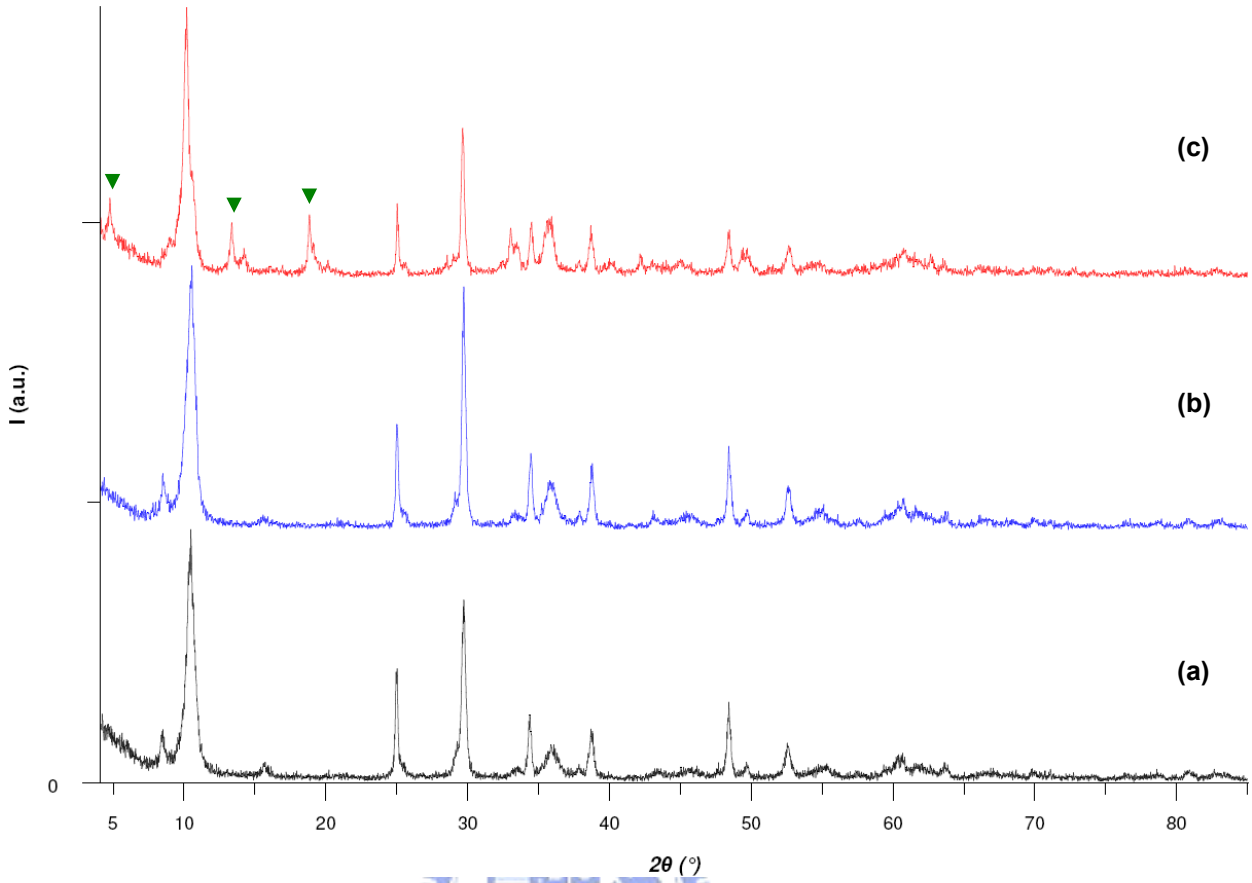

Figure 2.23. XRD diagrams of titanate nanoribbon from (a) amorphous (am10M180), (b) RDH (RDH10M180) and (c) rutile (rut10M180) at 180° C. (▼: the characteristic peaks of rutile-type.)

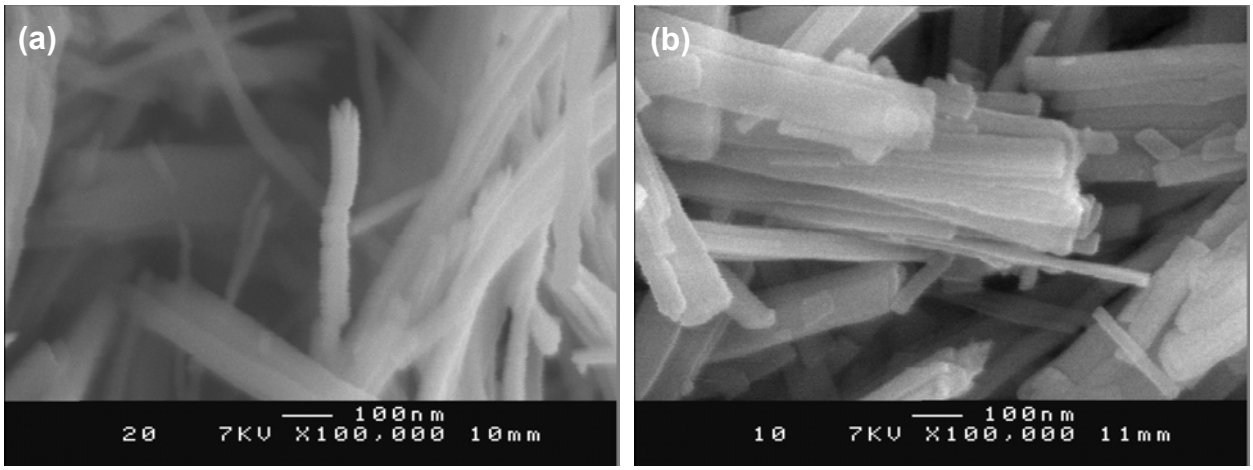

Figure 2.24. SEM images of titanate nanoribbon from (a) amorphous (am10M180) and (b) RDH (RDH10M180).

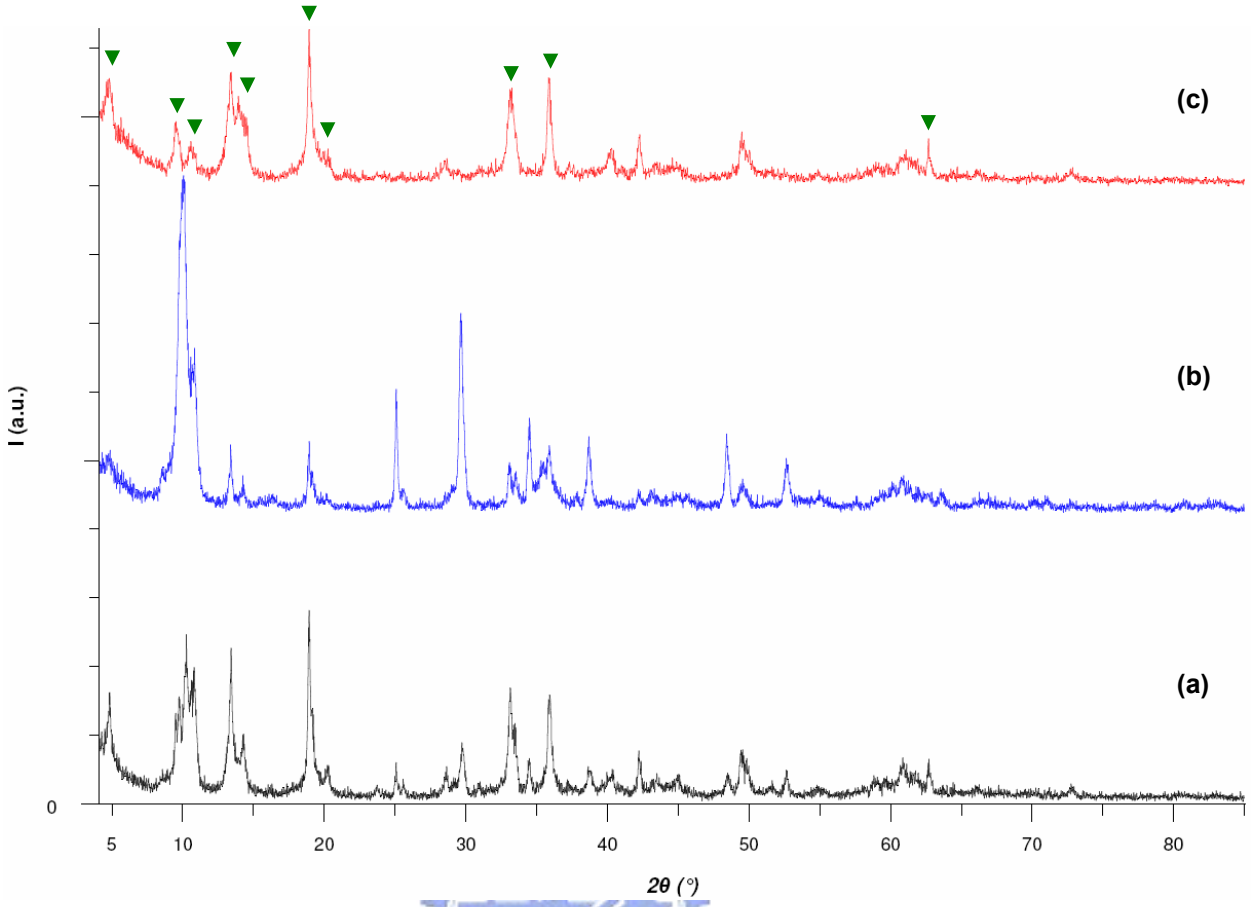

Figure 2.25. XRD diagrams of titanate nanoribbon from (a) amorphous (am10M220), (b) RDH (RDH10M220) and (c) rutile (rut10M220) at 220° C. (▼: the characteristic peaks positions of rutile-type phase submicro-stick.)

2.4.2. Temperature effect

In the previous paragraph, we have seen different products from one precursor at different temperature conditions (figure 2.17, 2.20, 2.23 and 3.25). We want to discuss the temperature effect for a particular precursor. This section is focused on the amorphous one (am10M120, am10M140, am10M180 and am10M220).

In the XRD results (figure 2.26), we observed that 120° C and 140° C ones have an

X-ray diffraction pattern similar to the samples with small curved lamellar structures (nanosheet, semi-nanotube and nanotube); the 180˚ C one is similar as nanoribbon; and the rutile type product became major mixed with a few of lepidocrocite type product at 220˚ C. We have inferred that the phase of final product is decided by intermediate form in last section (Section 2.4.1). However, there is an important point in this discussion. The amorphous is not crystallized but random arrangement. That means it may be not degraded to form constructive intermediates but it may directly grow. So that it has the most freedom to create different building block, either rutile type or anatase type (to form lepidocrocite), depending on the external chemical environment. According to XRD observation, it prefers to exhibit as rutile at 220˚ C and as anatase under 180˚ C. The small crystallite TiO_2 as P25 (small sized anatase mixed with 20% of rutile) has similar behavior, but exclude of 5nm one which always keeps anatase form to be lepidocrocite product even at 220˚ C. That is due to structural carbonate existed which will be discussed in Section 2.4.5.

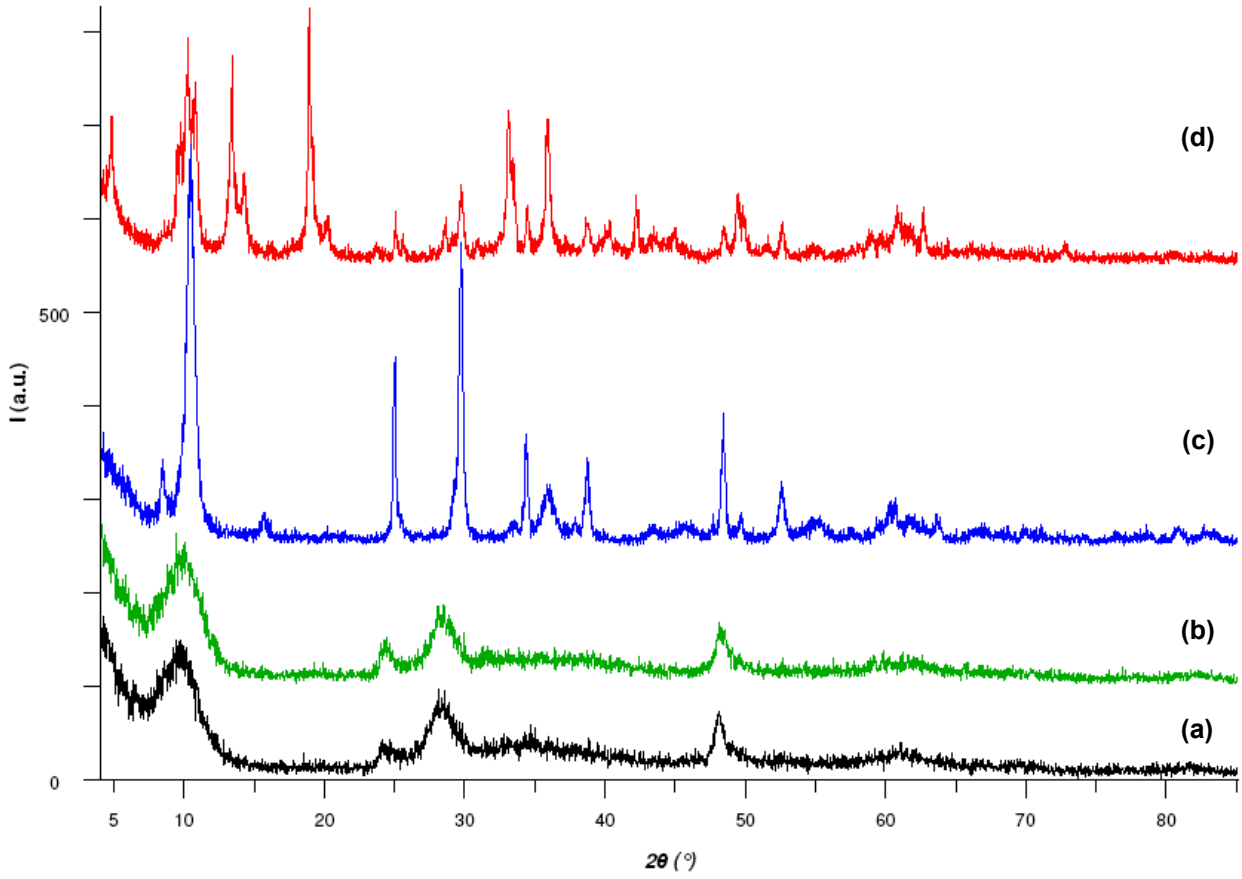

Figure 2.26. XRD diagrams of product from amorphous in 10M $NaOH_{(aq)}$ autoclaved at (a) 120ºC (am10M120), (b)140ºC (am10M140), (c)180ºC (am10M180) and (d)220ºC (am10M220) .

In EM images (figure 2.27 and 2.28), we observed that the product of amorphous (am10M120) is mostly semi-tubular (10nm-15nm diameter and 100nm-200nm length) and small lamellar (10nm-20nm width and 3nm thickness) as minor at 120˚ C. The 140˚ C one (am10M140) is tubular (8nm diameter and 100nm-200nm length) mostly and small lamellar. At 180˚ C (am10M180), we obtained nanoribbon but smaller and shorter than big anatase one (RDH10M180). In 220˚ C sample (am10M220) is major submicro-sticks mixed with nanoribbon.

By above observations, we found that the temperature condition is very critical for every individual phase when other parameters remain fixed. The elongation along c-direction of tianate layer increases by temperature until 180˚ C (layer width: semitube<tube<ribbon). On another side, the 220˚ C may high enough to make smaller or another form building block as rutile derives. As the effect of nature of precursor above-mentioned, we can also explain the influence of reaction temperature by different intermediate formations. Due to the product morphology is sensitively affected by temperature; these phenomena give us one of possible routes to adjust titanate nanostructures.

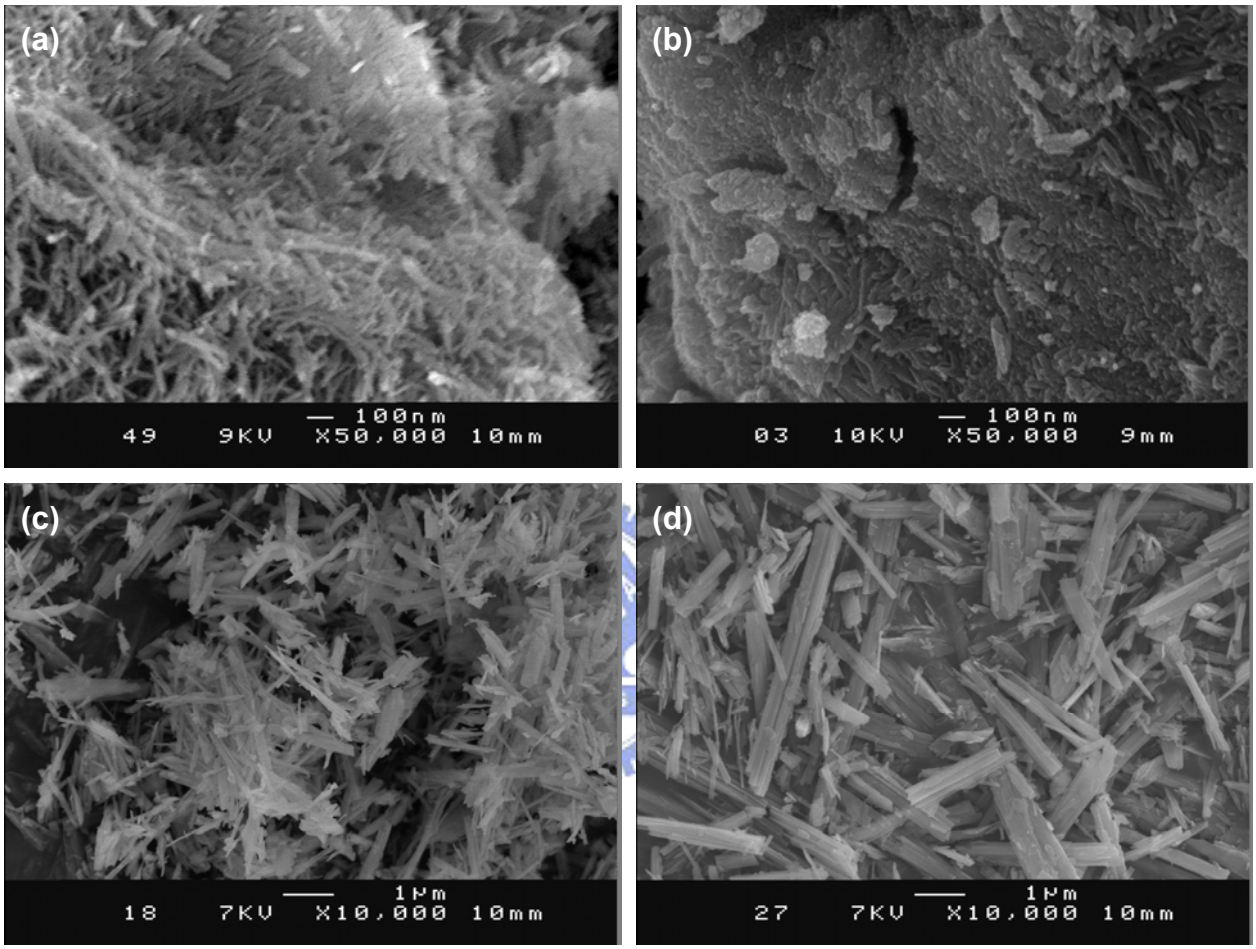

Figure 2.27. SEM images of product from amorphous in 10M $NaOH_{(aq)}$ autoclaved at (a) 120º C (am10M120), (b) 140º C (am10M140), (c) 180º C (am10M180) and (d) 220º C (am10M220) .

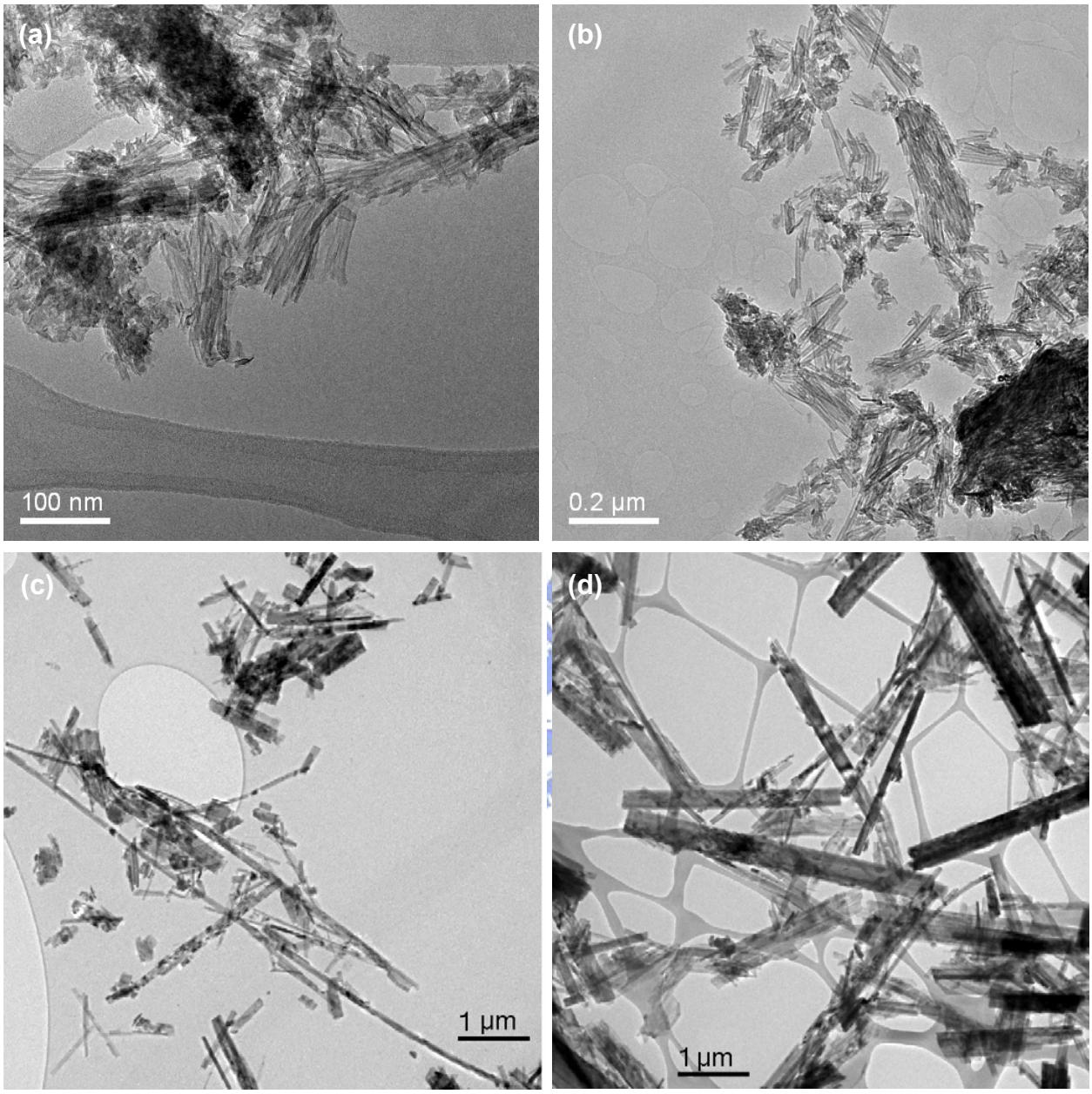

Figure 2.28. TEM images of product from amorphous in 10M $NaOH_{(aq)}$ autoclaved at (a) 120º C (am10M120), (b) 140º C (am10M140), (c) 180º C (am10M180) and (d) 220º C (am10M220) .

2.4.3. Base concentration effect

The basic concentration effect has been discussed too. We chose amorphous as initiator for example 120° C autoclaved in 0M (deion water), 0.1M, 0.5M, 1M, 5M, 10M and 15M NaOH aqueous solution respectively to conclude the influence of different basic environment. We chose amorphous as discussed object because of its large reacted range of basic concentration. The RDH anatase can not transform to titanate under basic concentration lower than 10M. The 5nm one has still remained anatase observed in 5M NaOH condition. Not as the crystallized precursor, amorphous has obvious titanate peaks from 0.5M until 15M conditions (figure 2.29). In fact, it has been $TiO_2(OH)_x$ species, so that the degradation from TiO_2 crystallite to $[TiO_2(OH)_x]_n$ intermediate cluster by concentrated basic solution is not necessary. This degradation process for better crystallized TiO_2 needs stronger basic solution to carry out.

We found that the curvature and diameter of titanate layer increase with NaOH concentration from 0.5M until 15M. The 0.5M sample is smaller nanosheet; the 1M one is bigger nanosheet; the 5M one is semi-tubular as major; the 10M is mostly tubular; and the 15M product is almost amorphous. This process can be sorted out as two stages. The first stage from 0.1M to 1M is growth of titanate layer with more NaOH weighed in (figure 2.30b-d). In this stage, the NaOH is not saturated interlayer; more NaOH can enhance the growth of layer structure. The second stage from 1M to 15M is curvature and dispersion of titanate layers (figure 2.30d-g). In this stage, The NaOH intercalated interlayer has saturated for layer formation, the surplus NaOH continually intercalated into interlayer make stronger strain force to curve and over saturating the layer surface to disperse to monolayer. Therefore, we can observe the nanosheet more curved to form semi-tube, then dispersed to monolayer rolled up (nanotube) when basic concentration increase. Finally, when base is too much (over 15M in this case), it will be deconstructed to amorphous.

The product is anatase and little of brookite in 0M and 0.1M. The 0M sample is particle like (about 10nm) and has obvious preferred orientation of anatase by XRD result. In 0.1M condition, the anatase product became lower crystallized and brookite peak became more obvious.

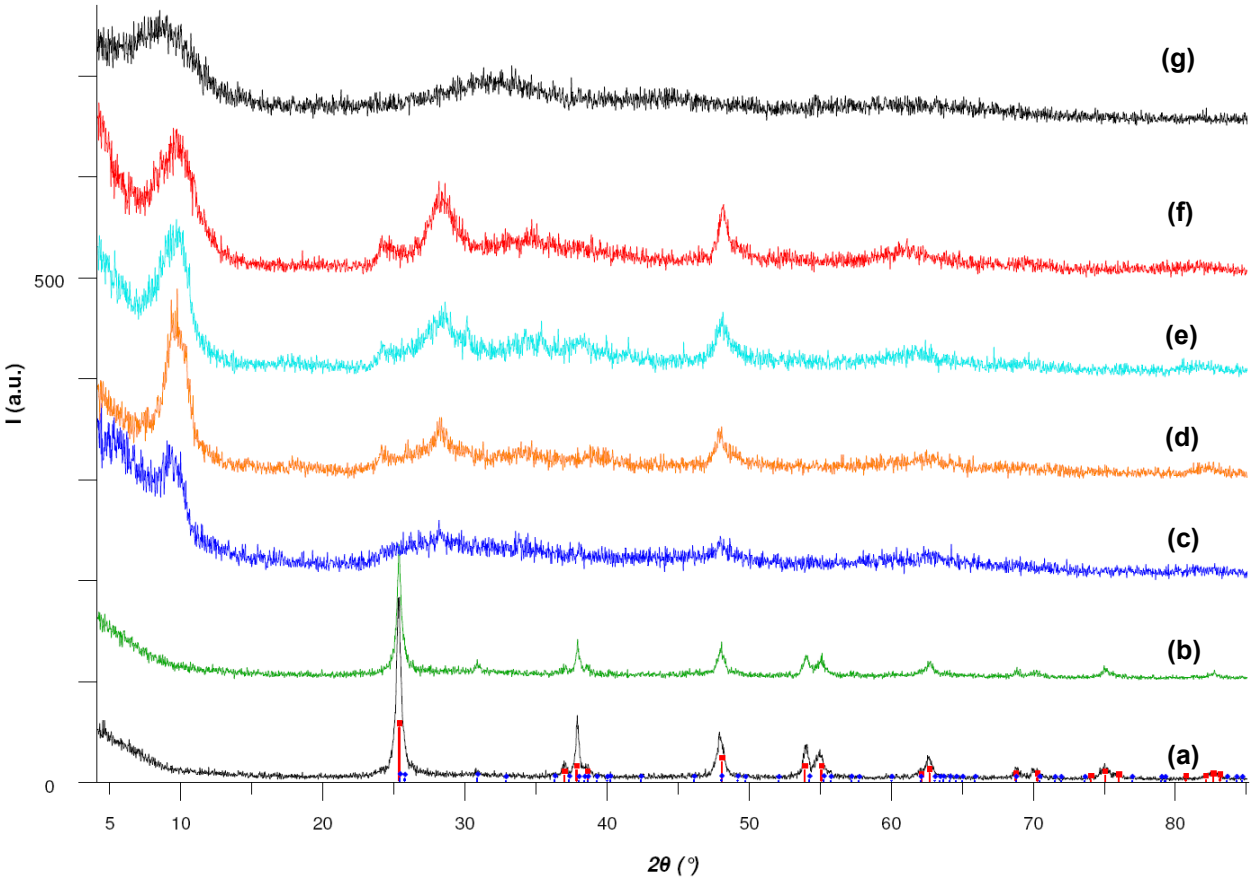

Figure 2.29. XRD diagrams of product from amorphous 120º C autoclaved in (a) 0M (am0M120), (b) 0.1M (am0.1M120), (c) 0.5M (am0.5M120), (d) 1M (am1M120), (e) 5M (am5M120), (f) 10M (am10M120) and (g) 15M (am15M120) NaOH aqueous solution.

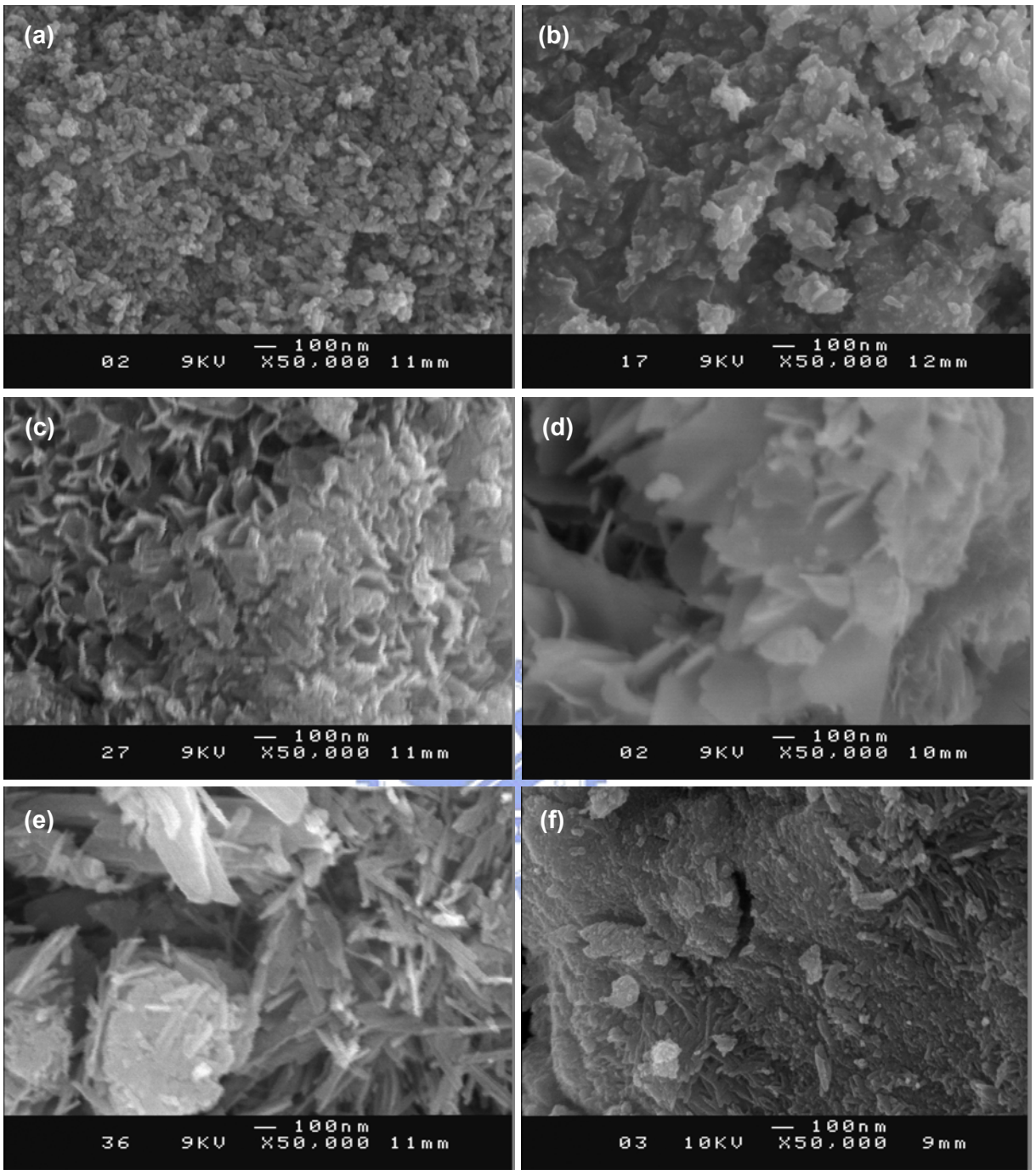
(a)
100nm
02 9KV X50,000 11mm
(b)
100nm
17 9KV X50,000 12mm
(c)
100nm
27 9KV X50,000 11mm
(d)
100nm
02 9KV X50,000 10mm
(e)
100nm
36 9KV X50,000 11mm
(f)
100nm
03 10KV X50,000 9mm
(g)
100nm
55 9KV X50,000 12mm

Figure 2.30. SEM images of product from amorphous 120º C autoclaved in (a) 0M (am0M120), (b) 0.1M (am0.1M120), (c) 0.5M (am0.5M120), (d) 1M (am1M120), (e) 5M (am5M120) and (f) 10M (am10M120) NaOH aqueous solution.

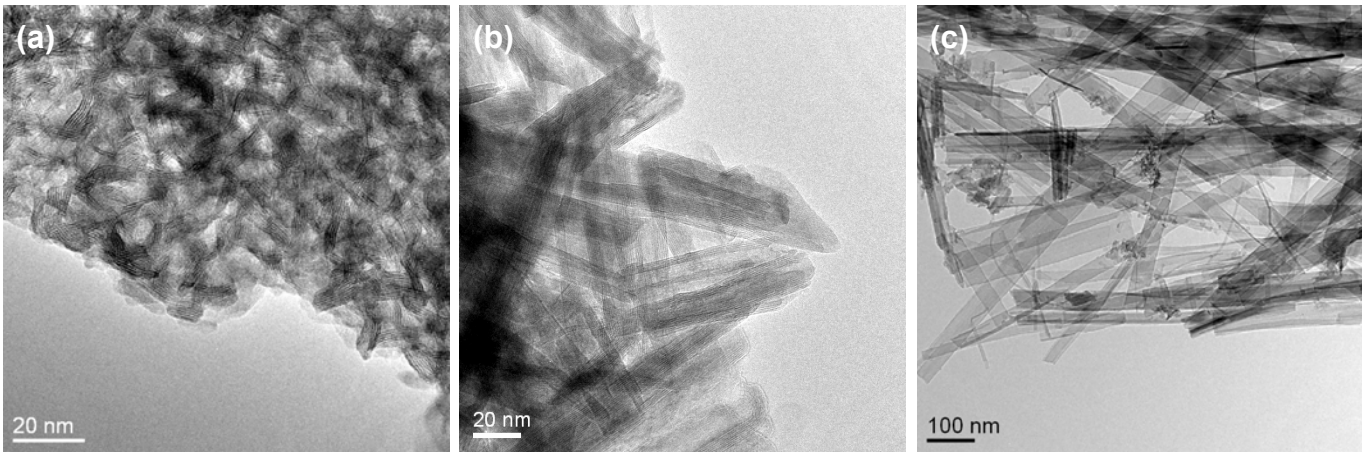

Figure 2.31. TEM images of 3 types of product in am5M120: (a) small lamellar, (b) semi-tubular (major) and (c) (band-like) lamellar.

2.4.4 Sodium chloride effect

In the above results and discussions, we know that the layer structure is deeply influenced by NaOH concentration. In low basic concentration condition, more sodium ion amount stabilizes and forms bigger layers (Section 2.4.3). However, the surplus OH ions deconstruct the lamellar structure under high basic concentration environment. Therefore, we added specially NaCl to study the influence of sodium ion for avoiding increased OH.

In 5nm 5M case, the additive NaCl indeed affects the product morphology. Originally, sample 5nm5M120 is semi-tubular (diameter: 30nm; length: 50nm-700nm) and remained anatase nanoparticles (diameter: 5nm), it became lamellar (diameter: 50nm-300nm; thickness: 10nm) and no survived anatase after additive NaCl (figure 2.32 and 2.33). However, additive

sodium ion does not affect on big grain precursor such as RDH anatase (figure 2.34). Even we have added 0.05mole NaCl in 10ml solution; we can not observe any change of XRD in either 5M or 10M case. The possible explanation is that OH is not enough to decompose RDH anatase in 5M case, therefore the anatase can not transform to titanate and the additive sodium does not work. In RDH 10M case, the sodium ion has saturated for titanate layer formation, so that more sodium ions are not helpful.

Consequently, the sufficient OH ion to decompose initiator is the most important prerequisite for other morphologic control artifices. When this premise was satisfied, adding sodium ion can flesh the intercalated ion interlayer out without increased strain or deconstruction, because we did not observe nanotube (curvature) or amorphous (decomposed) product increasing after adding NaCl. The sodium ion effect provides another good method to help growth of titanate layer structure.

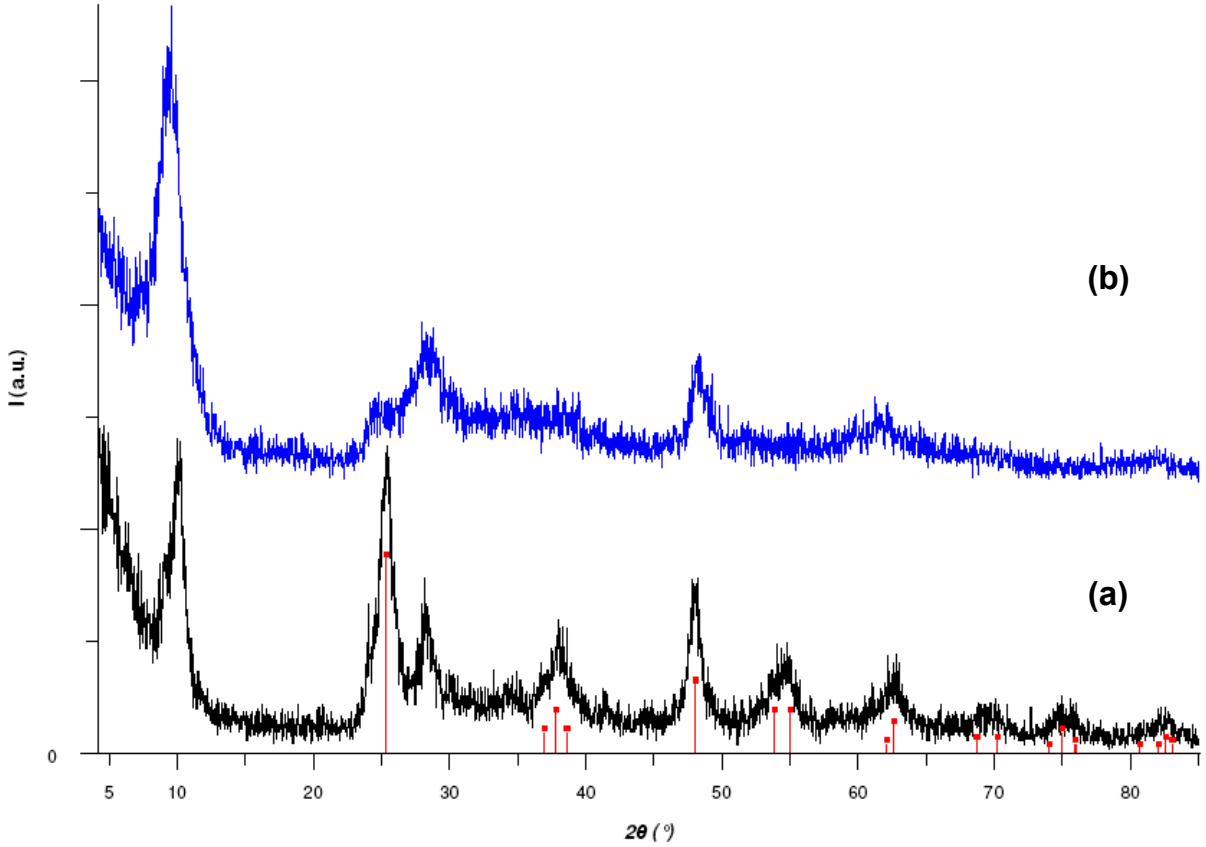

Figure 2.32. XRD diagrams of (a) product from 5nm in 5M $NaOH_{(aq)}$ autoclaved at 120ºC (5nm5M120) and (b) specially weighed 0.02 mole NaCl in.

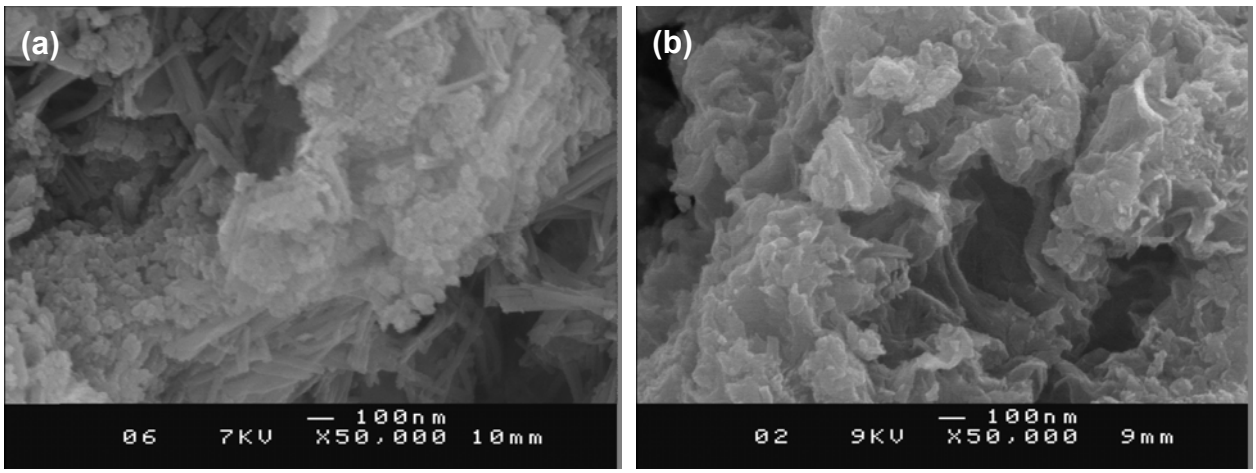

Figure 2.33. SEM images of (a) product from 5nm in 5M $NaOH_{(aq)}$ autoclaved at 120ºC (5nm5M120) and (b) specially weighed 0.02 mole NaCl in.

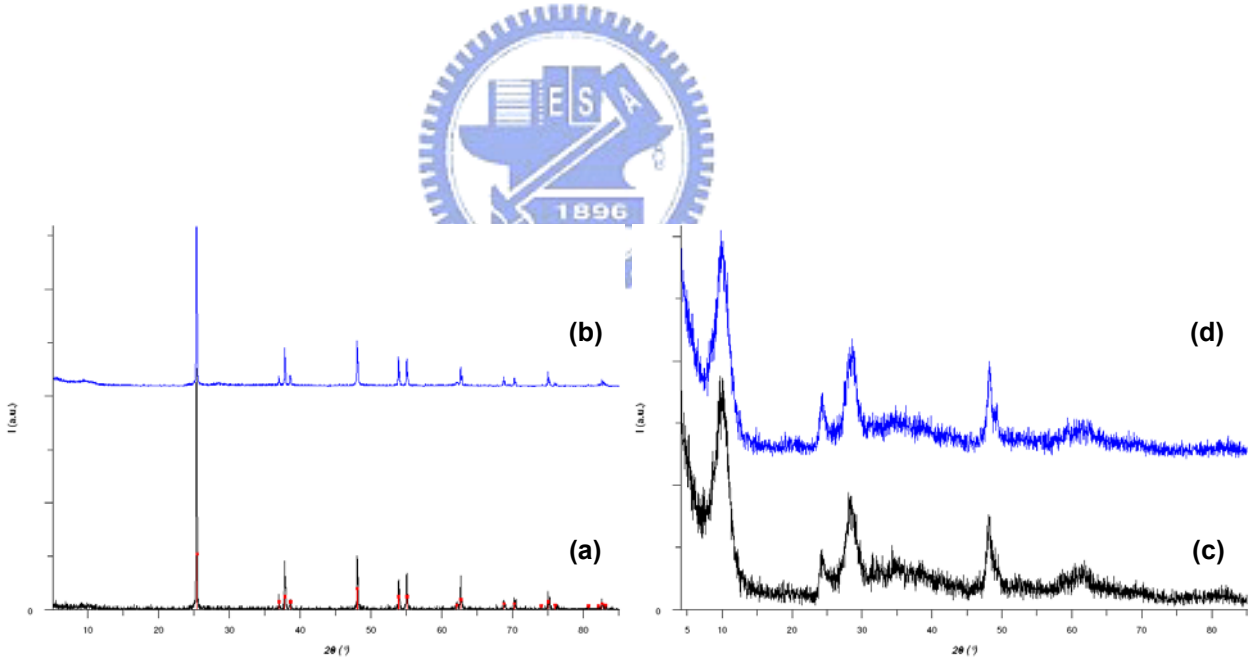

Figure 2.34. XRD diagrams of (a) RDH5M120 and (b) specially weighed 0.05 mole NaCl in (RDH5M120-4NaCl); (c) RDH10M120 and (d) RDH10M120-4NaCl. (■: anatase TiO_2 peaks)

2.4.5 Carbonate effect

The very different products between 120˚ autoclave and reflux in amorphous case prompted us to consider the influence of absorbed carbonate from air. By EM (figure 2.36) and XRD results (figure 2.35), we can see that the reflux sample (am10MR) is nanofiber (shorter nanoribbon), but the 120˚C autoclave one is semi-nanotube. The principle distinctions of environment between them are pressure and air, due to autoclave is a closed system. By our experiences, we knew the pressure effect is not important in low temperature (below 150˚ C), for example, the sample RDH10MR and RDH10M120 (or 140) are both mainly tubular phases. Besides, we observed stronger carbonate characteristic peaks of FT-IR (Section 2.6.), Raman (Section 3.5.) and TGA-MS (Section 2.6.) in all reflux cases than in autoclave ones. Therefore, we inferred that their differences are made by absorbed carbonate from air.

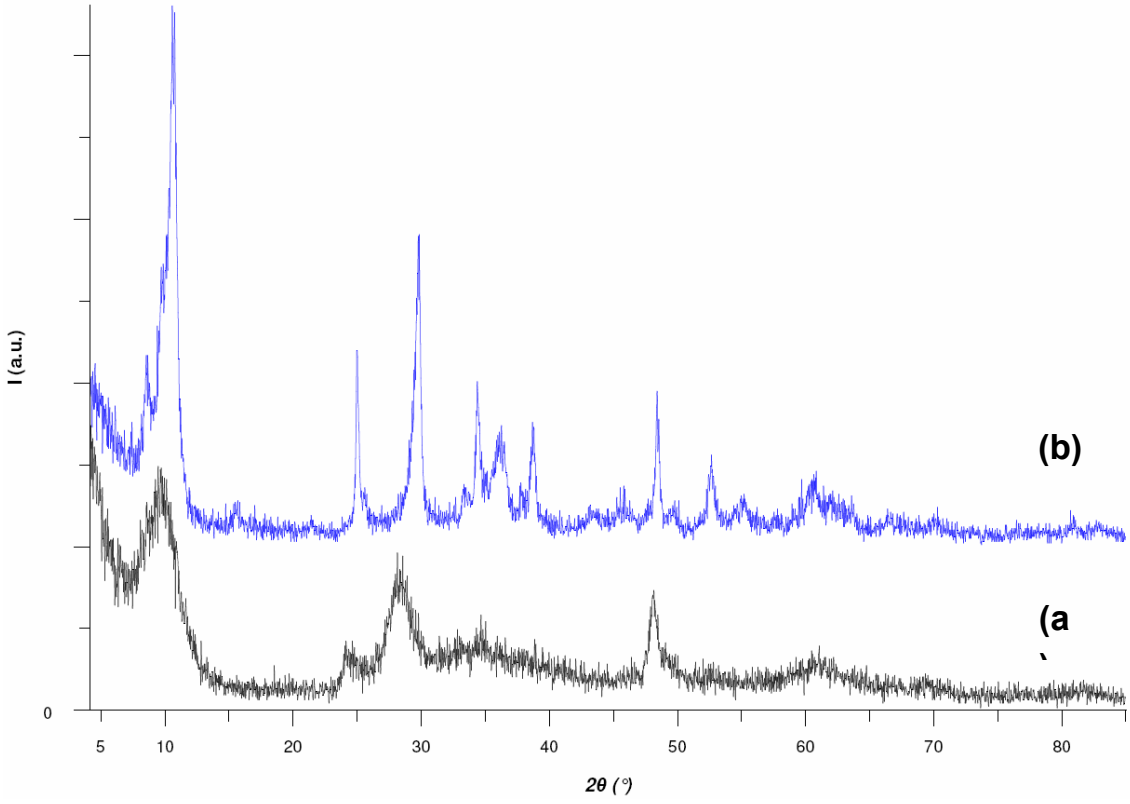

Figure 2.35. XRD diagrams of (a) am10M120 (autoclave) and (b) am10MR (reflux).

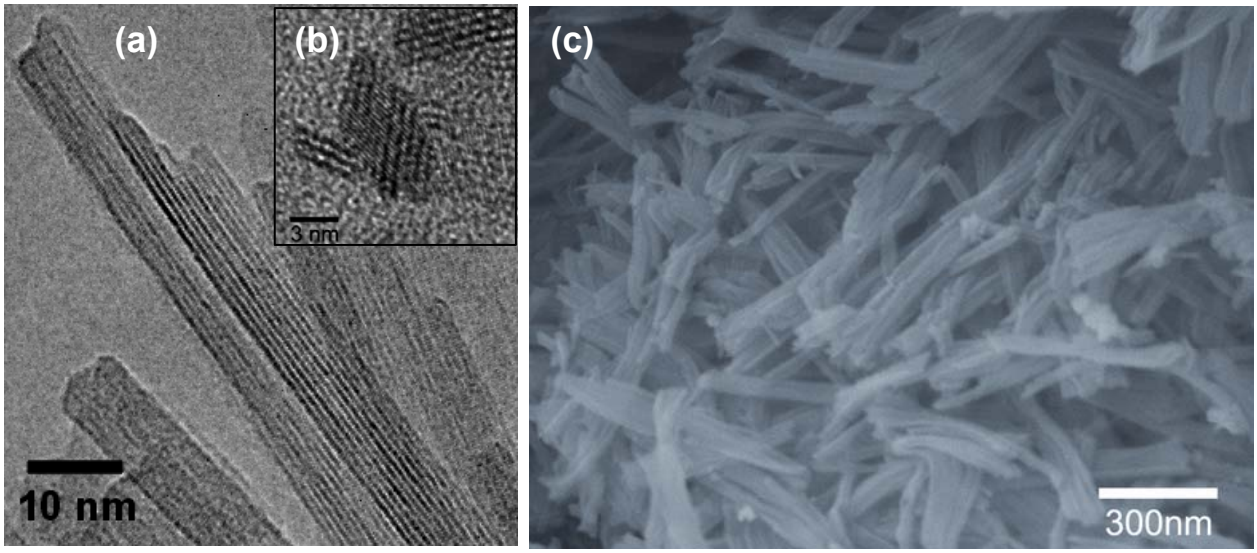

Figure 2.36. (a) the TEM image, (b) cross-section image and (c) the SEM image of titanate nanofibers. (am10MR)

The nanosheet from RDH15MR is another curious case of carbonate effect, which can form lamellar product. We knew all precursor are dissolved to amorphous autoclaved in 15M $NaOH_{(aq)}$ such strong basic condition, even RDH15M120 is also amorphous. For confirming our assumption of carbonate effect, we specially weighed sodium carbonate in RDH15M120. We discovered that RDH15M120-2CO3 is not amorphous again; it looks like sheet assembled by deconstructed nanotube (semi-nanotube) or hybrid with them. This observation is a powerful evidence of the morphologic influence of absorbed carbonate. If we can further adjust the carbonate additive amount even use dry ice to replace sodium carbonate, we could fabricate similar product as the reflux one.

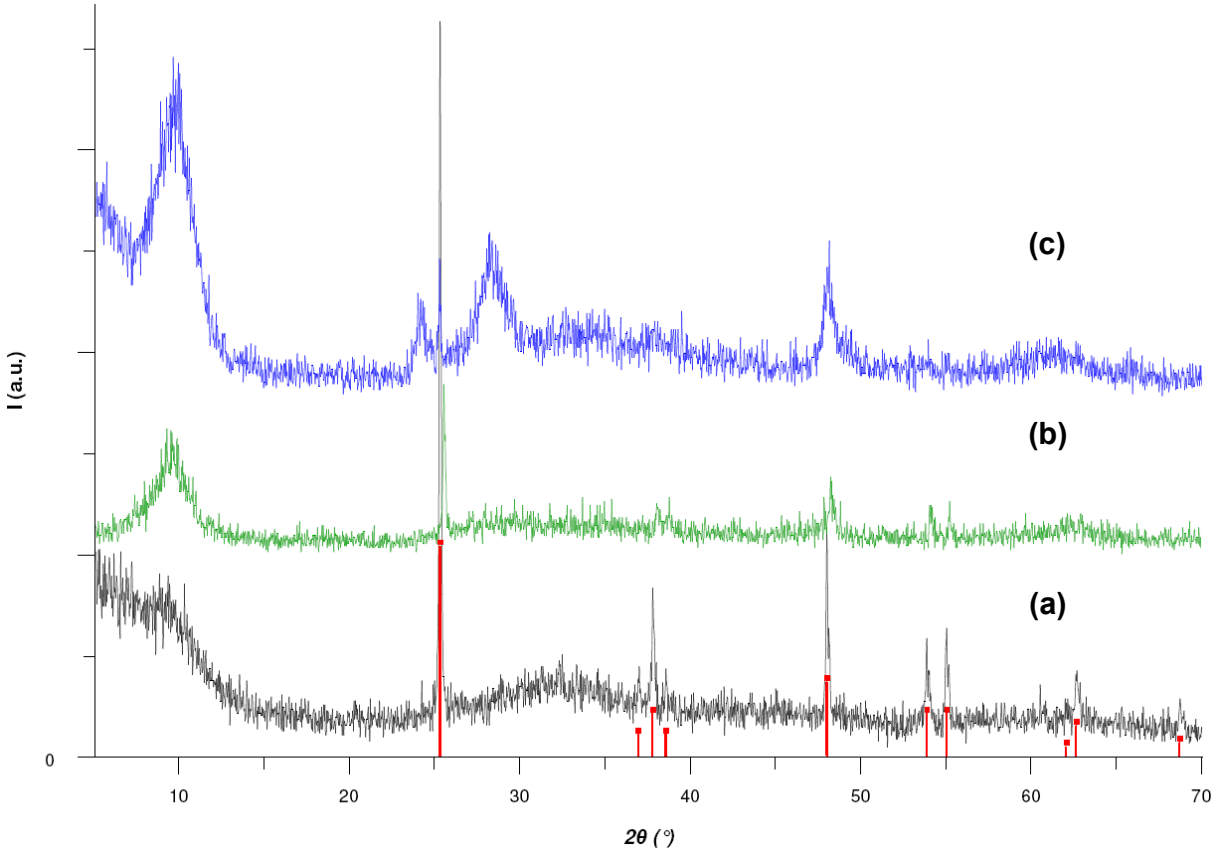

Figure 2.37. XRD diagrams of (a) RDH15M120, (b)RDH15MR and (c) RDH15M120-2CO3 (2.64g Na_2CO_3 added). (■: anatase TiO_2 peaks, JCPDS 21-1272)

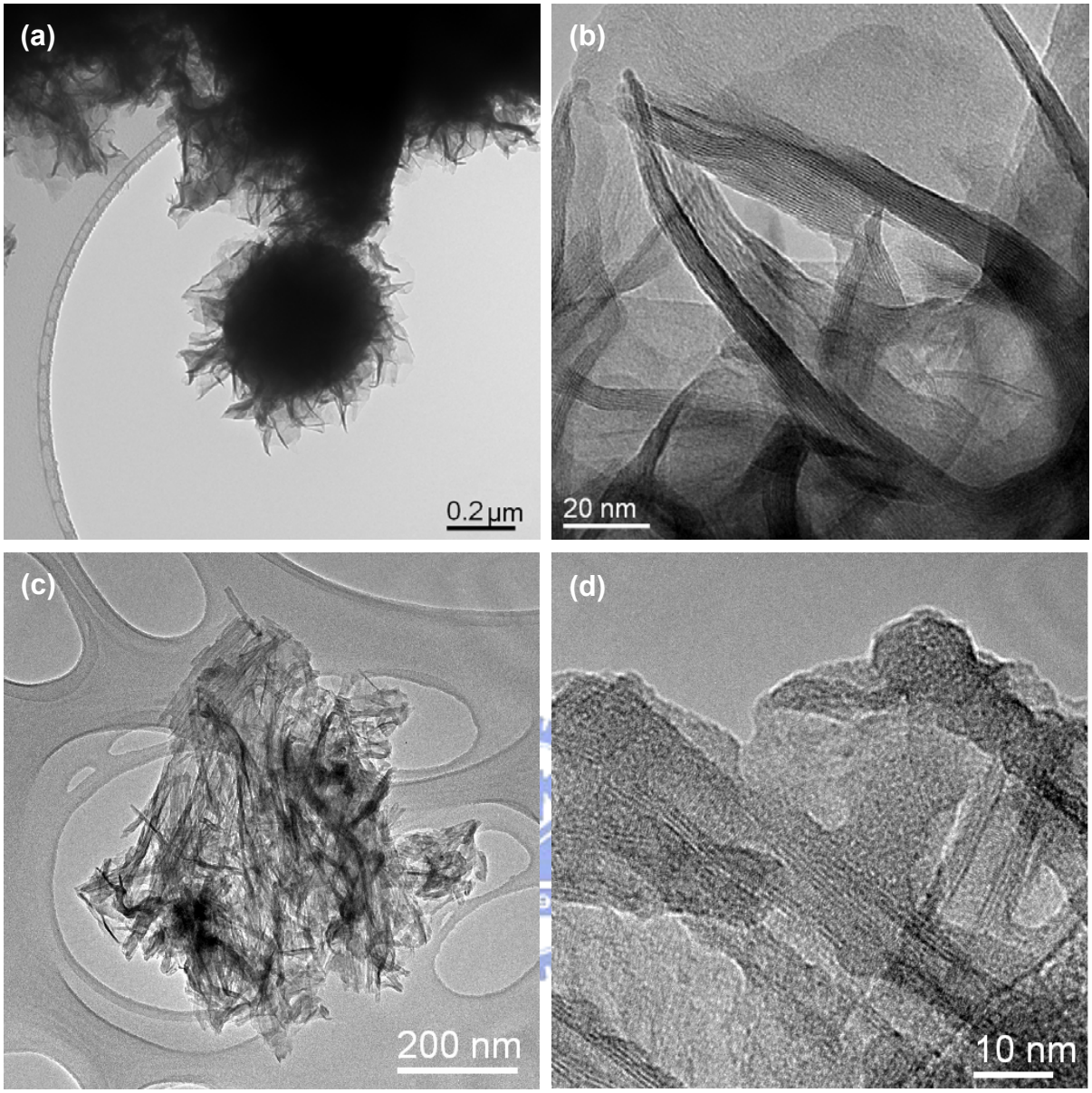

Figure 2.38. TEM images of (a), (b) RDH15MR and (c), (d) RDH15M120-2CO3.

For further comprehension of carbonate and sodium effect in our process, we employed different carbonate source such as $NaHCO_3$ on 5nm5M120. As results mentioned above, we discovered both sodium chloride and sodium carbonate additives can affect the product structure. However, carbonate can enhance the intensity of (100) peak (≈10°) more effectively in XRD (figure 3.35 and 3.36). To compare 5nm5M120-1.6NaCl and 5nm5M120-0.8CO3 (they have the same amount of sodium ion), the CO_3^{2-} one is more intense. The (100) relative

intensity enhancement implies preferred orientation along the a axis, indicating that the crystal growth takes place along b and c. Along with more additive sodium, the intercalated sodium was more saturated, the (100) peak intensity was little reduced and right-shift. Na_2CO_3 and $NaHCO_3$ cases with the same sodium concentration have the same reduced range, even though $NaHCO_3$ has double of CO_3^{2-}. That implies sodium is the main effect at least in reduce process. Unfortunately, we can not distinguish the function of sodium and carbonate separately in this experiment. We can only confirm the sodium carbonate effect on morphologic control better than sodium chloride. The dry ice may be better as a carbonate source without sodium for this case.

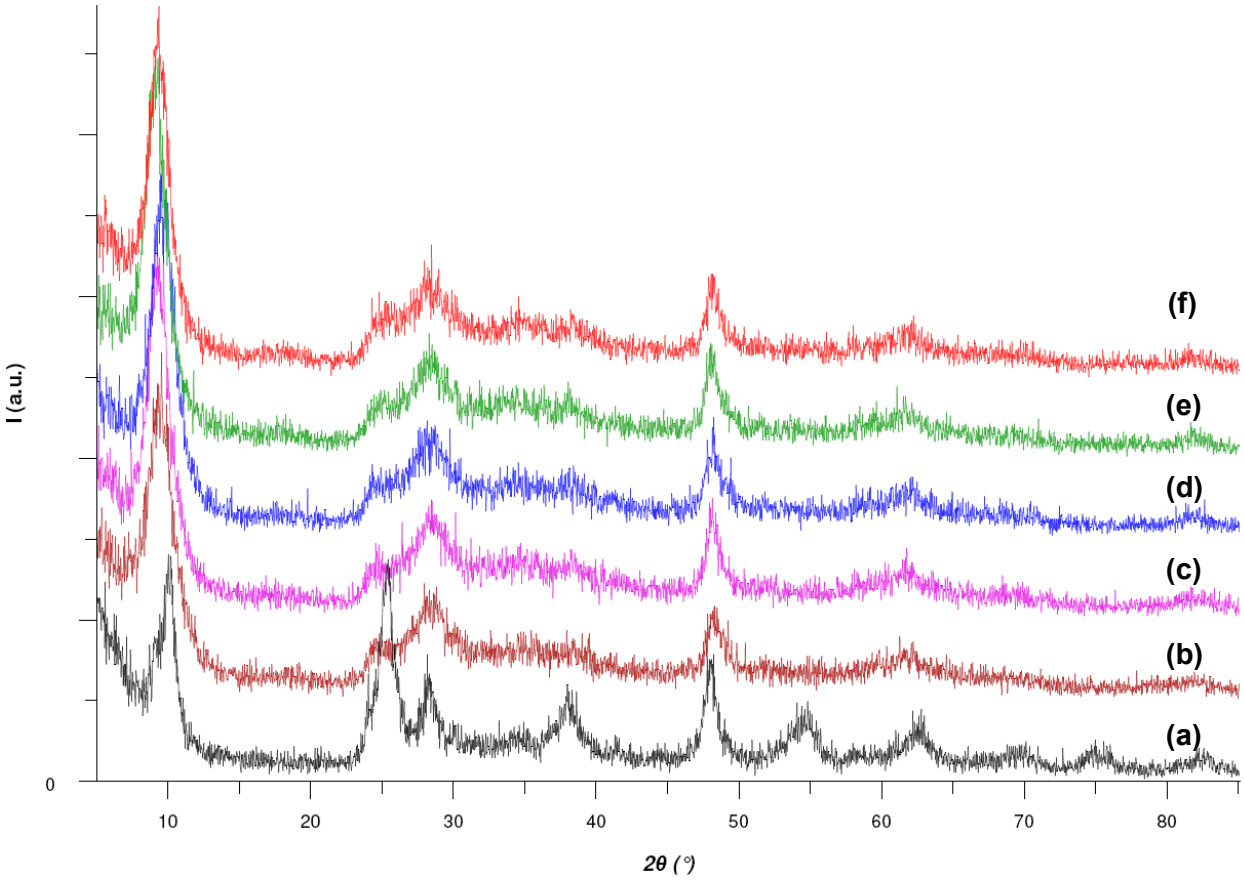

Figure 2.39. XRD diagrams of (a) 5nm5M120, (b) 5nm5M120-1.6NaCl, (c) 5nm5M120-0.5CO3, (d) 5nm5M120-0.8CO3, (e) 5nm5M120-0.4HCO3 and (f) 5nm5M120-0.8HCO3. (CO3: Na_2CO_3; HCO3: $NaHCO_3$)

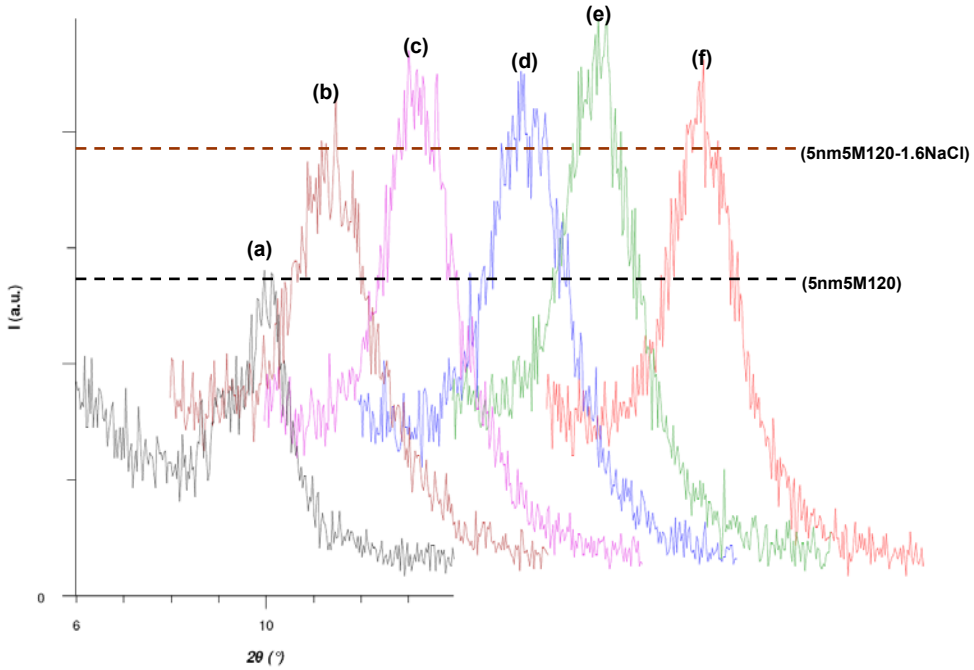

Figure 2.40. XRD diagrams of peak (100) (2θ=10˚) of (a) 5nm5M120, (b) 5nm5M120-1.6NaCl, (c) 5nm5M120-0.5CO3, (d) 5nm5M120-0.8CO3, (e) 5nm5M120-0.8HCO3 and (f) 5nm5M120-1.6HCO3. (CO3: Na_2CO_3; HCO3: $NaHCO_3$)

However, the added sodium carbonate is an easy artifice to adjust product morphologies. In am10M180 case, we can obviously observe the nanoribbon became longer than originally (without sodium carbonate added) (figure 2.42), and the enhancement of length (b-direction preferred) makes peaks of (100) and relative planes more intense in the XRD pattern (blue arrow marked positions).

By RDH15M samples, we have known the carbonate can affect the product phase. Although we have not understood how it works and what the difference with sodium effect, this influence indeed provides a convenient method to control product form. The further study about carbonate and sodium effect is still under progress.

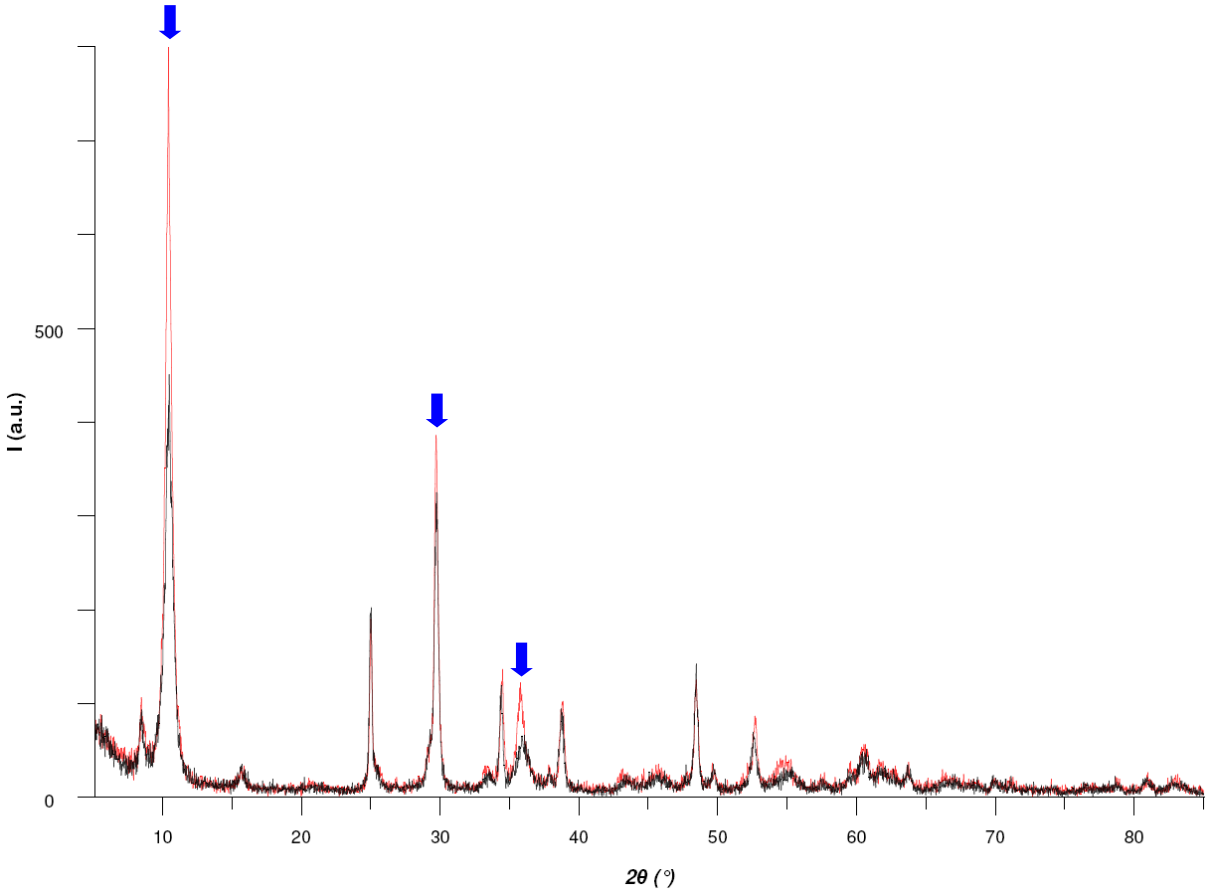

Figure 2.41. XRD diagrams of am10M180 (black) and am10M180-0.8CO3 (red).

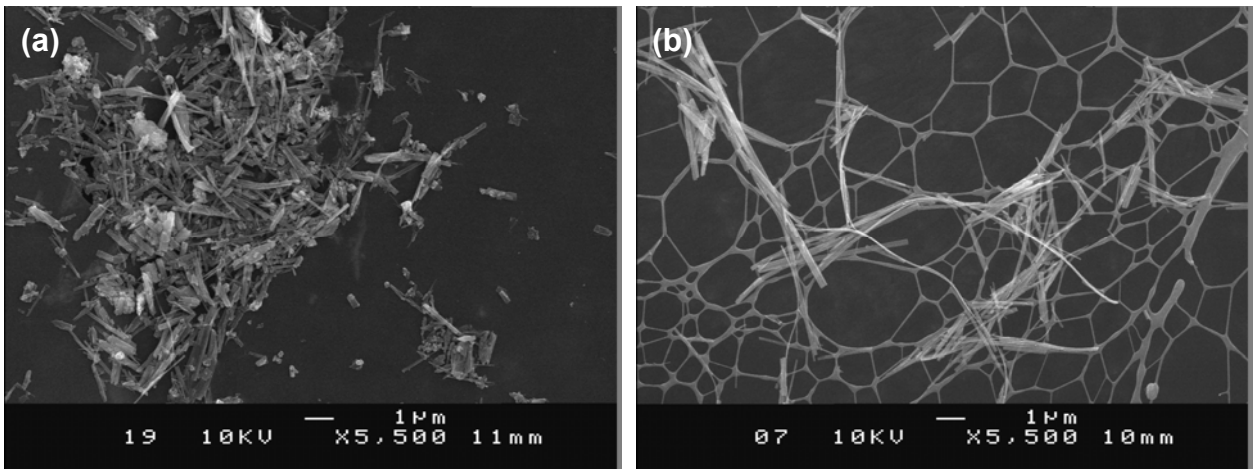

Figure 2.42. SEM images of (a) am10M180 and (b) am10M180-0.8CO3 (supported on grid with carbon film).

2.4.6. Morphologic study of nanostructurated TiO_2

The intercalated sodium and hydroxo group limit the applications of these titanate nanostructures, especially as electrode materials. Transformation to nanostructurated TiO_2 is a possible route to apply these products. That implies we regard titanate as a nanostructurated intermediate. We transform these intermediates to titania nanostructures through proton exchanging and heating up for dehydration.

In following represented XRD and TEM results, we can observe the titania product is able to keep the titanate shape and preferred orientation after exchanging and annealing. In nanosheet case (figure 2.43 and 2.44), it became lower crystallized because of loss of the coherent stacking of the layers after exchanging. After calcinations at 400˚ C during 4hours, it completely transforms to anatase nanosheet with more intense (101) peak. The titania nanosheets shrink and make many vacancy during condensation process. That is why the specific surface of titania nanosheet is bigger than original titanate nanosheet.

Nanotube has similar behavior, it transforms to anatase and TiO_2(B) biphase nanofiber (8nm as diameter and length as 50nm-100nm) and we can not observe more intense peak in XRD. We inferred that is due to the curvature of nanotube. The strain and distortion of titanate monolayer makes it forming many defaults during exchange and calcinations. These defaults let it less photoactive even though it has very big specific surface (see Chapter 5).

Nanoribbons transform to anatase through TiO_2(B) phase. At 400˚ C, it exists as TiO_2(B) nanoribbon (similar diameter as raw nanoribbon). This property is the same with bulk layered alkali titanate. And it transforms completely to anatase until 800˚ C due to a little of carbonate intercalated in its structure. We can monitor this course by TGA-MS (Section 2.6.).

Submicro-sticks is totally different from other samples, which tranforms directly to rutile phase sticks after exchanging and annealing to 400˚ C (figure 2.49). This stick assembles by linking rutile particles (figure 2.50). The low temperature formation of rutile implies that it is possibly rutile derive structure.

The titanate nanostructures are able to transform to titania and retain their original shapes after proton exchanging and 400˚ C annealing. This observation provides a good route to do the nanostructuration from bulk TiO_2 to nano TiO_2. Moreover, these titania nanostructures have preferrential orientation in order to potentially improve the property.

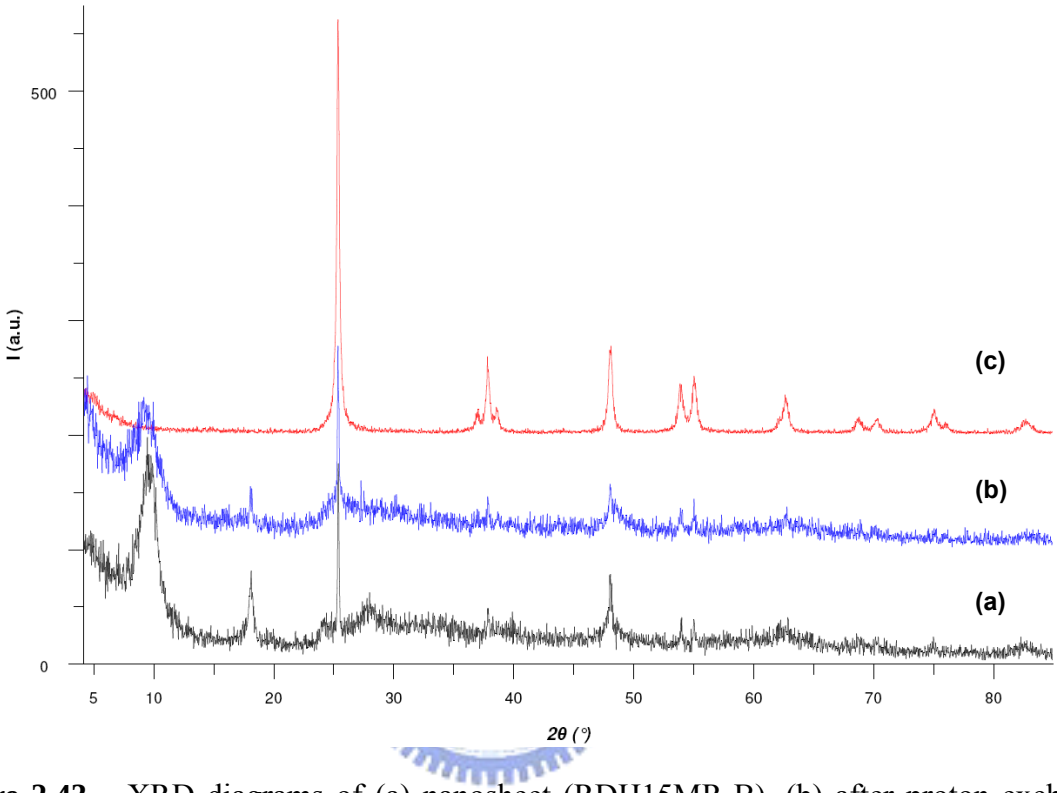

Figure 2.43. XRD diagrams of (a) nanosheet (RDH15MR-B), (b) after proton exchanged one and then (c) annealed at 400˚ C.

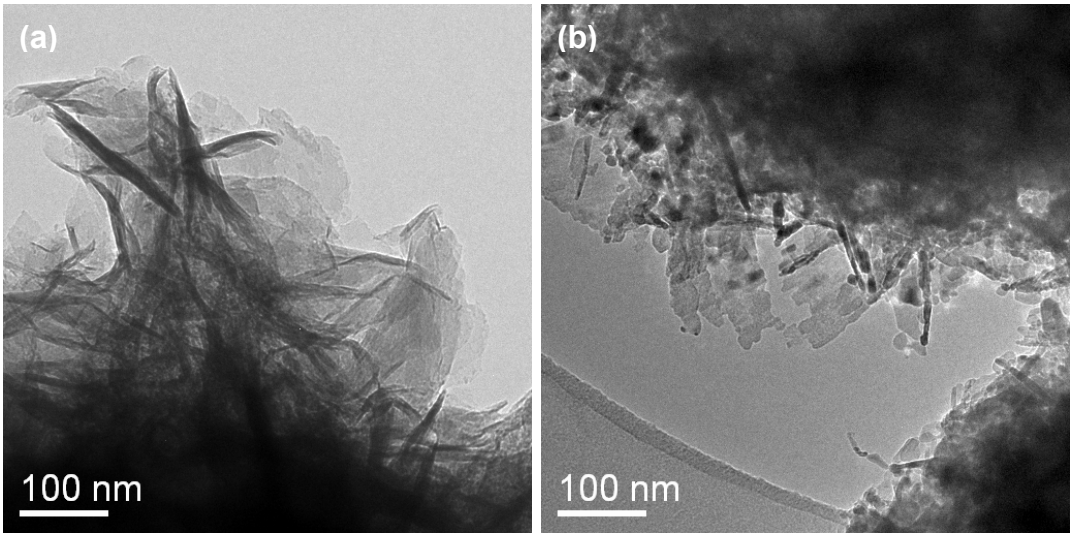

Figure 2.44. TEM images of (a) nanosheet after proton exchanging and then (c) annealed at 400˚ C.

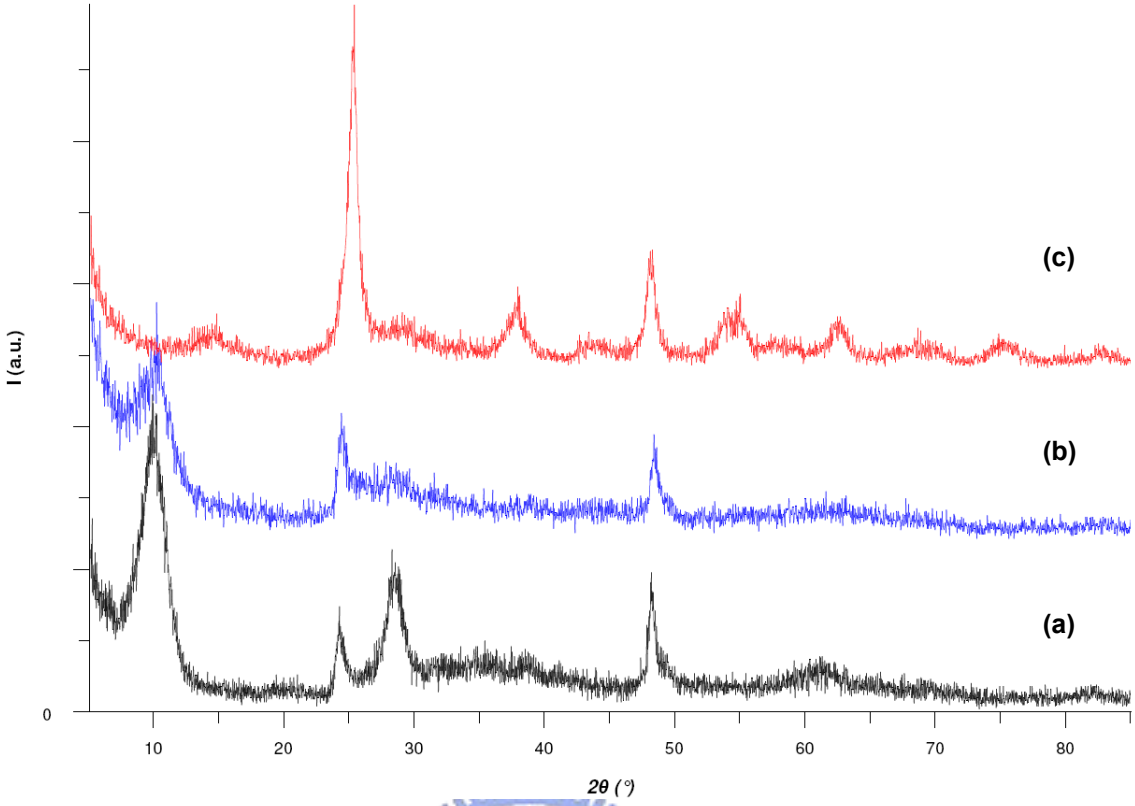

Figure 2.45. XRD diagrams of (a) nanotube (RDH10M140), (b) after proton exchanged one and then (c) annealed at 400˚ C.

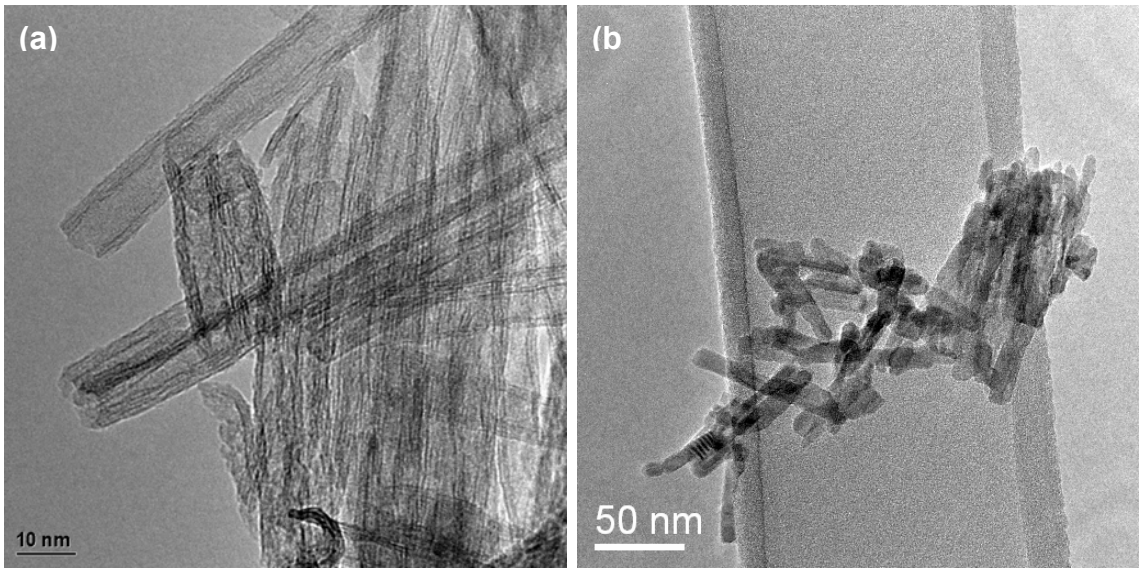

Figure 2.46. TEM images of (a) nanotubes after proton exchanging and then (c) annealed at 400˚ C.

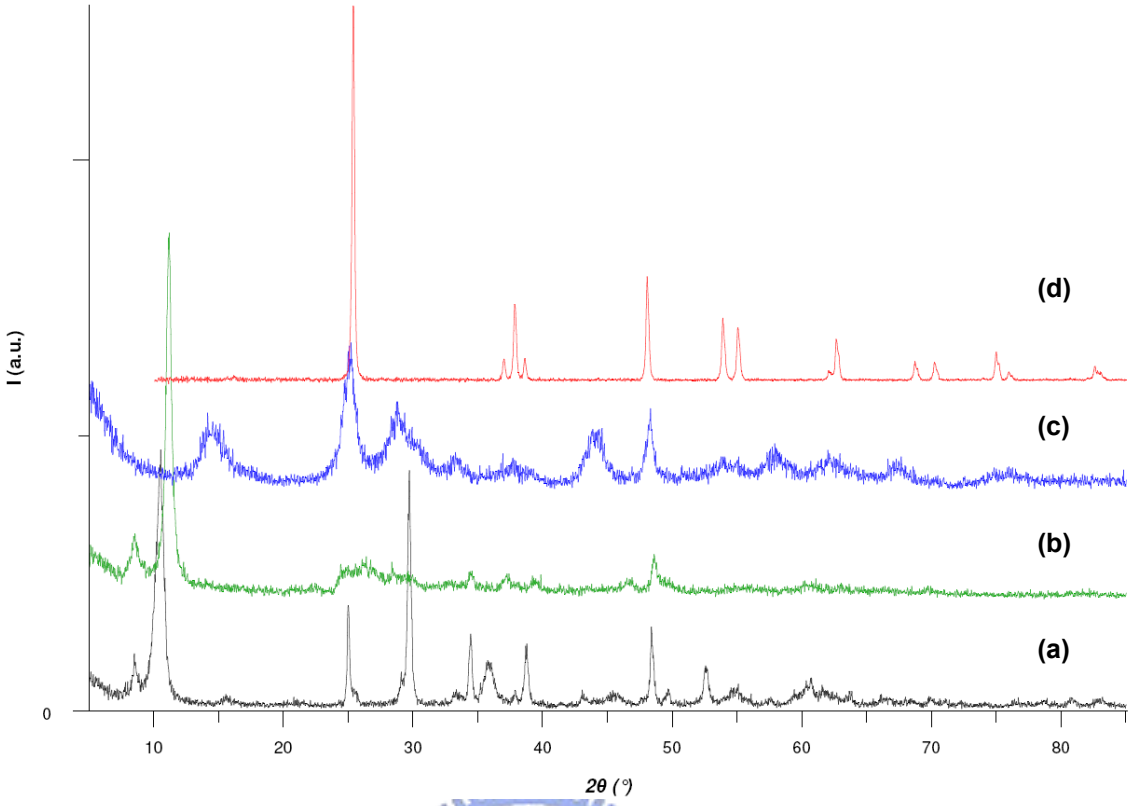

Figure 2.47. XRD diagrams of (a) nanoribbon (RDH10M180), (b) after proton exchanged one and then (c) annealed at 400° C, (d) at 800° C.

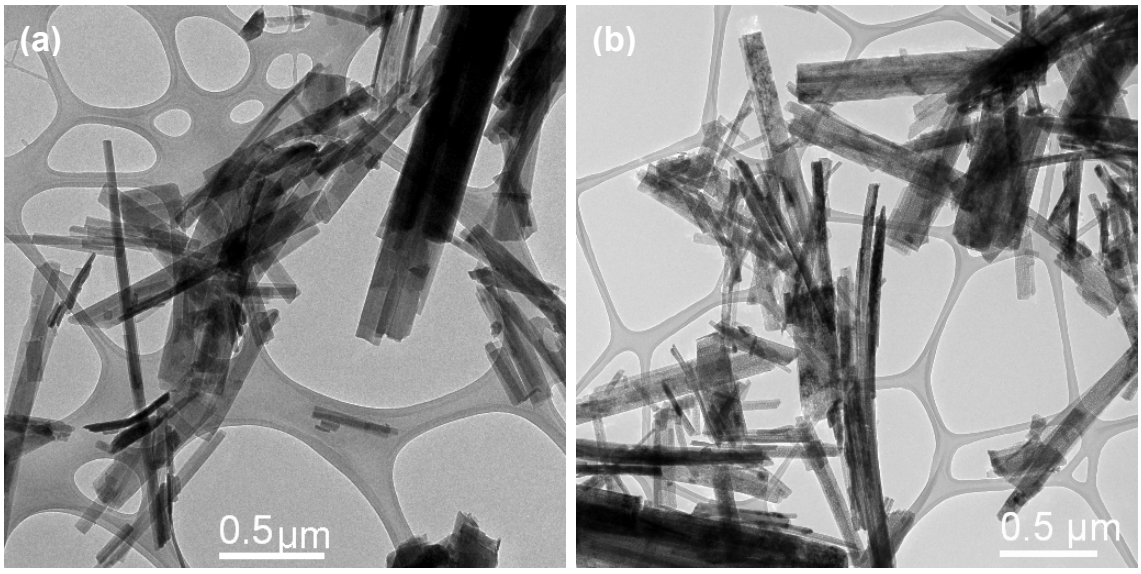

Figure 2.48. TEM images of (a) nanoribbons after proton exchanging and then (c) annealed at 400° C.

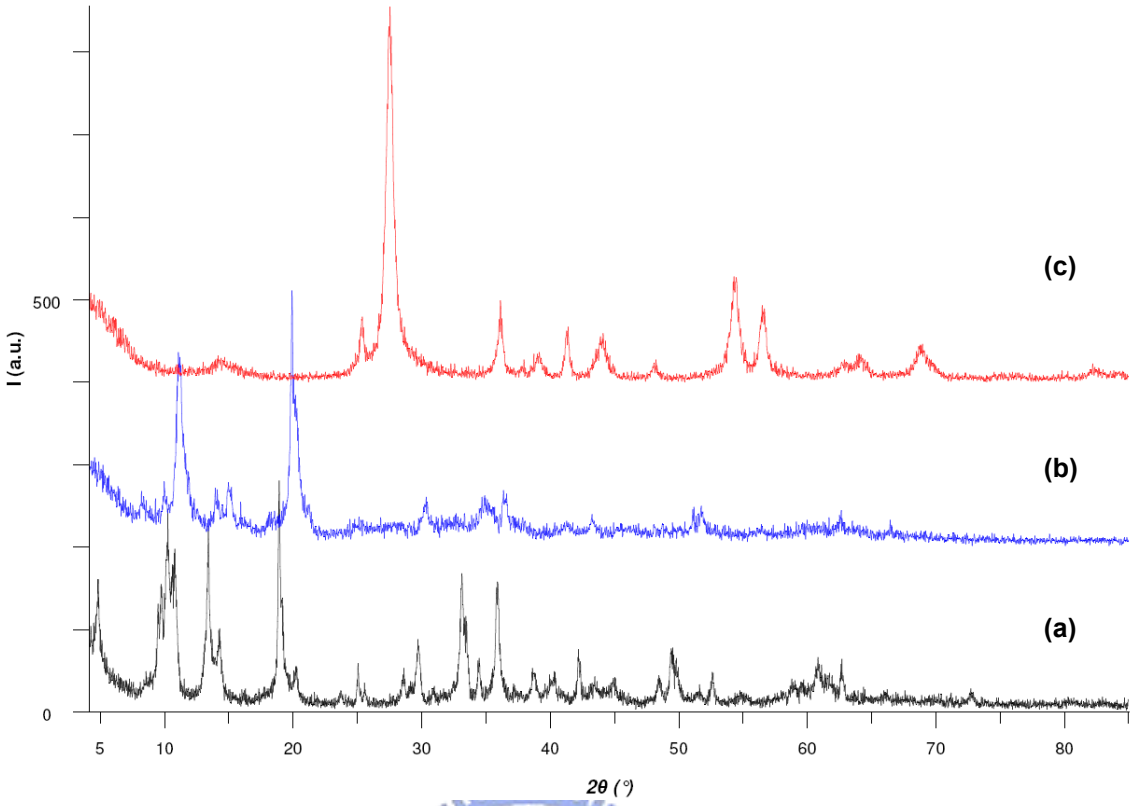

Figure 2.49. XRD diagrams of (a) submicro-sticks (am10M220), (b) after proton exchanged one and then (c) annealed at 400° C.

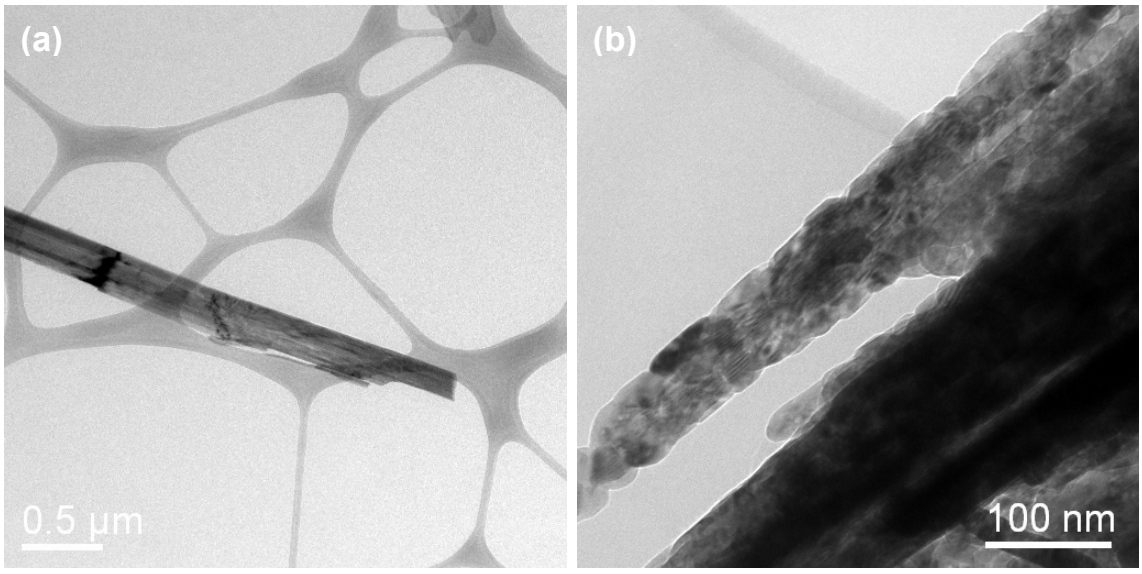

Figure 2.50. TEM images of (a) submicro-sticks after proton exchanging and then (b) annealed at 400° C.

2.4.7. Size control synthesis of potassium titanate nanofibers (KOH-TiO_2) by temperature effect

Potassium titanate with tunnel structure and fibrous shape such as $K_2Ti_6O_{13}$ is a well-known material used as reinforcement in plastics and metals.[11,12] These potassium titanates were usually synthesized by conventional solid-state and flux method. Titania powder and potassium carbonate or potassium peroxide were used as raw materials in these methods. The product morphology and size are difficult to control. Recently, the solvothermal synthesis (chimie-douce) from titanium metal or titania in KOH solution at low temperature (150˚ C-250˚ C) was employed to produce new phase[13] (figure 2.51) or nanostructure of potassium titanate (figure 2.52).[14-17] Size control is a very important way to adjust the properties of reinforcing materials. The nano-sized products are even regarded as possible candidates to develop new applications. Actually, the hydrothermally synthesized $K_2Ti_8O_{17}$ nanoribbons were discovered available to be anode material of lithium ion battery.[16] The results of intercalation tests reveal that the smaller crystallite product have better efficiency than the bigger one (figure 2.52).

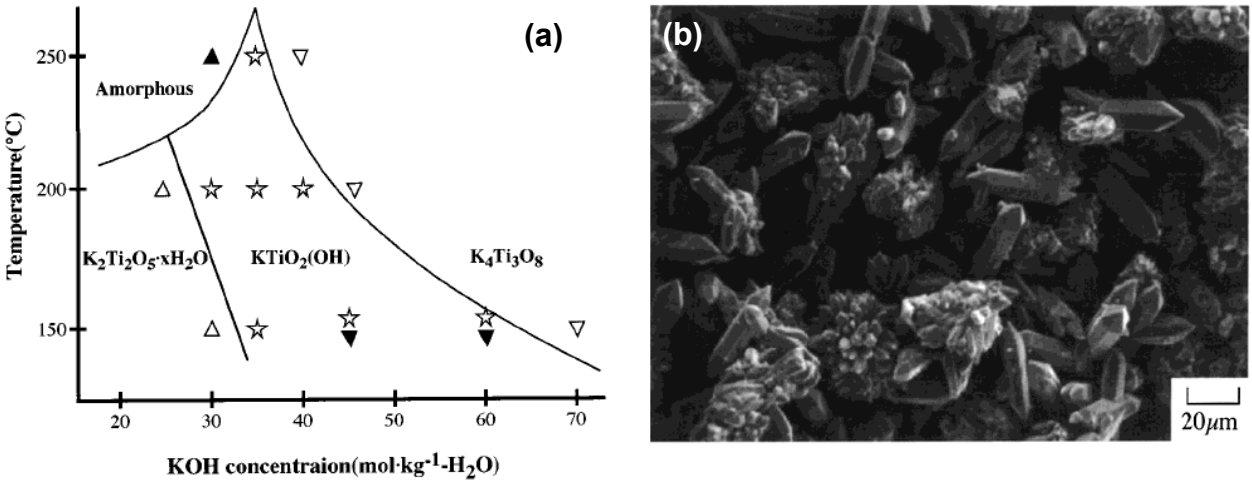

Figure 2.51. (a) Diagram of the formation of $KTiO_2(OH)$ in the Ti-KOH-H2O system; (b) SEM photograph of $KTiO_2(OH)$. [13]

Hydrothermal synthesis is a promising morphology controllable method involving many tunable parameters of operation, such as nature of precursor, temperature, concentration of solution, pH, time and additives.[18] In this part, solutions of $TiOCl_2$ as titanium source were reacted with KOH at different temperatures to enhance a possible size control on potassium titanate nanofibers.

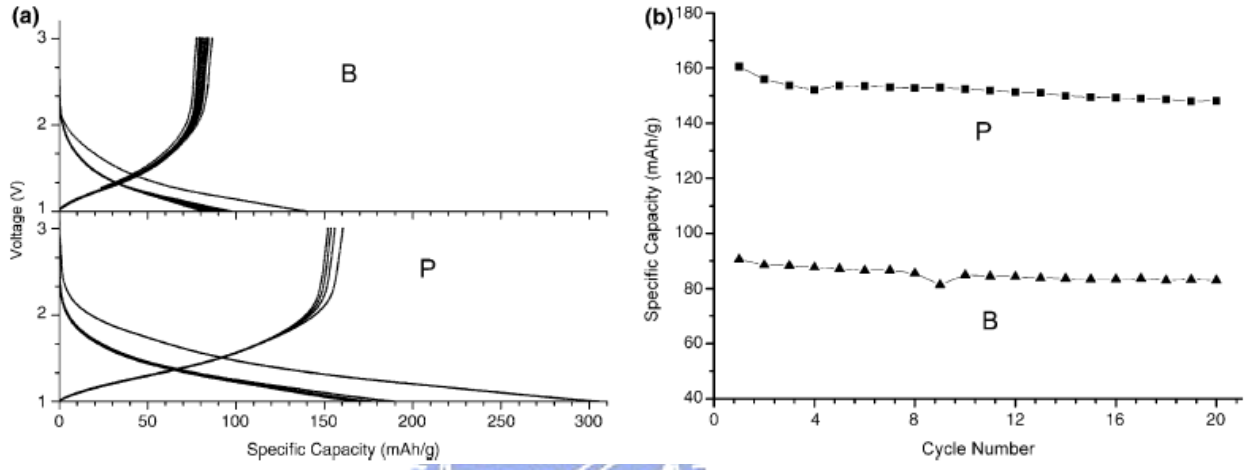

Figure 2.52. (a) The charge–discharge curves of the block products (made from Ti plate) (labeled by B) and the powder products (made from Ti powder) (labeled by P) showing good electrochemical performance of the products as anode materials for lithium ion battery. (b) The cycle performance of the products showing excellent reversible capacities of the block products (labeled by B) and the powder products (labeled by P).[16]

In this study, 2 ml of $TiOCl_2$ solution was put into a sealed 50 ml Teflon tubular container with weighted KOH pellets (purchased from Merck Company, 97% purity) and then kept at different temperatures (110˚ C, 120˚ C, 150˚ C, 180˚ C or 220˚ C) during 24 hours in the autoclave. The products were later rinsed with de-ion water and collected by centrifuge repeatedly until pH<12, after then the powders were dried in an oven at 70˚ C in air. The products were characterized by XRD, SEM, TEM, TGA, FT-IR and Raman. The conditions were described as experimental section above.

A. Temperature effect

We used $TiOCl_2$ solution (in 2M HCl aqueous solution) as precursor react with stoichiometric KOH pure pellets, the reaction can be expressed as following:

$$TiOCl_2 \cdot 1.4HCl \cdot 7H_2O + (3.4+x)\ KOH \rightarrow (KOH\cdot)_x \cdot TiO_2\ ,\ 9.4H_2O + 3.4KCl$$

We discovered that the products completely transform to potassium titanate when x>1. When x<1, some rutile or brookite are detected in the X-ray diffraction pattern(figure 2.3). Therefore, in the following, x was fixed to 1 in order to study the temperature effect on the sample morphology.

By XRD, we can observe that potassium titanate are more and more crystallized along with increasing autoclave temperature. Comparison with the JCPPDF files cannot lead to a unique conclusion, since $K_2Ti_6O_{13}$ and $K_2Ti_8O_{17}$ present very similar X-ray diffraction patterns. In addition, the samples exhibit broad peaks which increase the imprecision of the phase identification. In TEM, we discovered that the nanoribbons became longer and thicker in higher temperature condition. At 110° C, the nanoribbon is 3nm thick and 10nm long; at 220° C, the nanoribbon assembled as bundle of 20nm thick and 250nm-1000nm long. These observations imply that the size can indeed be controlled by the temperature. We are able to use this property to adjust the size of potassium titanate nanoribbon, which is regarded as a simple artifice to adjust its reinforcement and lithium intercalation property, according to the literature.[16]

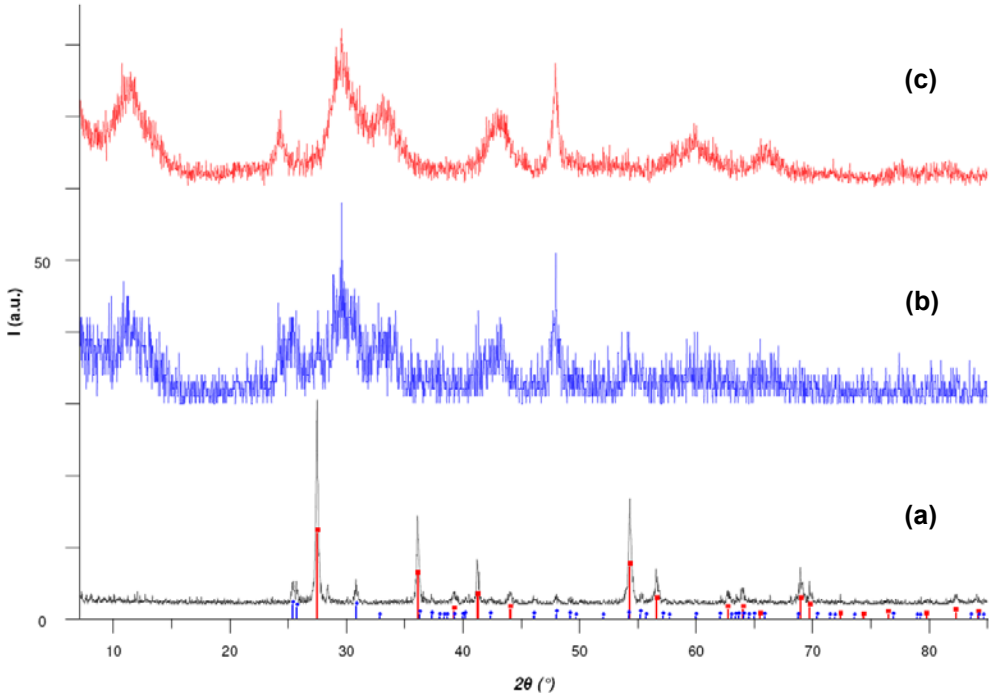

Figure 2.53. XRD diagrams of product by the reaction $TiOCl_2 \cdot 1.4HCl \cdot 7H_2O$ + (3.4+x) KOH at 180˚ C 24 hours: (a) x = 0, (b) x = 0.5 and (c) x = 1. (red bars : rutile, blue bars: anatase)

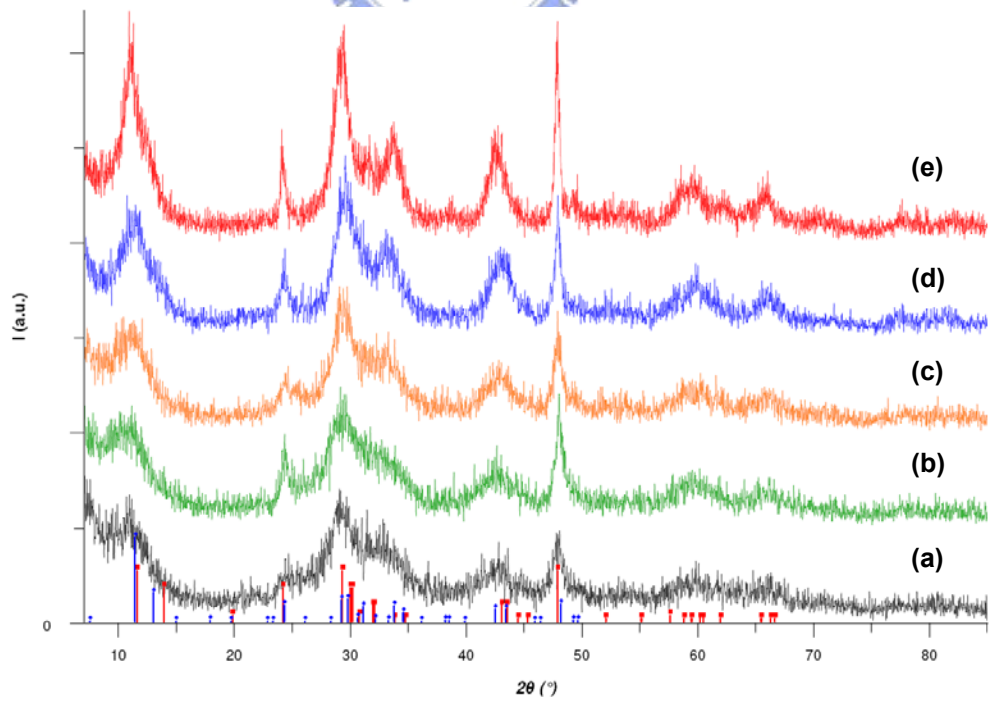

Figure 2.54. XRD diagrams of product by the reaction $TiOCl_2 \cdot 1.4HCl \cdot 7H_2O$ + 4.4 KOH at (a) 110˚ C, (b) 120˚ C, (c) 150˚ C, (d) 180˚ C and (e) 220˚ C 24hours. (■: $K_2Ti_6O_{13}$; ♦: $K_2Ti_8O_{17}$)

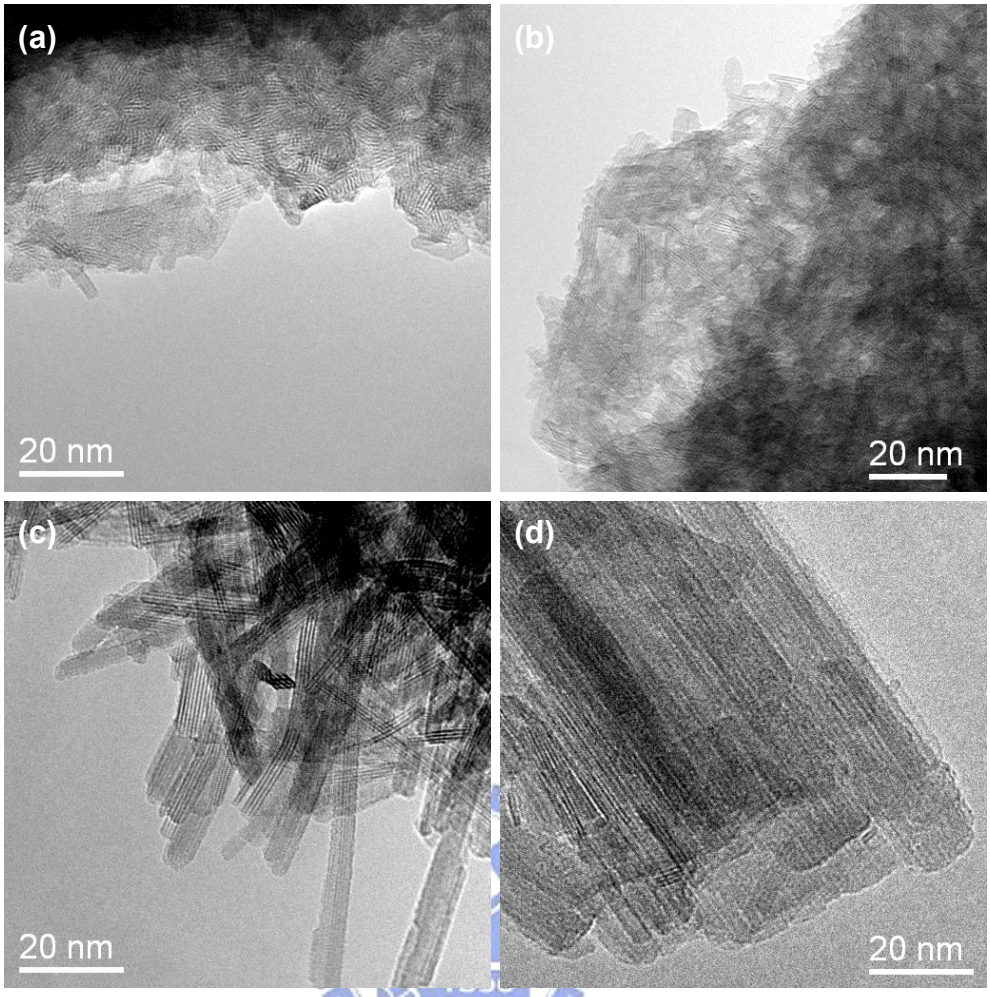

Figure 2.55. TEM images of potassium titanate nanoribbons obtained at (a) 110˚ C, (b) 150˚ C, (c) 180˚ C and (d) 220˚ C.

B. Composition and Structural study

The study of chemical composition of potassium titanate nanoribbon was performed by EDX, FT-IR and TGA. By EDX, we found that the K/Ti ratio in the nanoribbons is about 0.4 after washing by de-ion water until pH<12. Among the titanates, $K_2Ti_5O_{11}$ has a K/Ti ratio close to this value. In the FT-IR-ATR spectra, we observed obvious characteristic peaks of

water at X cm-1 and some carbonate at X cm-1. The latter was absorbed from air (figure2.6). We further studied the containing amount of water by TGA. We observed that the powder smoothly loses 8.5% (weight) from 50˚ C to 400˚ C (5K/min in air). This weight loss accounts for 2.5 H_2O molecules, assuming the final product is indeed $K_2Ti_5O_{11}$. To sum up with theses results, the chemical composition of the nanoribbons could be written as "$K_2{\cdot}(TiO_2)_5(OH)_2$,1.5$H_2O$". However, the X-ray diffraction pattern cannot be interpreted with a $K_2Ti_5O_{11}$ structure.

Moreover, this composition is not in agreement with the one reported in the literature in the past. B. L. Wang et al. reported that it is $K_2Ti_8O_{17}$ and X. Meng et al. were of the opinion that it is $K_2Ti_6O_{13}$. In our opinion, the nanoribbon's structure is closer to a Ti_8O_{17} framework according to XRD results (figure 2.54 and 2.57). In addition the potassium quantity is closer to the one of $K_3Ti_8O_{17}$, K/Ti=0.375. However, $K_3Ti_8O_{17}$ is black due to the insertion of one more potassium atom than in $K_2Ti_8O_{17}$. We inferred that the extra potassium intercalated as KOH,·xH_2O group and thus the solid still remains white. Taking into account all the information, the solid can be written as $K_{3.2}Ti_8O_{17}(OH)_{0.6}$, 3.4$H_2O$.

The experiment of proton exchange reconfirms that the nanoribbons exhibit a tunnel titanate structure. The intercalated potassium ion can not be totally exchanged by acid solution in ambient condition, and the nanoribbon always seems to retain its original structure after acidification process (figure 2.57). However, the (020) peak in the XRD patterns is right shifted from $K_3Ti_8O_{17}$ (b=3.809Å) to $K_2Ti_8O_{17}$ (b=3.775Å). The Raman spectrum also reveals that the nanoribbon is very different from $K_2Ti_6O_{13}$ (figure 2.58).In addition, the EDX result leads to the following K/Ti=0.27. Our conclusion may be that the extra intercalated KOH can be exchanged after immersion in acid and the structure is thus closer to the one of $K_2Ti_8O_{17}$, after partial H^+ exchange.

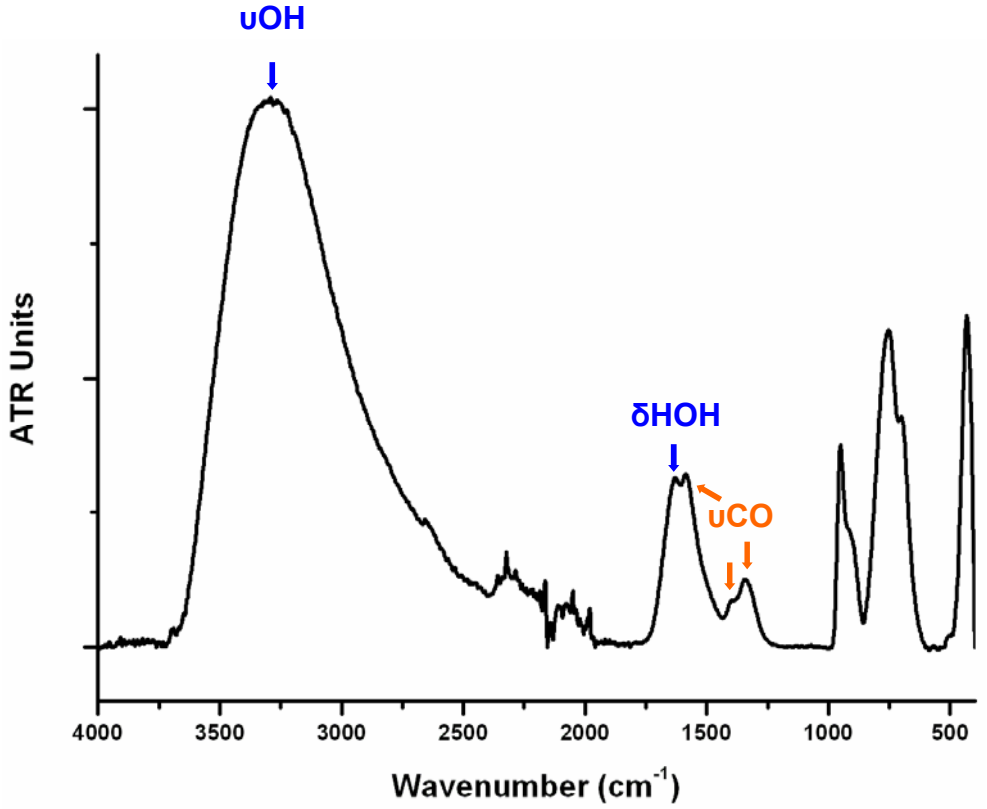

Figure 2.56. FT-IR-ATR spectrum of potassium titanate nanoribbon obtained at 220˚ C.

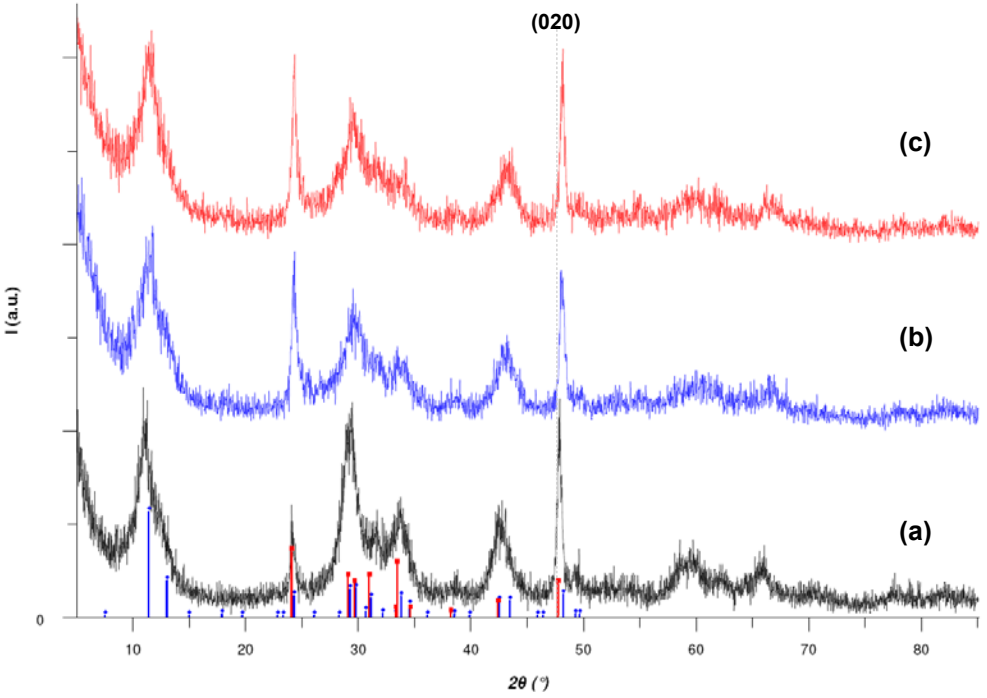

Figure 2.57. XRD diagrams of (a) potassium titanate nanoribbon, (b) after 0.1M HNO_3 washing and then (c) annealed to 400˚ C. (■: $K_3Ti_8O_{17}$; ♦: $K_2Ti_8O_{17}$)

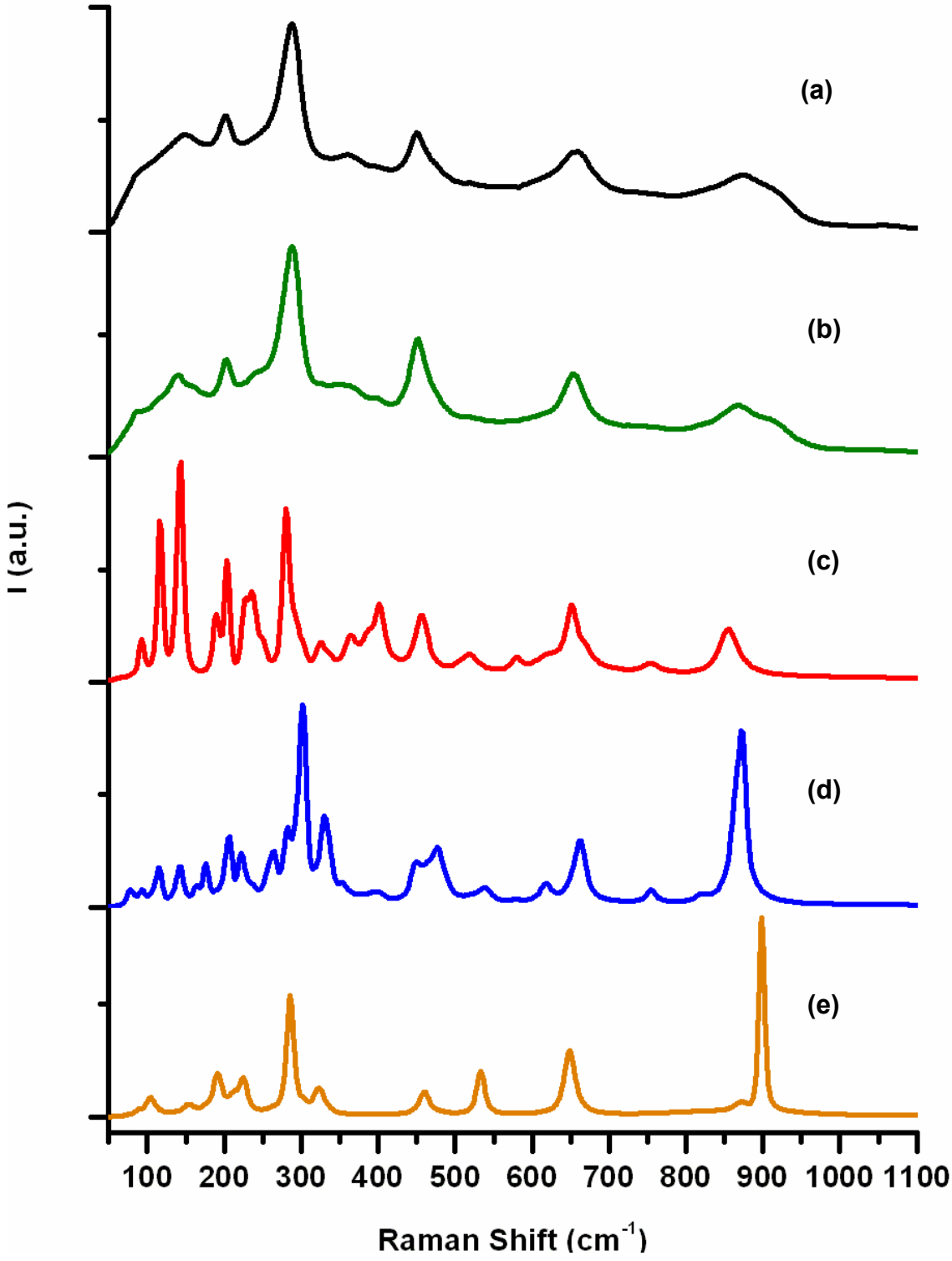

Figure 2.58. FT-Raman spectra of potassium titanate nanoribbon obtained at (a) 110˚ C and (b) 220˚ C; (c) $K_2Ti_6O_{13}$; (d) $K_2Ti_4O_9$; (e) $K_2Ti_2O_5$.

In this experiment, we discovered the temperature effect of potassium titanate nanoribbon synthesis. We used $TiOCl_2$ as precursor reacting with KOH to obtain various sized nanoribbon in different autoclaved temperature condition. The size of nanoribbon is bigger along with enhanced temperature. The influence of other operation parameters is under studying.

The chemical composition of nanoribbon is $K_{3.2}Ti_8O_{17}(OH)_{0.6}$, $3.4H_2O$ after washing by water. The potassium ion intercalated into the Ti_8O_{17} tunnel structure as KOH form. The composition can transform to $K_2Ti_8O_{17}$ after acid treatment, even though they have similar structure.

2.5. Conclusions

In this chapter, we study the relationships between synthesis conditions and various morphologies of sodium hydroxo titanate products to improve the comprehension of adjustable titanate nanostructures. We changed reaction conditions such as various grain size and structure of precursors, autoclaved temperatures, basic concentrations and varying quantities of additive sodium or carbonate.

We discovered that bigger grain sized precursor can form larger titanate layer when these precursors have the same phase. The anatase initiator preferably leads to lepidocrocite type product, and rutile one forms rutile derives. That implies the intermediate structure and size is designed by the nature of precursor. The temperature and basic concentration also sensitively affect intermediate phase. We can observe more condensed phase in higher temperature. That may be due to higher pressure and smaller intermediate building block. Besides, the more basic environment makes titanate layer more curved and dispersed until monolayer rolls up as tubes. When basic concentration is over saturated, the product is amorphous. The additive sodium or carbonate source allows one to adjust titanate product morphology, which can effectively enhance the growth along b and c direction.

These titanate nanostructures can transform to titania and retain their special shapes after proton exchanging and annealing. This property provides a novel simple route to TiO_2 nanostructuration (from bulk TiO_2 to nano TiO_2).

For size controlled synthesis of potassium titanate nanoribbon, we used $TiOCl_2$ as precursor reacting with KOH, to obtain various sized nanoribbon in different autoclaved temperature condition. The size of nanoribbon is bigger along with enhanced temperature.

We will deeply discussed these structures and possible growth mechanisms in following chapter, then describe their photocatalytic and intercalation properties in Chapter 4.

2.6. Annex

2.6.1. Chemical composition study of various products (EDX and TGA results)

The principal composition of sodium hydroxo titanate is sodium, titania and water (or hydroxyl species). Therefore, we used EDX to characterize the ratio of sodium/titanium and TGA/MS to gauge the amount of hydroxyl species. Their conditions were described in experimental section (Section 2.2). The results were summarized as table following (table A2.1, A2.2 and A2.3). Moreover, the spectra of TGA/MS were exhibited also.

Table A2.1. Na/Ti ratio of various morphologies of titanate by EDX/SEM

	Raw Nanosheet (RDH15MR)	Nanosheet (RDH15MR-B)	Nanotube (RDH10M140)	Nanofiber (am10MR)	Nanoribbon (RDH10M180)	Submicro-stick (rut10M220)
Na/Ti	0.54	0.33	0.38	0.55	0.52	0.57

Table A2.2. TGA-MS reports of various morphologies of titanate

	weight loss %		H_2O (mass 18)		CO_2 (mass 44)		CO (mass 28)	
	<400˚C	>400˚C	T (˚C)	area	T (˚C)	area	T (˚C)	area
Raw Nanosheet (RDH15MR)	11.5%	1.3%	157	6.6	96	9.1		
			201	13.7	134	2.8		
			281	6.5	646	8.4	645	7.1
Nanosheet (RDH15MR-B)	14%	2%	114	3.3	97	0.8		
			183	12.6	160	2.1		
			261	12.3	534	12.4	539	8.3
Nanotube (RDH10M140)	12.2%	0.4%	138	12.6	99	1.9		
			185	7.3			(no data)	
			304	5.3				

Nanofiber (am10MR)	13%	3.6%	207 370	8.9 6.9	112 140 570 659	10.0 5.0 23.6 7.4	112 564	0.9 5.9
Nanoribbon (RDH10M180)	9%	1%	169 241	3.5 11.1	104 612	7.6 4.8	(no data)	
Submicro-stick (rut10M220)	4.6%	0.1%	119 182 278	0.9 0.8 8.6	108 157	1.0 0.7	(no data)	

According to the observation of TGA/MS spectra, there are three types of hydroxyl species leaving as water molecular at 100˚ C, 200˚ C and 300˚ C, respectively. We assign them respectively to surface adsorbed water, surface hydroxyl group and interlayer hydroxyl group. We can observe that smaller (more specific surface) sample has more (stronger) water out at 200˚ C (surface hydroxyl group). This observation can be one of powerful evidence to our assignment of hydroxyl chemical environment. Besides, we observed the carbonate species existing and leaving out as carbon oxide or carbon dioxide in annealing. They occurred at 100˚ C, 200˚ C and 600˚ C-700˚ C, respectively. We assign them to adsorbed carbon dioxide from air, unidentate carbonato group and bidentate carbonato group (see Section 2.6.2, FT-IR study). The vaporize temperature of enlarged nanosheet after boiling in water were down to 600˚ C and carbon monoxide occurred in the same time. We infer that is due to bridging bidentate one or carboxyl species after proton exchanging. We can only observe it in the reflux cases. These carbonate species are only small containing amount (<1% weight loss) and much reduced after acidification in our samples, but critical to morphologic control (see Section 2.4.5).

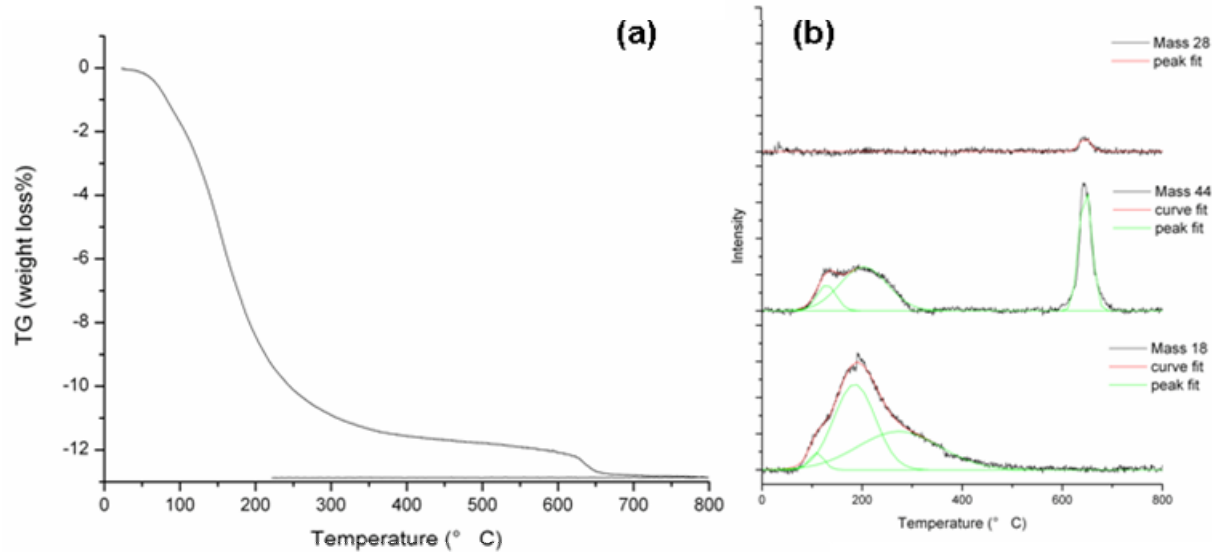

Figure A2.1. (a) TG weight loss % diagram and (b) TG-Mass spectra of raw nanosheets (RDH15MR).

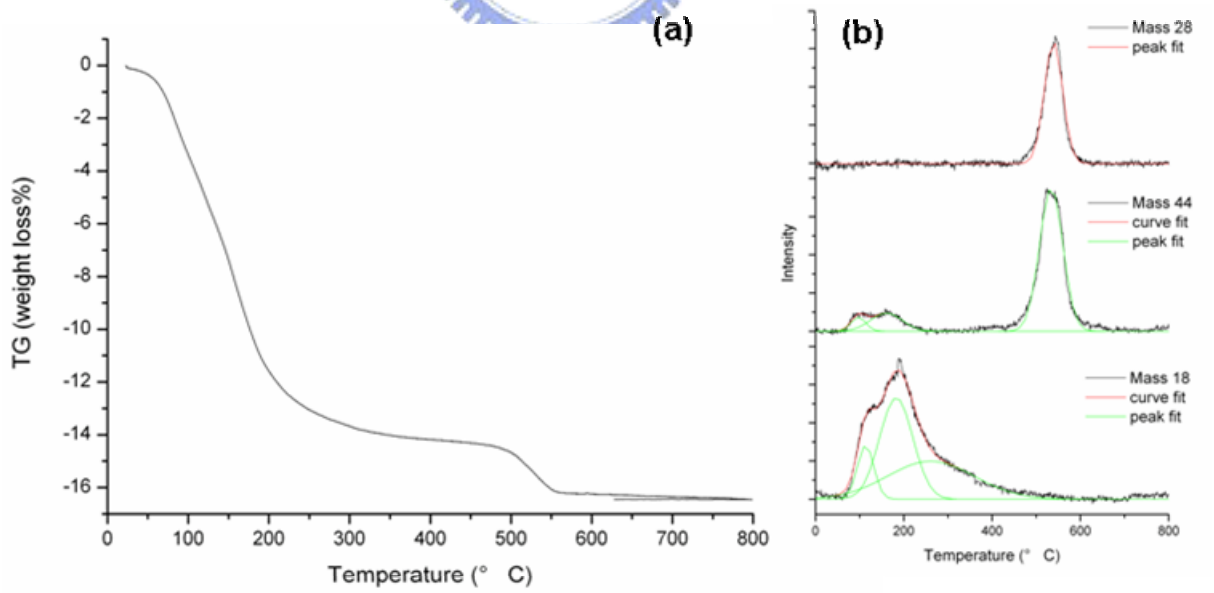

Figure A2.2. (a) TG weight loss % diagram and (b) TG-Mass spectra of nanosheets (RDH15MR-B).

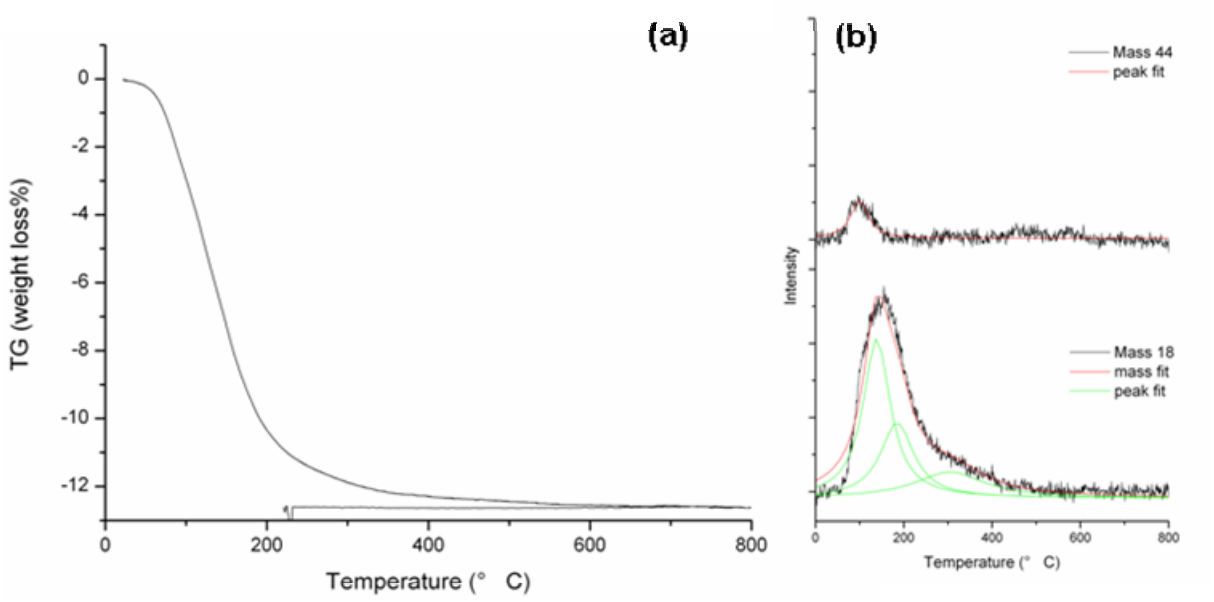

Figure A2.3. (a) TG weight loss % diagram and (b) TG-Mass spectra of nanotubes (RDH10M140).

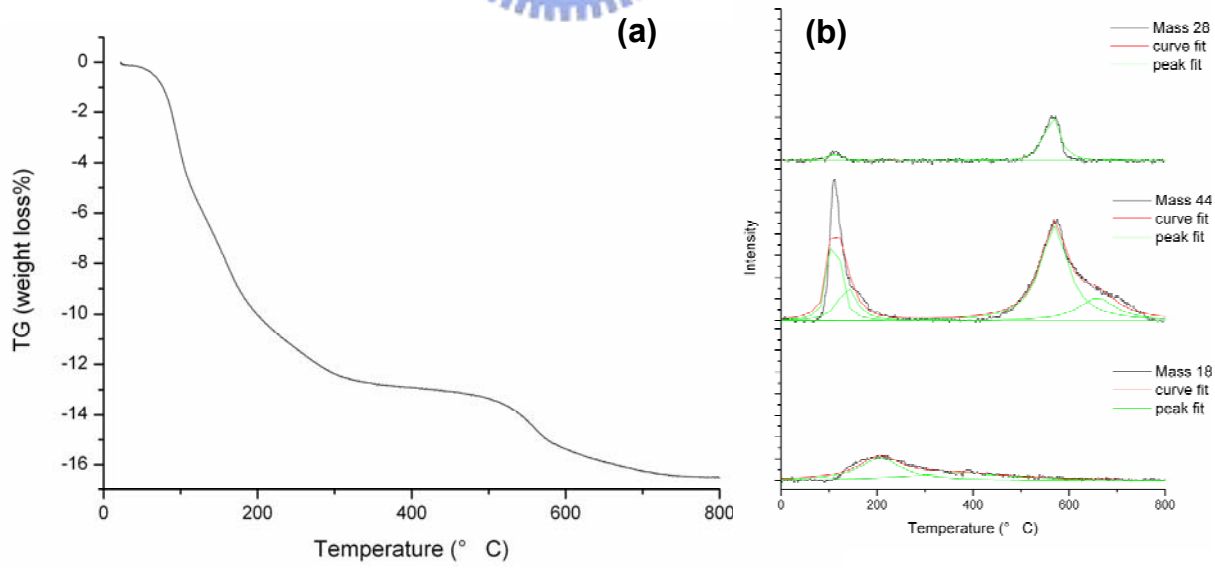

Figure A2.4. (a) TG weight loss % diagram and (b) TG-Mass spectra of nanofibers (small ribbon) (am10MR).

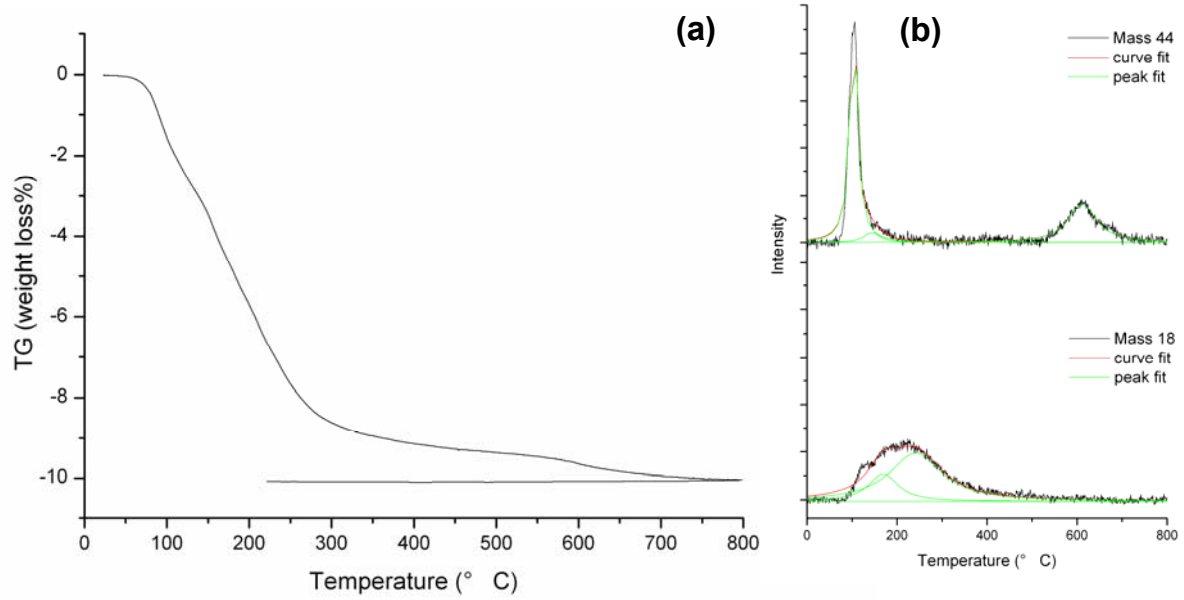

Figure A2.5. (a) TG weight loss % diagram and (b) TG-Mass spectra of nanoribbons (RDH10M180).

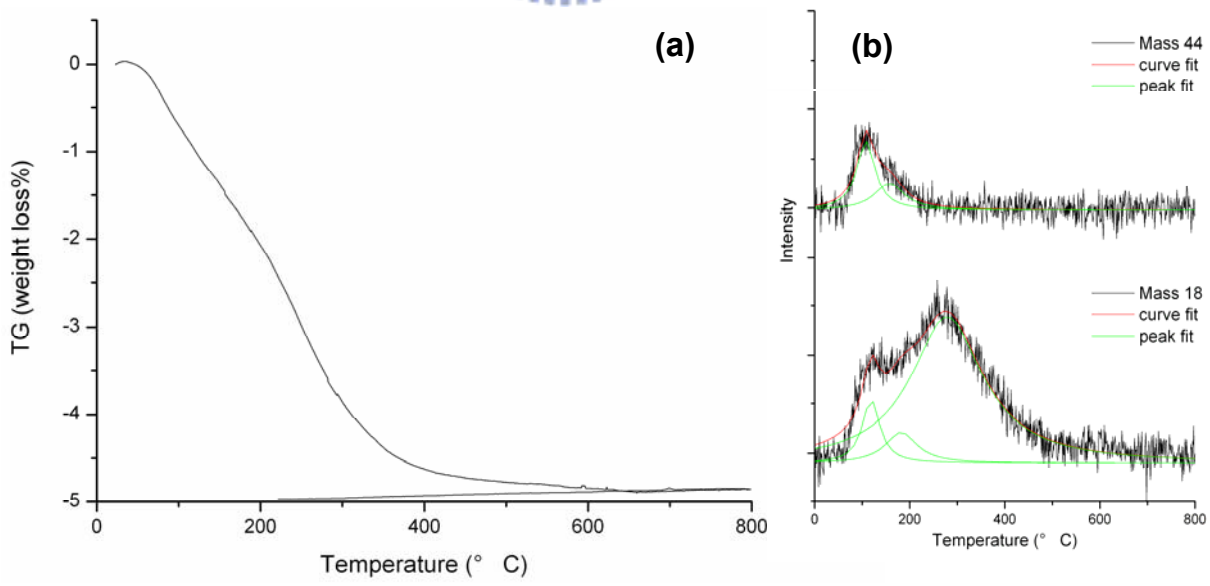

Figure A2.6. (a) TG weight loss % diagram and (b) TG-Mass spectra of submicro-sticks (rut10M220).

Table A2.3. TGA-MS reports of various morphologies of H-titanate (after proton exchanged).

	weight loss %		H_2O (mass 18)		CO_2 (mass 44)		CO (mass 28)	
	<400˚C	>400˚C	T (˚C)	area	T (˚C)	area	T (˚C)	area
H-Nanosheet (RDH15MR-B-H)	11.5%	3%	148	9.0	174	1.3	162	1.3
			217	6.0	537	2.4	532	2.4
					562	2.0	561	0.9
H-Nanotube (RDH10M140-H)	10%		141	1.8				
			179	2.2				
			260	2.2				
H-Nanofiber (am10MR-H)	14.5%	2.2%	212	3.0				
			277	5.5	245	2.0		
			401	4.9	566	2.3	558	3.4
H-Nanoribbon (RDH10M180-H)	14.6%	0.6%	163	6.9				
			214	7.0	204	19.0		
			314	11.1	362	18.5	(no data)	
					661	7.9		
					735	5.0		
H-Submicro-stick (am10M220-H)	10%		186	5.9				
			267	7.4				

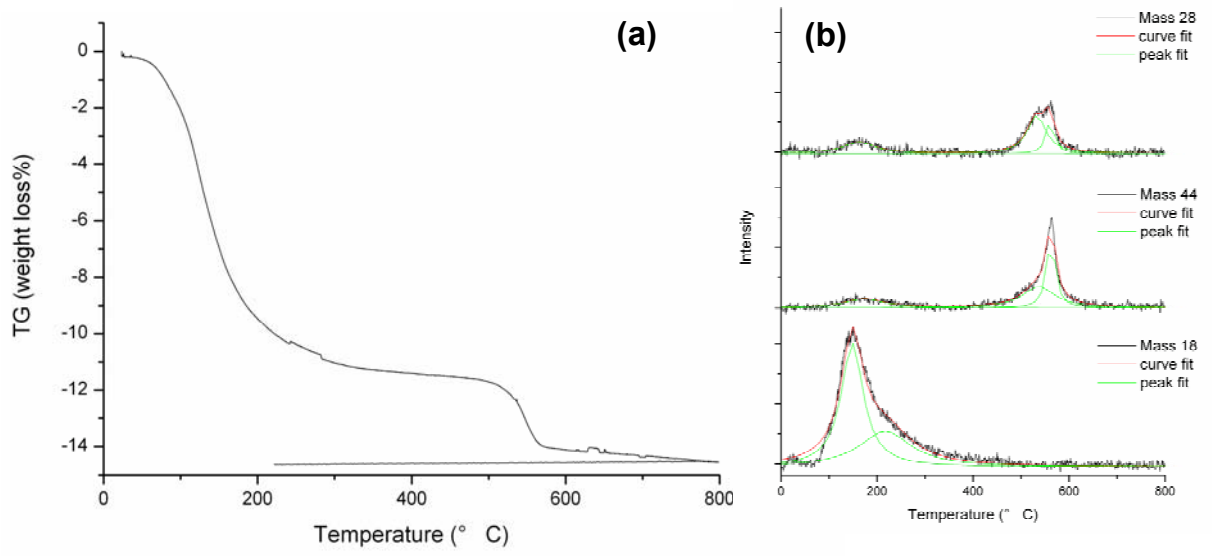

Figure A2.7. (a) TG weight loss % diagram and (b) TG-Mass spectra of proton exchanged nanosheets (RDH15MR-B-H).

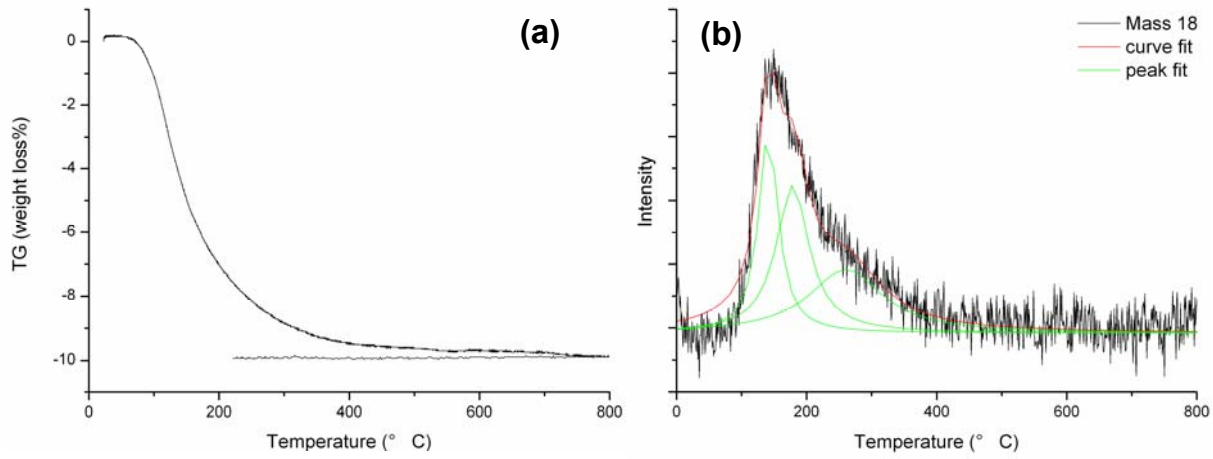

Figure A2.8. (a) TG weight loss % diagram and (b) TG-Mass spectra of proton-exchanged nanotubes (RDH10M140-H).

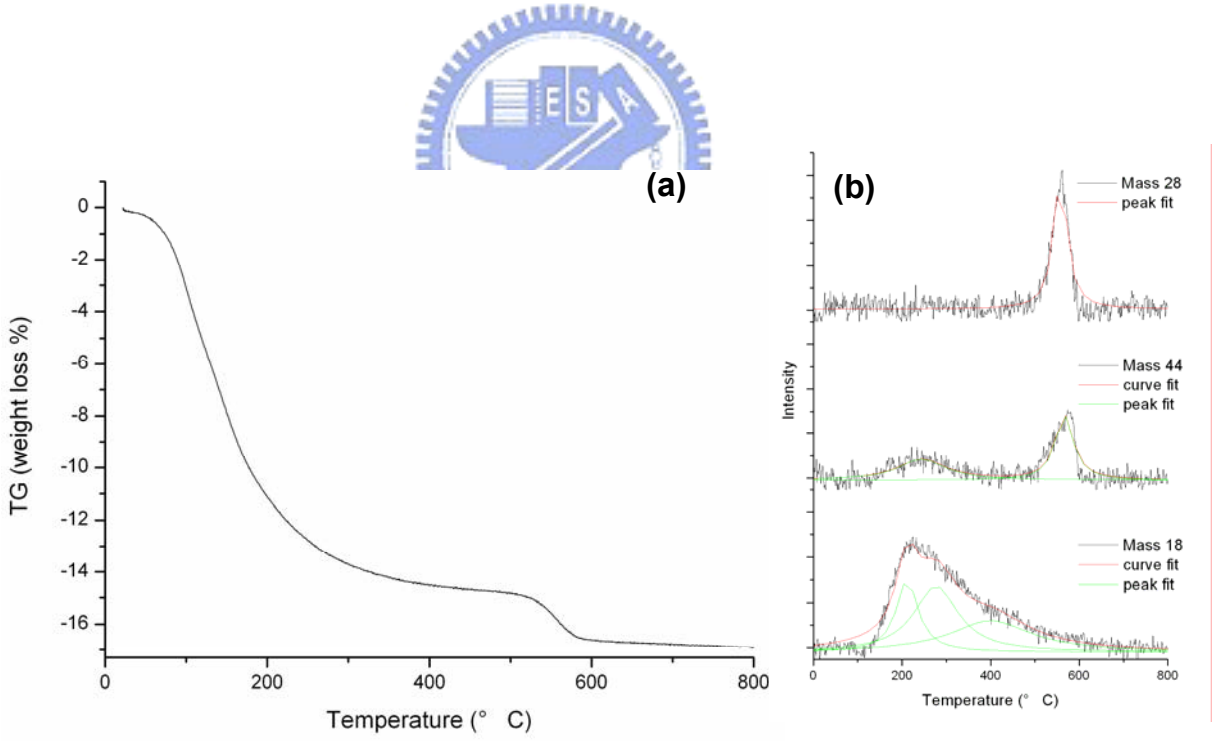

Figure A2.9. (a) TG weight loss % diagram and (b) TG-Mass spectra of proton-exchanged nanofibers (small ribbon) (am10MR-H).

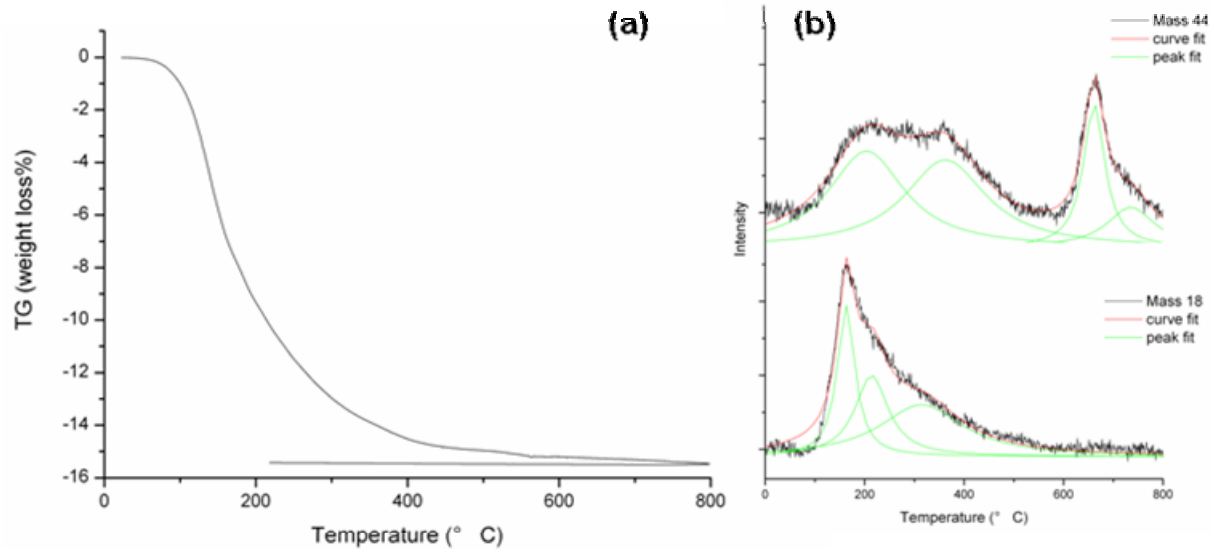

Figure A2.10. (a) TG weight loss % diagram and (b) TG-Mass spectra of proton-exchanged nanoribbons (RDH10M180-H).

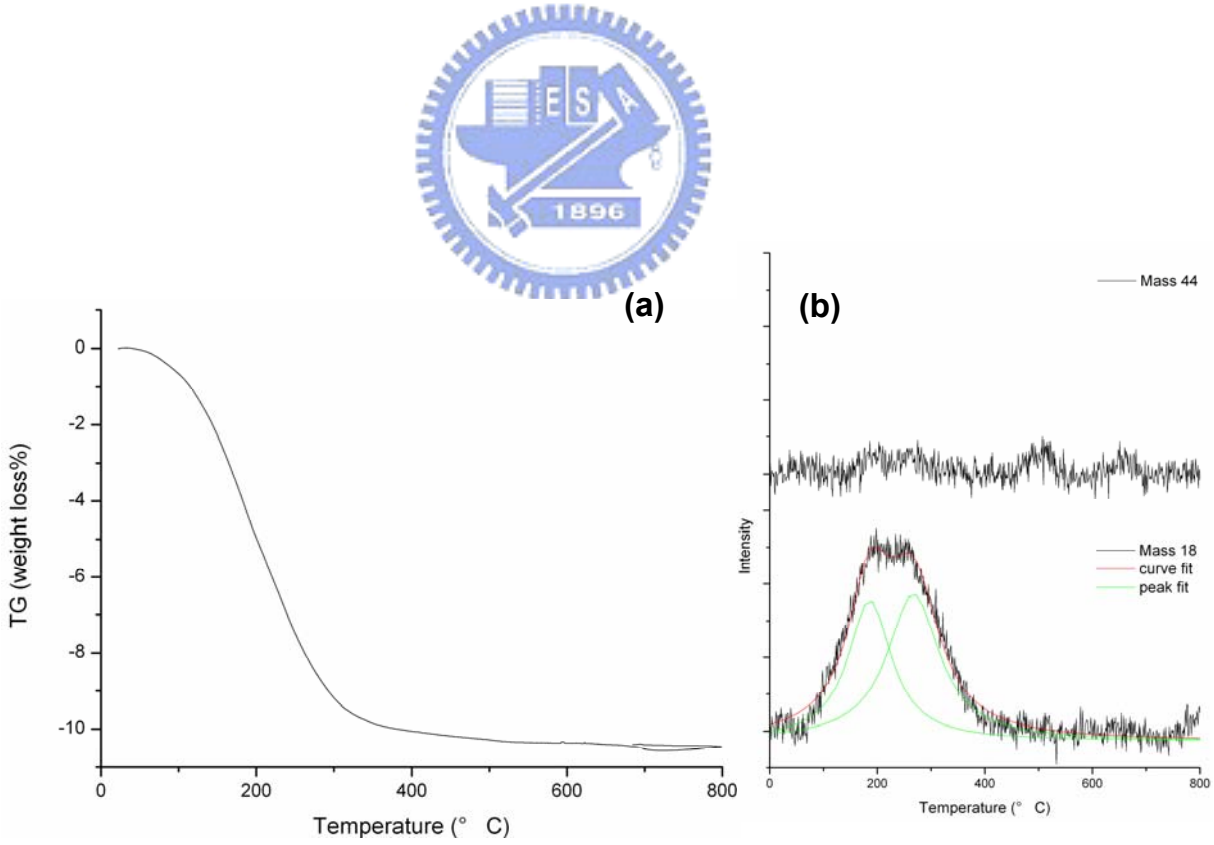

Figure A2.11. (a) TG weight loss % diagram and (b) TG-Mass spectra of proton-exchanged submicro-sticks (am10M220-H).

2.6.2. FT-IR study of various products

The unidentate and bidentate (chelating) coordinations shown below are found in the majority of carbonato complexes.[19]

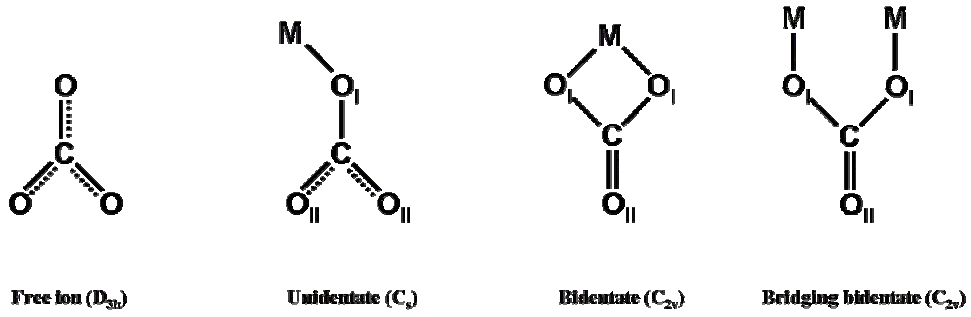

Figure A2.12. Various types of carbonato groups.[19]

Although the number of infrared-active fundamentals is the same for C_{2v} (bidentate) and C_s (unidentate), the splitting of degenerate vibrations is larger in the bidentate than in the unidentate complex.[20] Fujita et al. carried out normal coordinate analysis on unidentate and bidentate carbonato complexes of Co(III).[21] According to their results of CO stretching force constant (in unit of mdyn/Å), which is 5.46 (1163 cm^{-1}) for the free ion, becomes 6.0 (1219 cm^{-1}) for C-O_{II} bonds and 5.0 (1113 cm^{-1}) for the C-O_I bond of the unidentate complex, whereas it becomes 8.5 (1451 cm^{-1}) for the C-O_{II} bond and 4.1 (1008 cm^{-1}) for the C-O_I bonds of the bidentate complex. In terms of these data, the splitting of degenerate vibration $\Delta\upsilon$ is about 100 cm^{-1} for the unidentate complex and about 450 cm^{-1} for the bidentate.

In the IR spectra, we can obviously observe that O-H vibration band at 3000 cm^{-1}-3500 cm^{-1} and 1630 cm^{-1}, C-O bands at 1750 cm^{-1} , 1550 cm^{-1}, 1450 cm^{-1}, 1350 cm^{-1}, and Ti-O vibration bands below 1000 cm^{-1}. For analyzing the FT-IR spectra, we need to compare them

with the results of TGA-MS. In submicrostick sample, we can only observe a weak band of adsorbed carbon dioxide and unidentate carbonate at 100˚ C -200˚ C (figure A2.6). Therefore, the peak of the IR spectrum (figure 2.14e) occurred at 1530 cm^{-1} and 1330 cm^{-1} may be assigned to C-O_I bond and C-O_{II} bond of unidentate carbonato group respectively on titania layer with $\Delta\upsilon\approx200$ cm^{-1}. This pair of vibration band can be observed in all of cases, the TGA-MS spectra also reconfirmed this observation. The pair of C-O_I at 1720 cm^{-1} and C-O_{II} at 1450 cm^{-1} which we assigned to bidentate one due to $\Delta\upsilon\approx300$ cm^{-1}can only be found in the case of nanoribbon. The characteristic peaks of bridging bidentate or carboxyl group in nanosheet and exchanged product can be obseved at 1120 cm^{-1} and 1170 cm^{-1}.

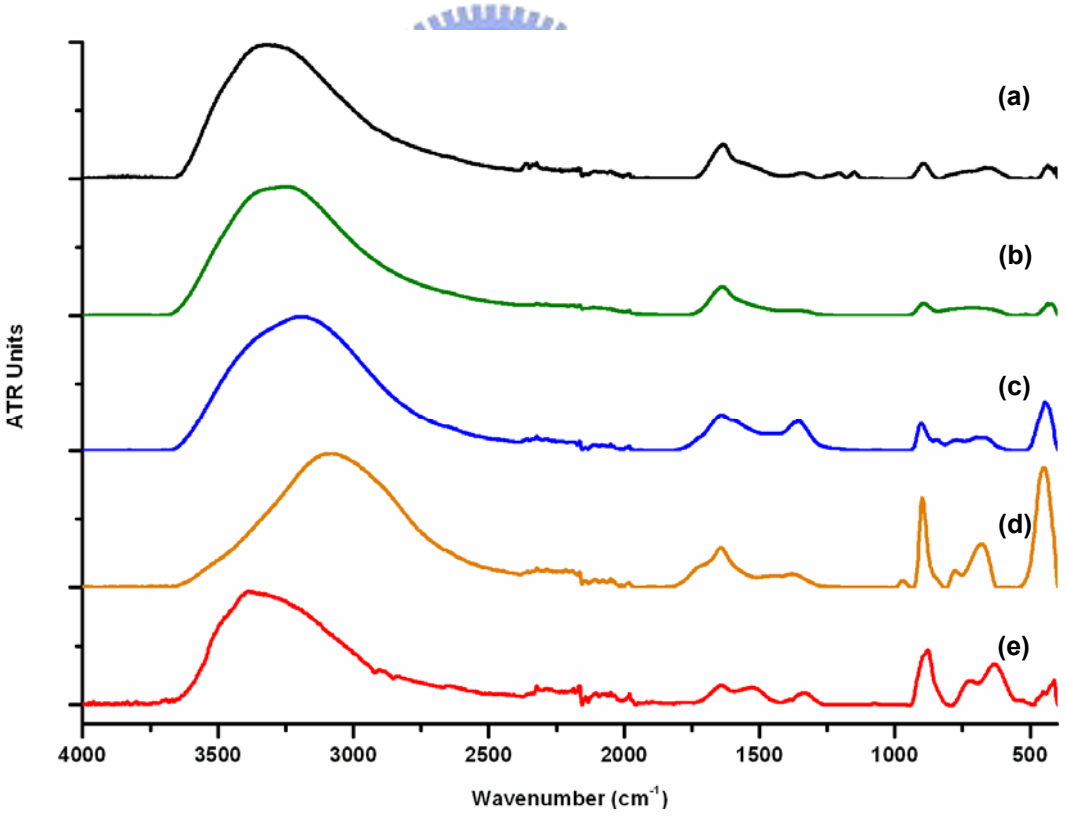

Figure A2.13. The FT-IR spectra of (a) nanosheet (RDH15MR-B), (b) nanotube (RDH10M140), (c) nanofiber (am10MR), (d) nanoribbon (RDH10M180) and (e) submicrostick (rut10M220).

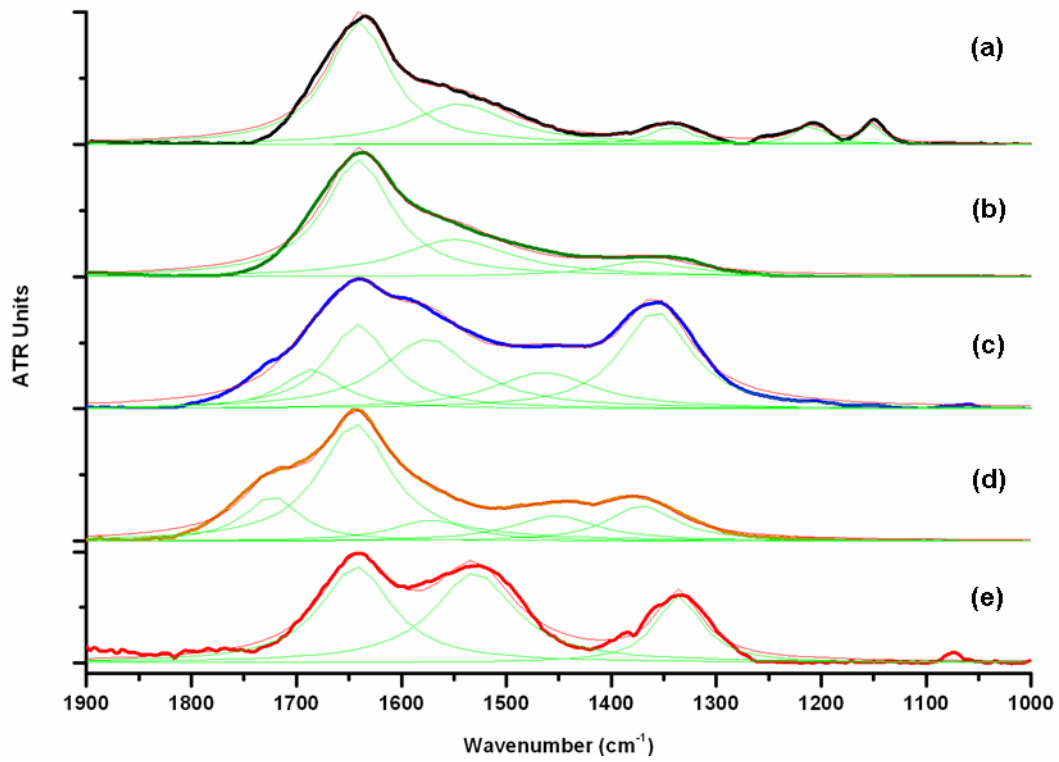

Figure A2.14. The FT-IR spectra in range of 1000cm^{-1}-1900cm^{-1} of (a) nanosheet (RDH15MR-B), (b) nanotube (RDH10M140), (c) nanofiber (am10MR), (d) nanoribbon (RDH10M180) and (e) submicrostick (rut10M220).

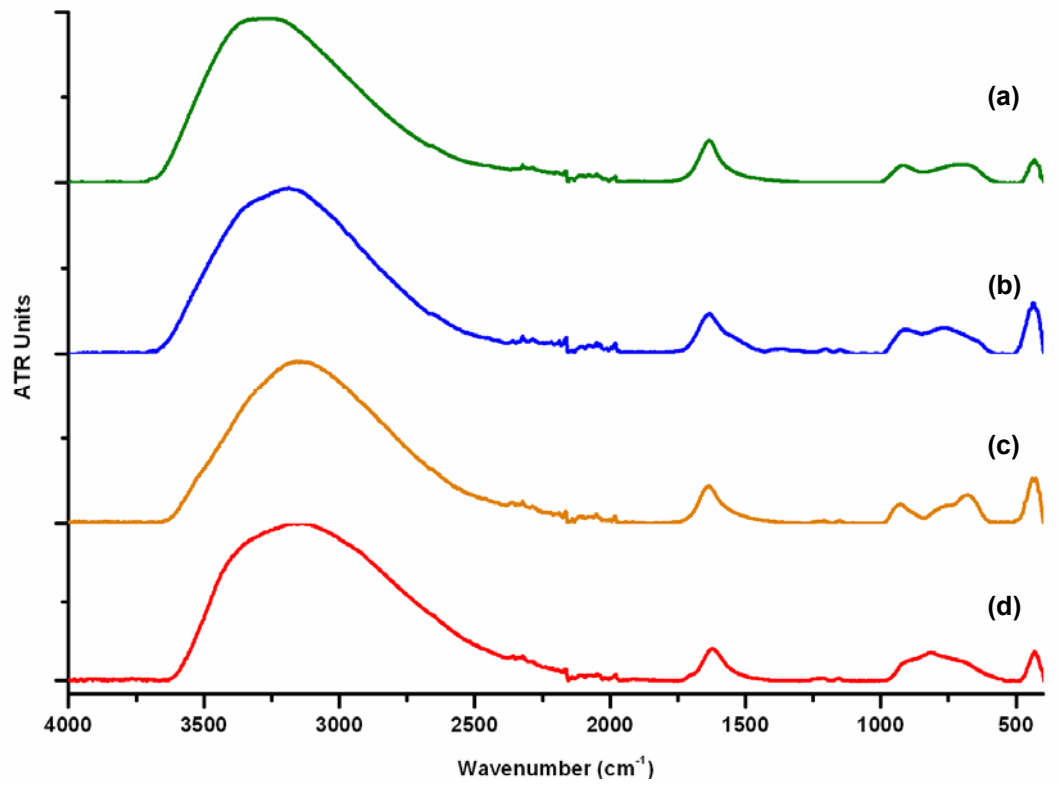

Figure A2.15. The FT-IR spectra of proton exchanged (a) nanotube (RDH10M140-H), (b) nanofiber (am10MR-H), (c) nanoribbon (RDH10M180-H) and (d) submicrostick (am10M220-H).

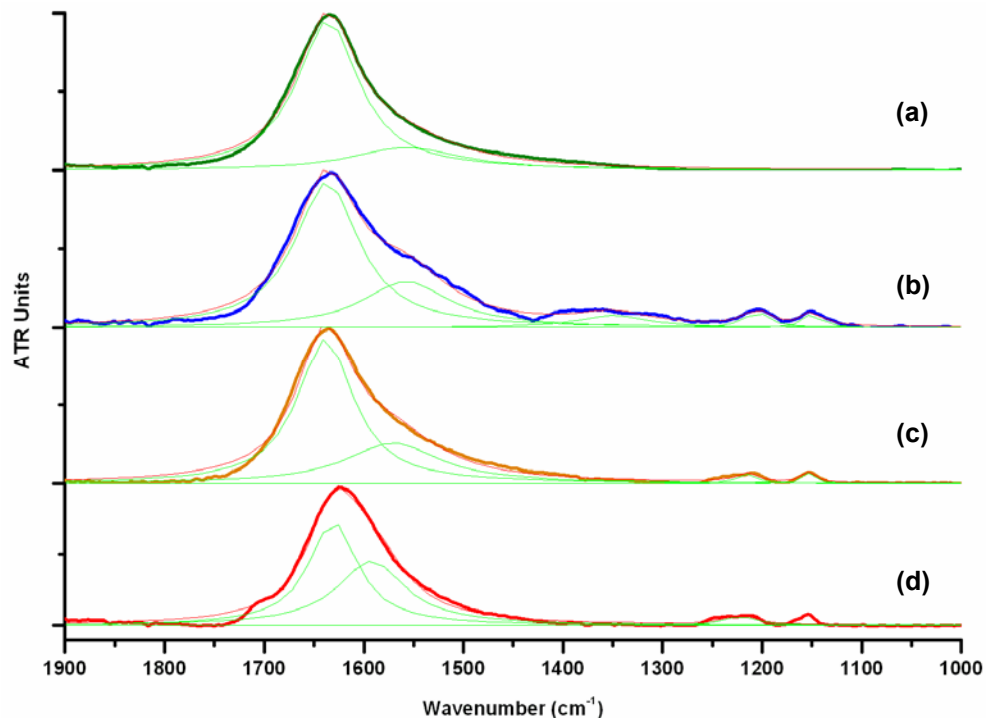

Figure A2.16. The FT-IR spectra in range of 1000cm^{-1}-1900cm^{-1} of proton exchanged (a) nanotube (RDH10M140-H), (b) nanofiber (am10MR-H), (c) nanoribbon (RDH10M180-H) and (d) submicrostick (am10M220-H).

2.6.3. $TiOCl_2$ + x NaOH

For discussion of correlation of the quantity of NaOH and formation of titanium oxolation building block, we used $TiOCl_2$ as precursor to autoclave with stoichiometric NaOH. The $TiOCl_2$ is more active and has no problem of solubility; we apply it as bottom up unit. Moreover, there is much fewer water than the experiments mentioned in this system, we can less consider possible influence of solvent pressure. The real composition of our TiOCl2 reagent is "TiOCl2 • 1.4 HCl • 7H2O", hence we must add more 3.4 unit of NaOH for reduce and neutralize those Cl existed. We added 0.01 mole $TiOCl_2$ for each experiment. All x in this study mean OH/ Ti, actually we added "3.4+x" NaOH. All the solvothermal condition are 180 ˚C during 24h. We have tested various temperature from 110˚C to 180˚C to ensure the temperature has no obvious influence to the product morphologies in this study.

In the XRD results (figure A2.19), we can observe that there is no titanate structure when x=0, and all titanate structure after x>1. When 2<x<4, there is another titanate phase which occur in 10M NaOH 220˚C autoclaved condition as hollandite type structure (see Section 2.3 and Chapter 3) appearing. When x>4, we can only observe amorphous due to over saturated basic environment.

In the TEM images (figure A2.18), we observe that the product in x=0.63 is nanosheet, the product in x=1.26 is demi-nanotube, tube and sheet, x=1.5 is demi-tube and tube, and x=2 is more straight demi-tube and tube. Along with more x, the structure of product is more curved and straight. That infers that the building block with more OH forms more rolled product.

The x=3 sample is nanosheet on big fiber which is hollandite type product (see Section 2.3). The x=5 sample is amorphous particle.

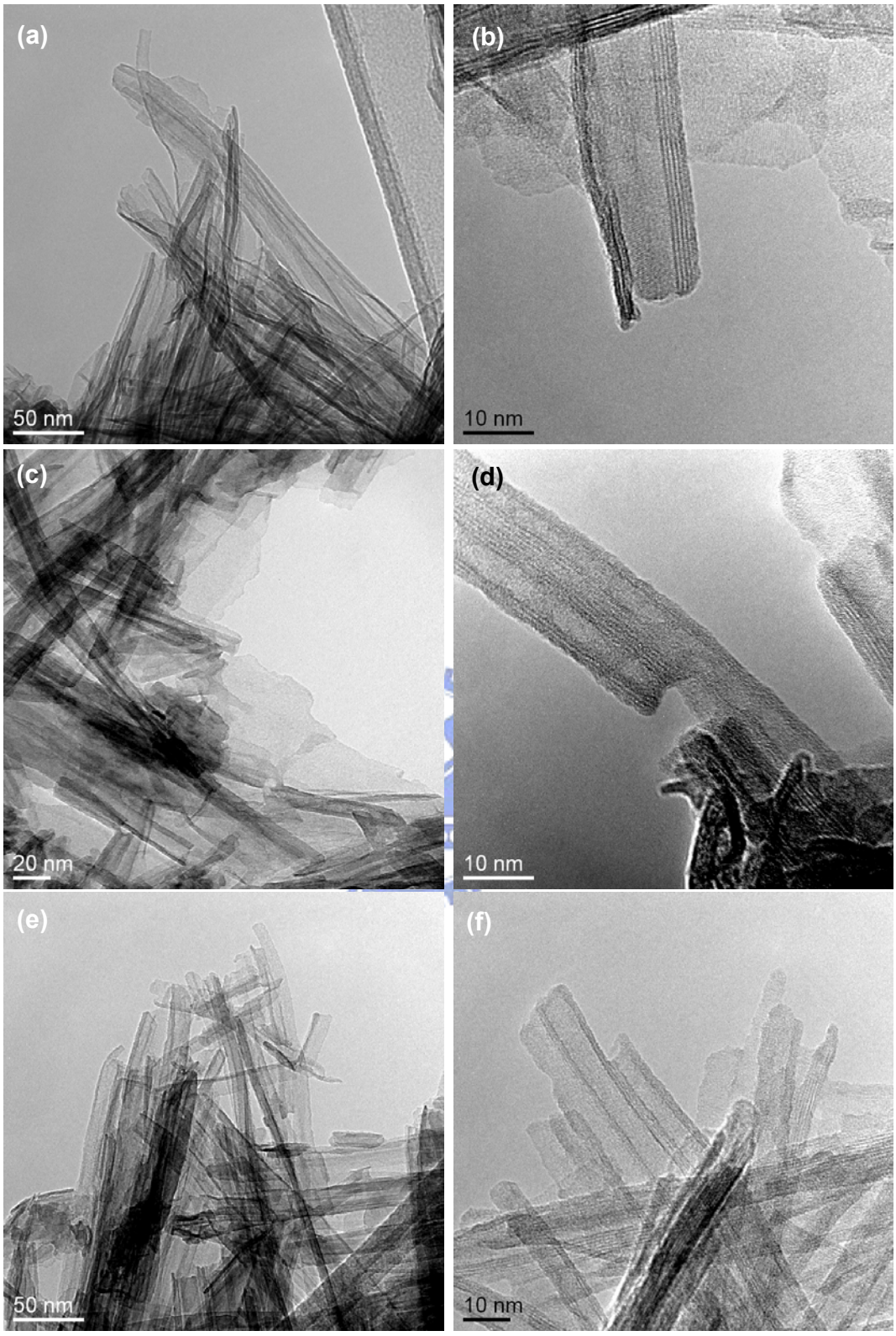

Figure A2.17. (a) low and (b) high magnification of TEM images of titanate nanosheets from TiOCl2 + (x+3.4) NaOH, x=0.63, 180°C autoclaved 24h; (c), (d) nanosheets and demi-tube with x=1.26; (e), (f) ribbon-like nanosheet and demi-nanotubes with x=1.5

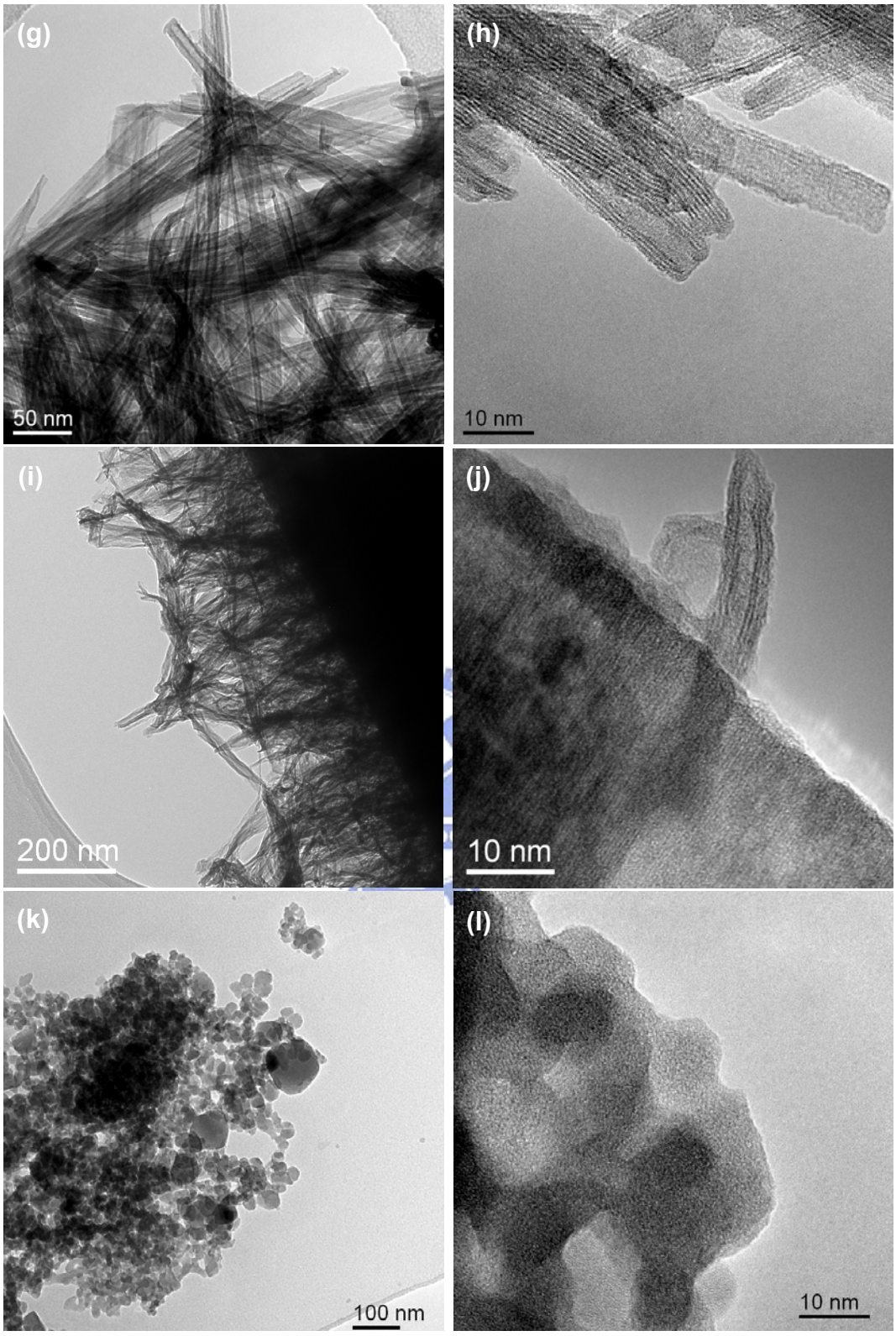

Figure A2.17. (cont.) (a) low and (b) high magnification of TEM images of titanate demi-nanotubes and nanotubes from TiOCl2 + (x+3.4) NaOH, x=2, 180°C autoclaved 24h; (c), (d) fiber and nanosheets with x=3; (e), (f) amorphous particles with x=5.

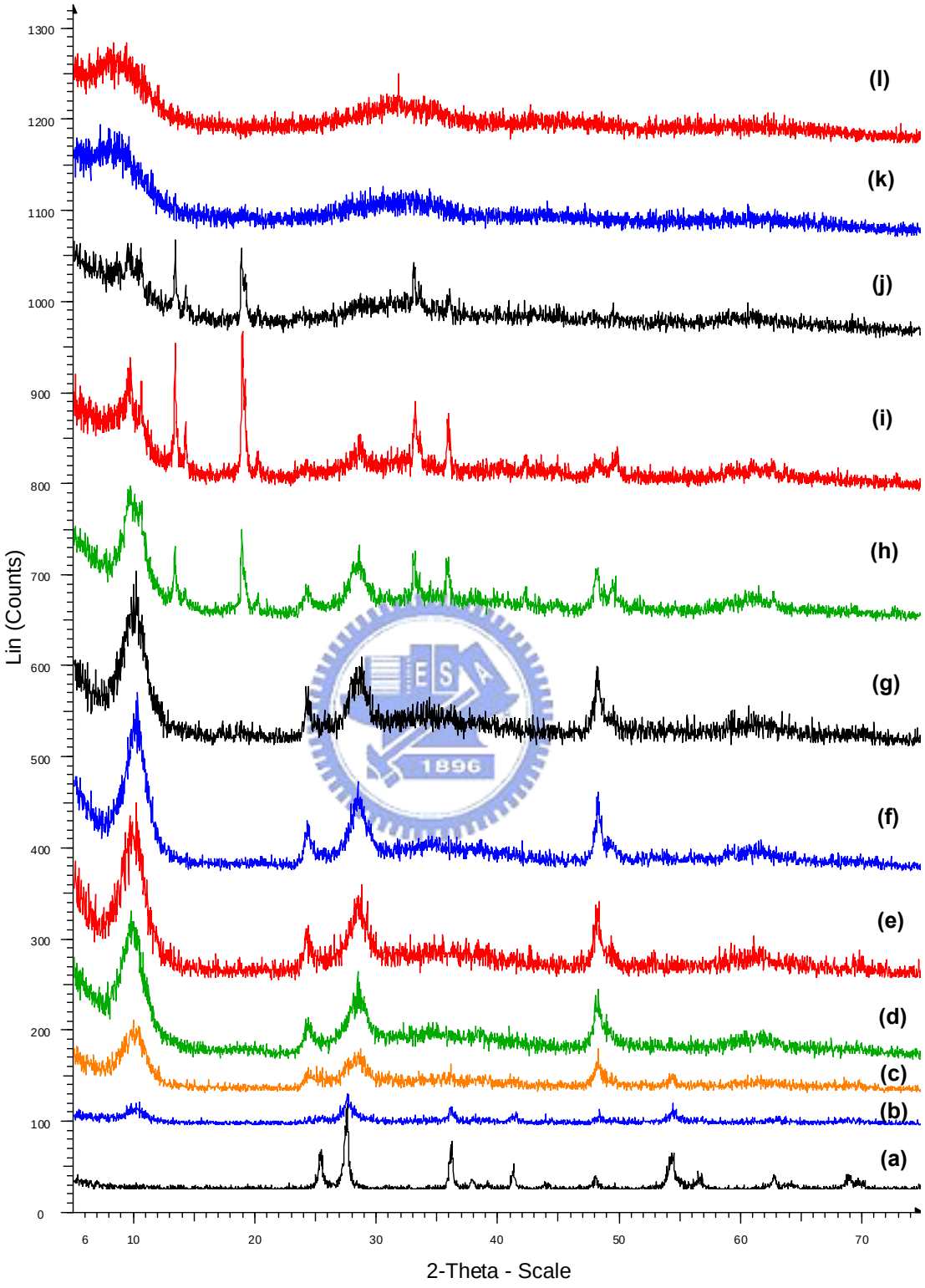

Figure A2.18. XRD diagrams of products from $TiOCl_2$ 180°C autoclaved with stoichiometric (x+3.4)NaOH, x = (a) 0 , (b) 0.5, (c) 0.63, (d) 1, (e) 1.26, (f) 1.5, (g) 2, (h) 2.5, (i) 3, (j) 3.5, (k) 4, (l) 5.

2.6.4. Enlargement of nanosheet from RDH15MR by treatment of boiling in water

We can enlarge the area of nanosheet from RDH15MR by treatment of boiling in water. In XRD (figure A2.19), we can obviously observe that peaks of lepidocrocite type titante become sharper than the raw material, which infer that crystallite of product after water boiling is larger than the raw product. In SEM observation (figure A2.20), we discovered that the nanosheets enlarged clearly, the width enhanced to 100nm from 20nm. In the TEM images (figure A2.21), we saw the same results, the nanosheet enlarged.

The pH of water (pH=7) is smaller than our raw nanosheet product (pH≈12). We measured the pH solution after water boiling, which is 9. And the precipitate becomes pH≈7-8 and Na/Ti=0.33 (0.54 in raw material) after washing and centrifuging. Therefore, we can regard the water boiling as a partial proton exchanging process. Besides, the extra OH species saturated the surface of raw nanosheet were moved and the oxolation to grow up may proceed. The IR spectrum after water boiling also exhibits as other IR spectra after proton exchanging. In Section 2.2.4 and Section 2.4.4, we concluded that less OH and appropriate amount of sodium are constructive to form sheet-liked titanate product. The observations of enlargement of RDH15MR also agree with this conclusion.

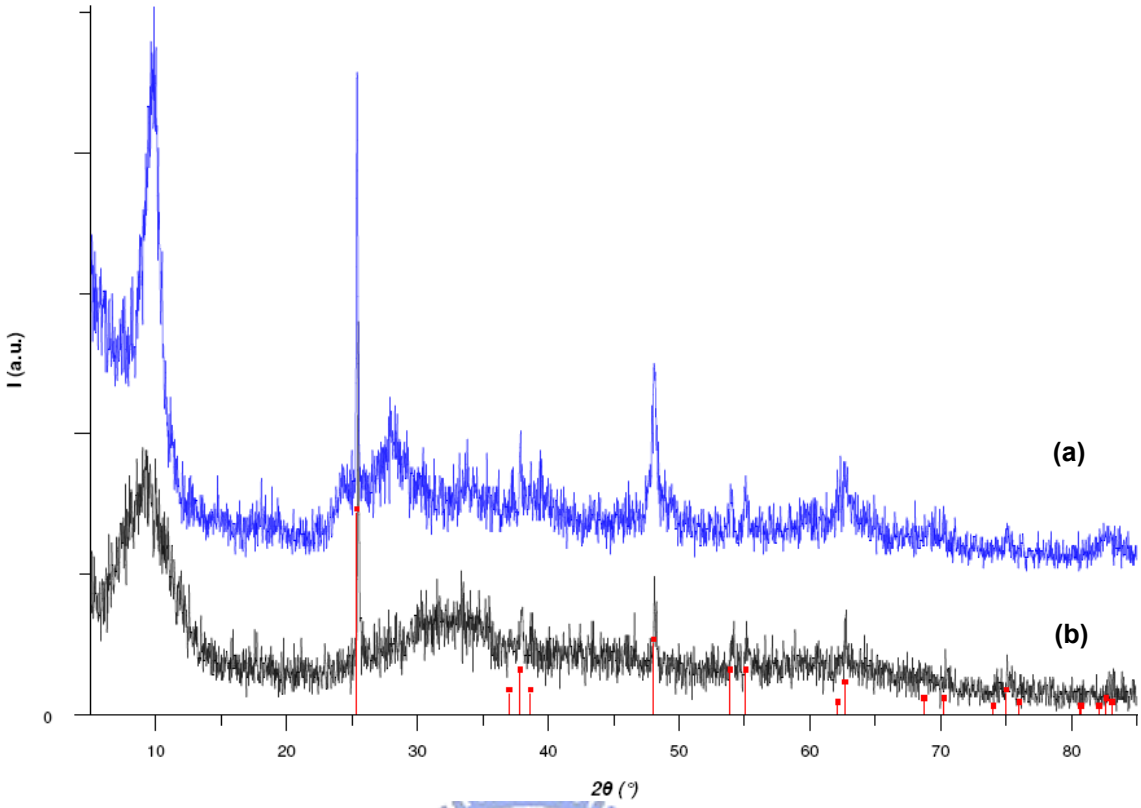

Figure A2.19. XRD diagrams of (a) nanosheet (RDH15MR) and (b) enlarged one after boiling in water during 48 hours (RDH15MR-B).

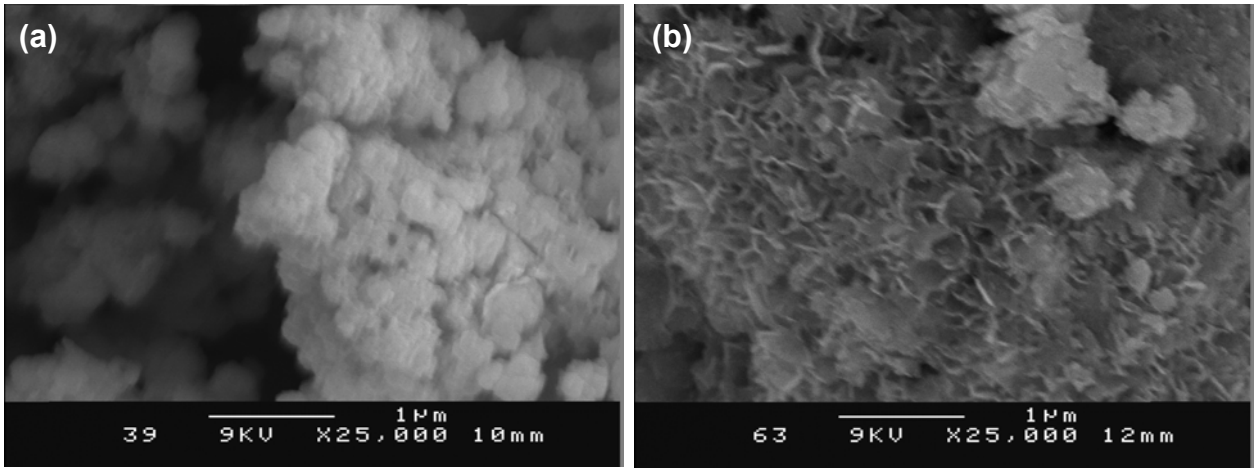

Figure A2.20. SEM images of (a) nanosheet (RDH15MR) and (b) enlarged one after boiling in water during 48 hours (RDH15MR-B).

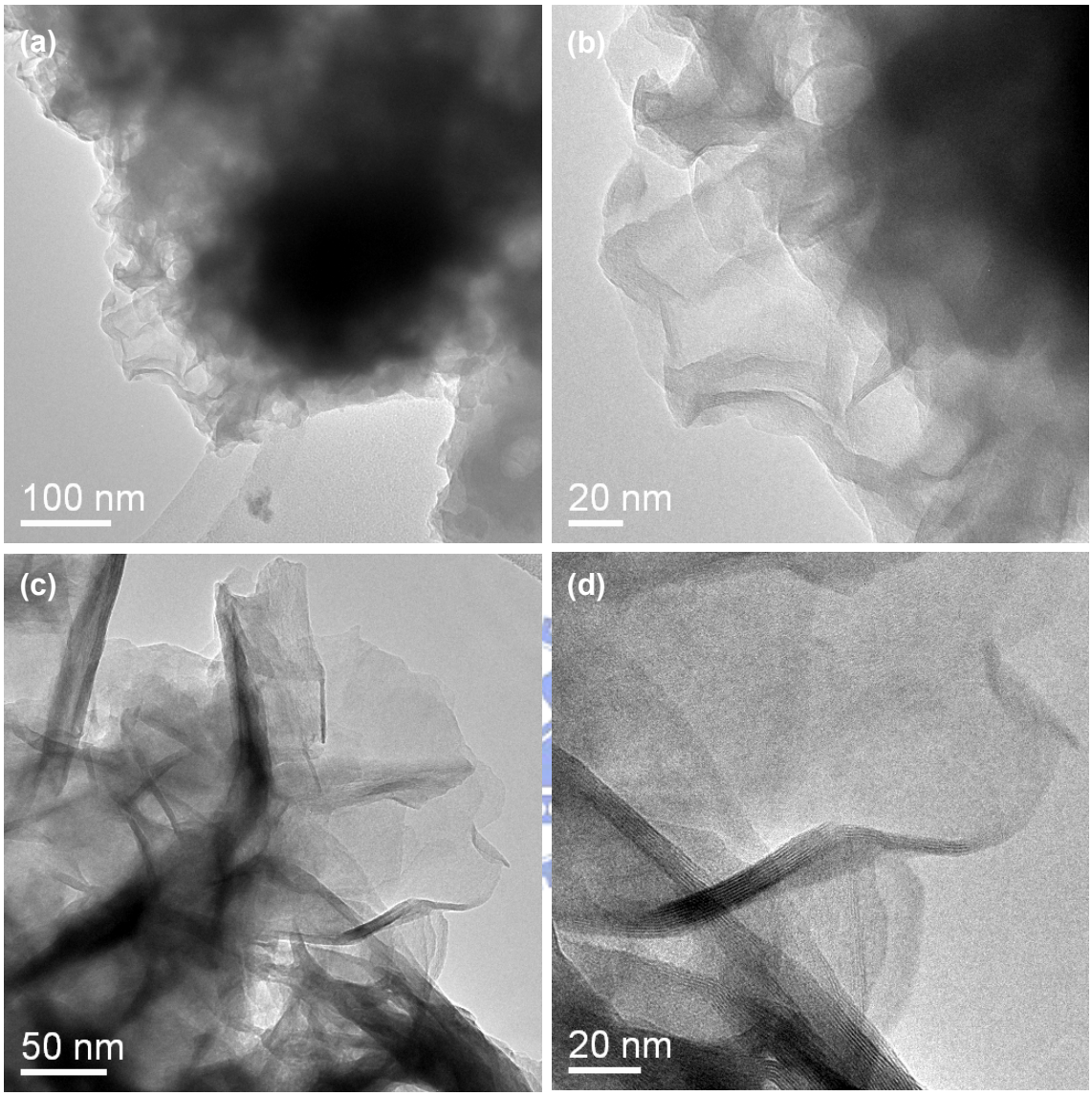

Figure A2.21. TEM images of (a), (b) nanosheet (RDH15MR) and (c), (d) nanosheet enlarged after boiling in water during 48 hours (RDH15MR-B).

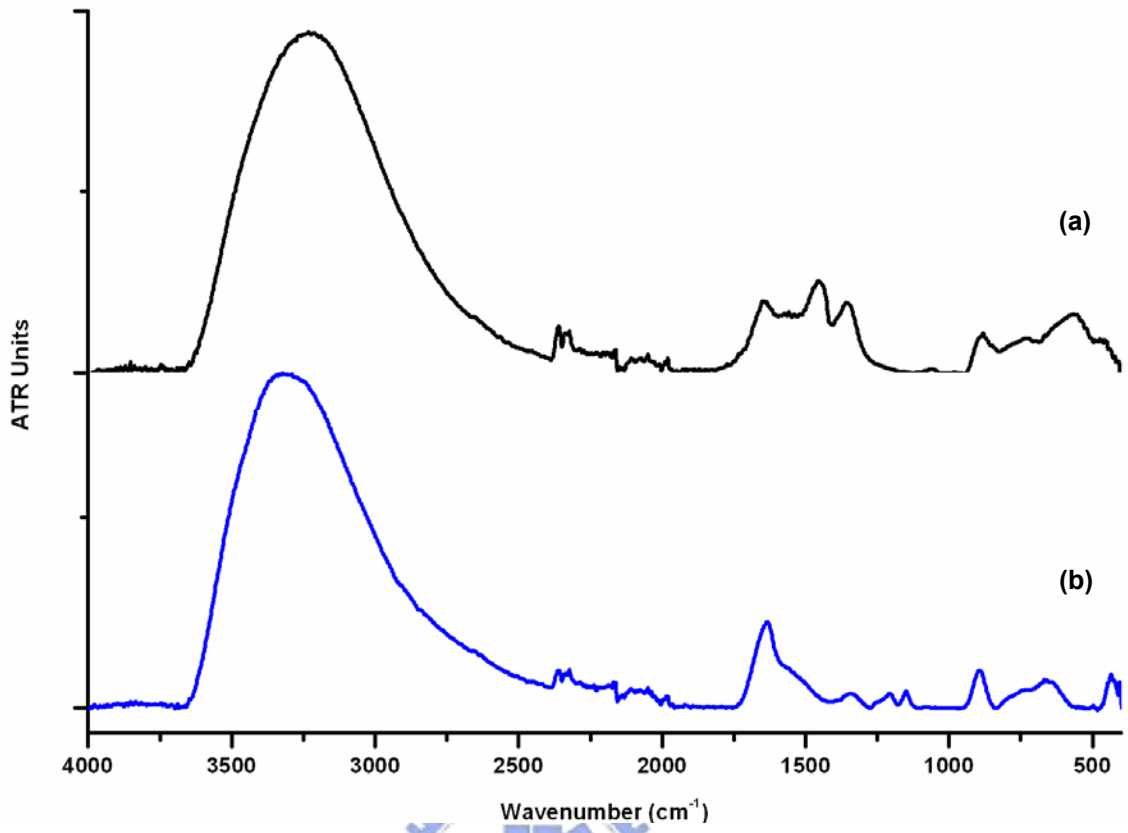

Figure A2.22. FT-IR spectra of (a) nanosheet (RDH15MR) and (b) nanosheet enlarged after boiling in water during 48 hours (RDH15MR-B).

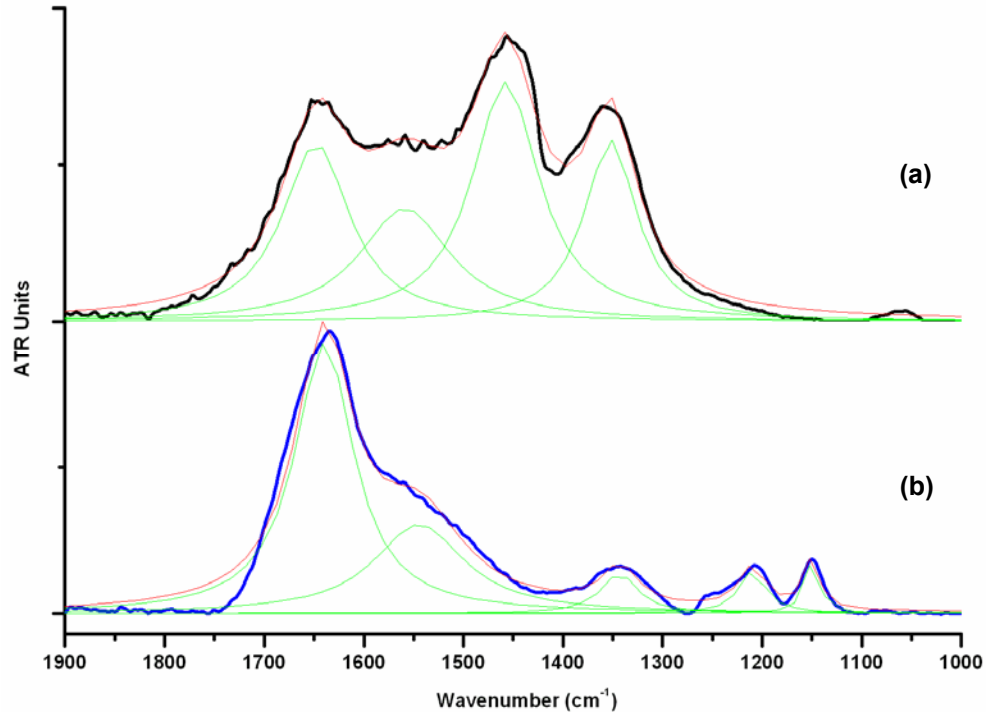

Figure A2.23. FT-IR spectra in range of 1000 cm^{-1}-1900 cm^{-1} of (a) nanosheet (RDH15MR) and (b) nanosheet enlarged after boiling in water during 48 hours (RDH15MR-B).

2.6.5. Reaction time effect of am10MR (from semi-nanotube to nanoribbon)

The am10MR case can form short nanoribbon product. If we stop this reaction in different duration as 24 hours, 48 hours and 72 hours, we can obtain different sized products. In XRD results (figure A2.24), we can observe the phase of product is as lamellar type product (nanotube, semi-nanotube or nanosheet) in the beginning (<24 hours), and transform to nanoribbon when duration >48 hours. The peaks become sharper with longer duration. That implies the crystallite of product become larger. In TEM images (figure A2.25), we observed the product is semi-nanotube in 24 hours one and nanoribbon in 48 hours and 72 hours. Along with longer reaction duration, the nanoribbons become longer. In autoclave cases, this effect is not obvious. This implies that the reaction time effect may due to the amount of adsorbed carbonate. Longer duration of contacting with air let it adsorb more carbonate and form a product straighter and longer (see Section 2.4.5). These results also prove that the nanoribbon and semi-nanotube are similar structures, their differences are size and curvature. Moreover, this effect provides a route to control the size of nanoribbon product. It is very helpful to improve the properties of titanate nanoribbon.

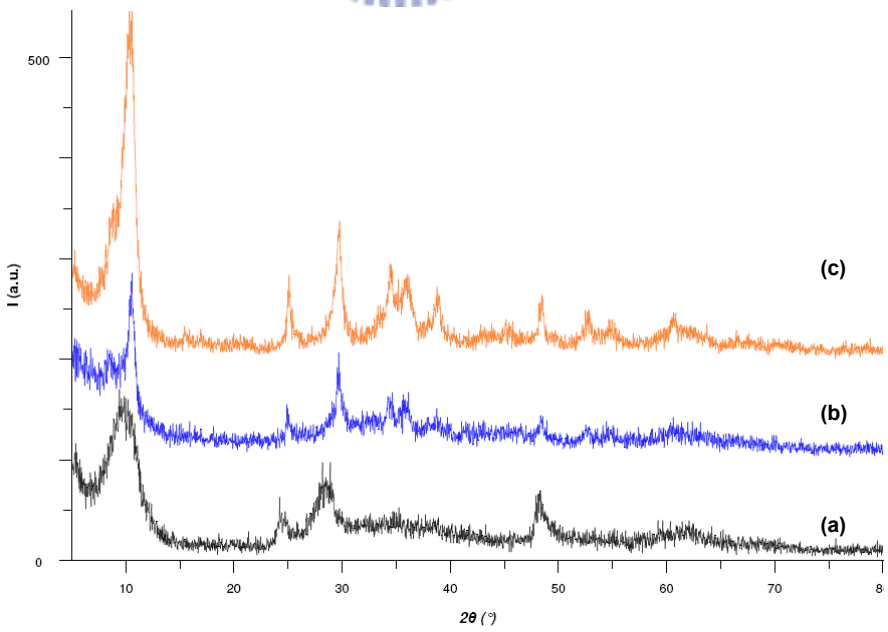

Figure A2.24. XRD diagrams of am10MR reflux during (a) 24 hous, (b) 48 hours and (c) 72 hours.

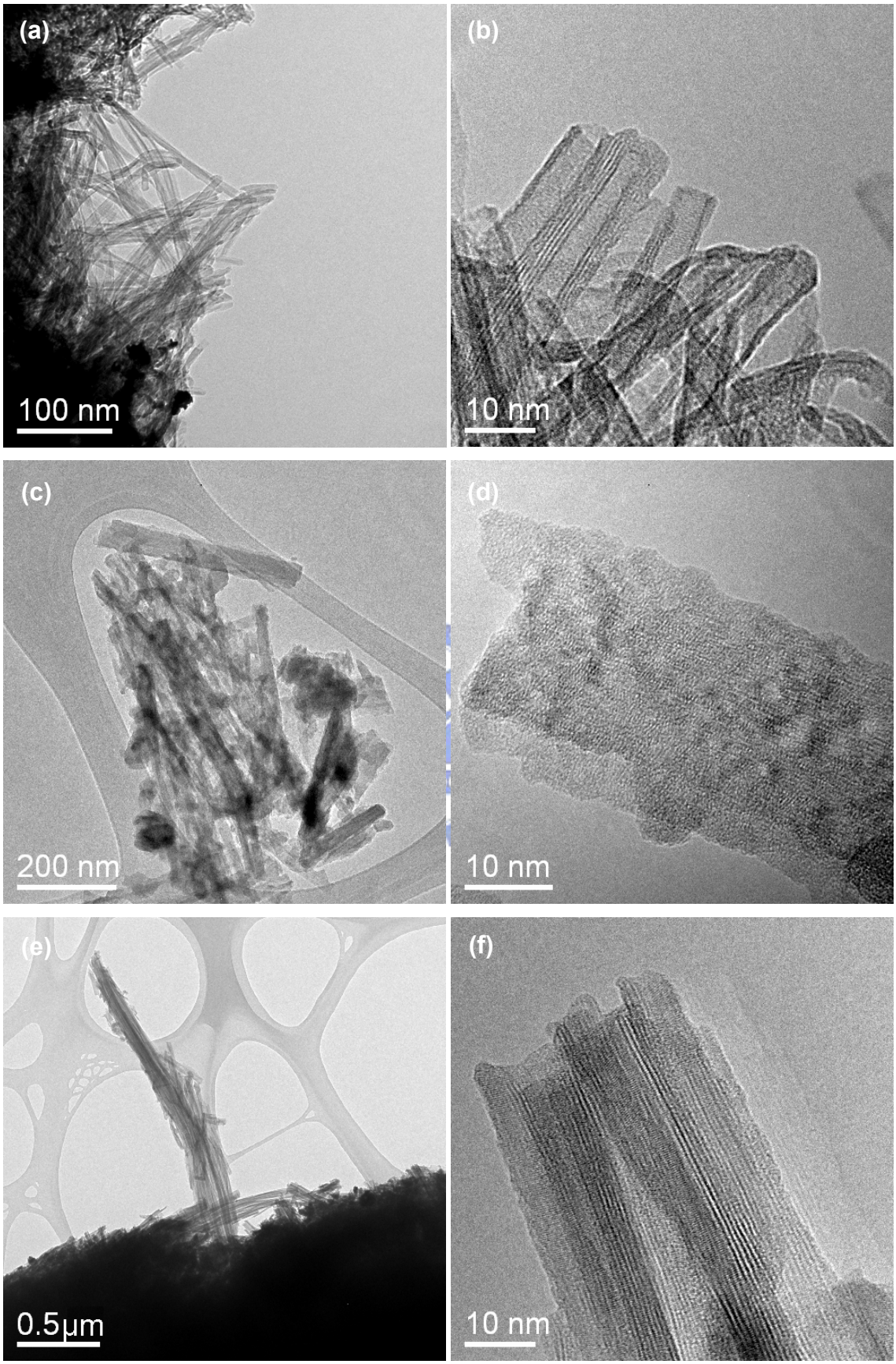

Figure A2.25. TEM images of am10MR reflux during (a), (b) 24 hous, (c), (d) 48 hours and (e), (f) 72 hours.

2.6.6. 5nm5M120-xNa_2CO_3

We added different amount of sodium carbonate into 5nm5M120 system to study the effect of carbonate amount. We found that the product morphology changes very much when we add small amount of sodium carbonate. However, when we add more than 1.06g Na_2CO_3 (CO_3^{2-}/Ti=0.8), the morphology almost do not change, even more destructive with adding more sodium carbonate. This observation infers that the system has a saturated limit of sodium carbonate. This limit may due to the saturation of sodium ion (Section 2.4.4 and Section 2.4.5). The carbonate effect is not well distinct from sodium ion effect instead. However, the small amount of additive can strongly change the product morphology indeed.

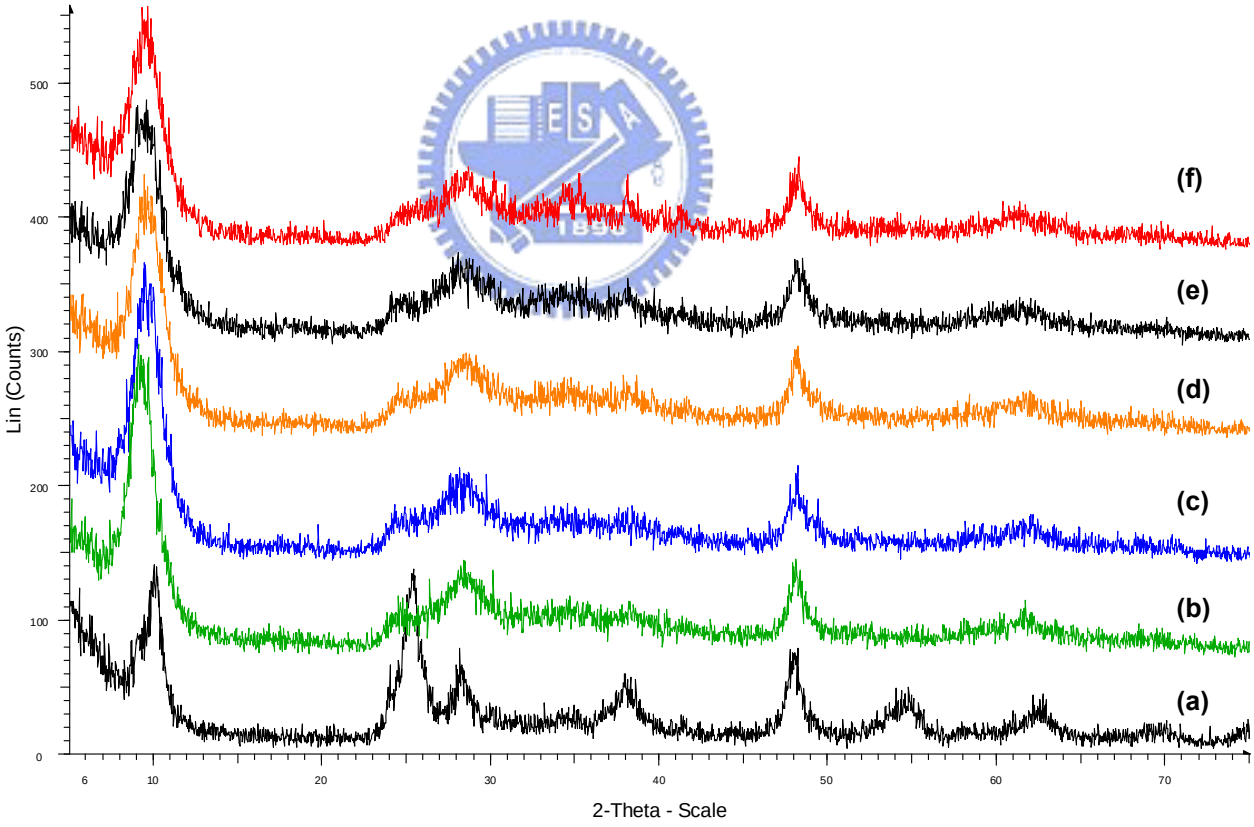

Figure A2.26. XRD diagrams of products from 5nm anatase TiO_2 in 120°C autoclave with (a) 5M NaOH, (b) specially add 0.66g Na_2CO_3 (CO_3^{2-}/Ti=0.5), (c) 1.06g Na_2CO_3 (CO_3^{2-}/Ti=0.8), (d) 1.33g Na_2CO_3 (CO_3^{2-}/Ti=1), (e) 2.65g Na_2CO_3 (CO_3^{2-}/Ti=2), (f) 5.30g Na_2CO_3 (CO_3^{2-}/Ti=4).

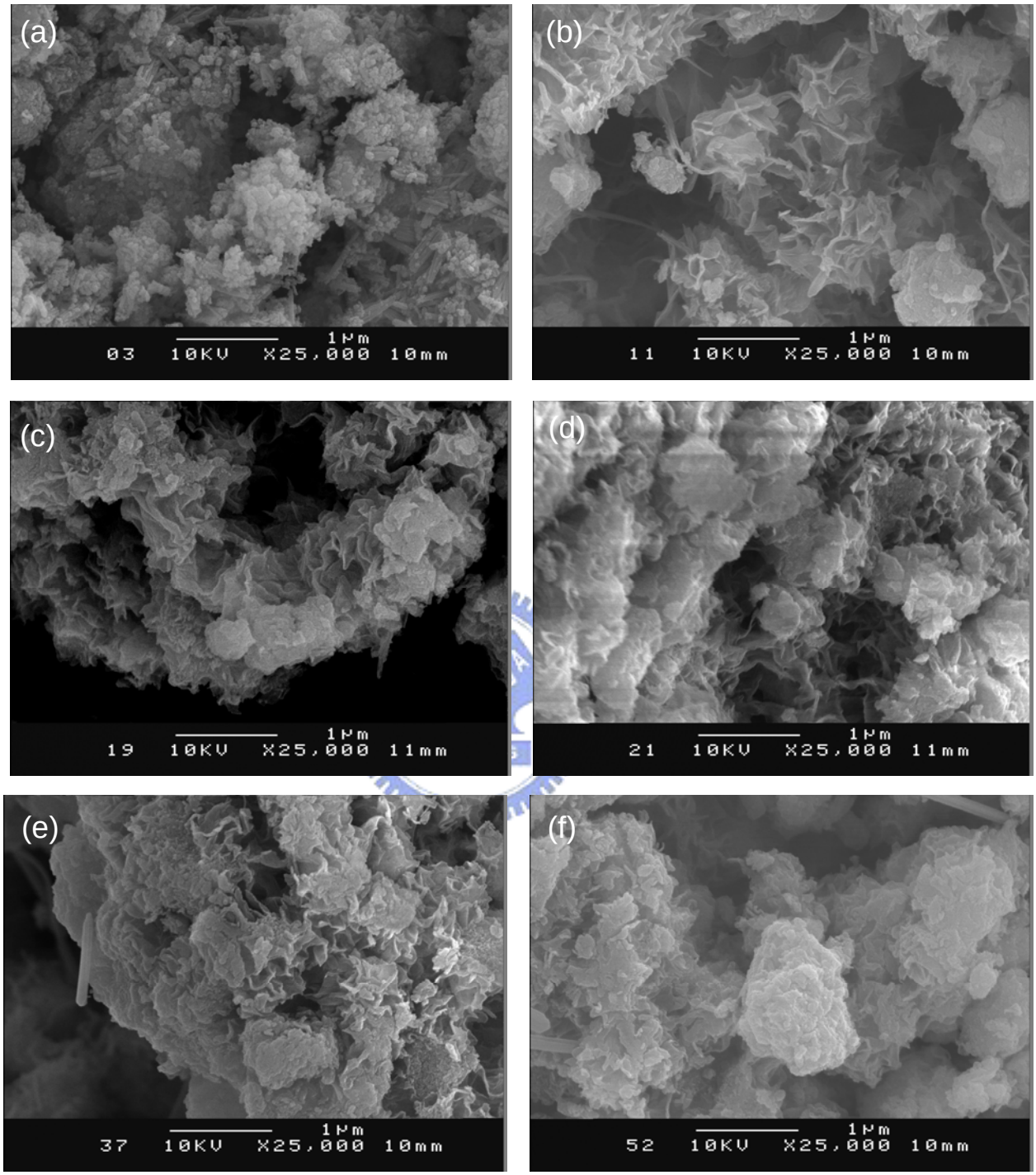

Figure A2.27. the SEM images of products from 5nm anatase TiO_2 in 120°C autoclave with (a) 5M NaOH, (b) specially add 0.66g Na_2CO_3 (CO_3^{2-}/Ti=0.5), (c) 1.06g Na_2CO_3 (CO_3^{2-}/Ti=0.8), (d) 1.33g Na_2CO_3 (CO_3^{2-}/Ti=1), (e) 2.65g Na_2CO_3 (CO_3^{2-}/Ti=2), (f) 5.30g Na_2CO_3 (CO_3^{2-}/Ti=4).

2.7. Reference

[1] M. Zhang, Z. Jin, J. Zhang, X. Guo, J. Yang, W. Li, X. Wang and Z. Zhang, *Journal of Molecular Catalysis A: Chemical* **2004**, *217*, 203–210.

[2] G. Armstrong, A. R. Armstrong, J. Canales and P. G. Bruce, *Angew. Chem. Int. Ed.* **2004**, *43*, 2286 –2288

[3] G. Armstrong, A. R. Armstrong, J. Canales and P. G. Bruce, *Chem. Commun.* **2005**, 2454–2456

[4] Graseby SpecAG, *User Manual of Golden Gate™ Single Reflection Diamond ATR (10500 series)*, 1.

[5] M. Sugita, M. Tsuji and M. Abe, *Bull. Chem. Soc. Jpn.* **1990**, *63*, 1978-1984.

[6] C. C. Tsai and H. Teng, *Chem. Mater.* **2004,** *16,* 4352-4358.

[7] T. Kasuga, M. Hiramatsu, A. Hoson, T. Sekino and K. Niihara, *Adv. Mater.* **1999**, *11*, 1307-1311.

[8] F. Miyaji, T. Yoko, H. Kozuka, S. Sakka, *J. Mater. Sci.* **1991**, *26*, 248.

[9] H. M. Kim, F. Miyaji, T. Kokubo, *J. Mater. Sci.: Mater. Med.* **1997**, *8*, 341.

[10] A. Kudo, T. Kondo, *J. Mater. Chem*. **1997**, *7*, 777.

[11] M. L. Halberstadt, S. K. Rhee and J. A. Mansfield, *Wear* **1978**, *46*, 109.

[12] R. Murakami and K. Matsui, *Wear* **1996**, *201*, 193.

[13] N. Masaki, S. Uchida, H. Yamane and T. Sato, *Chem. Mater.* **2002**, *14*, 419-424.

[14] X. Sun, X. Chen and Y. Li, *Inorg. Chem.* **2002**, *41*, 4996-4998.

[15] G. H. Du, Q. Chen, P. D. Han, Y. Yu and L. M. Peng, *Phys. Rev. B* **2003**, *67*, 035323.

[16] B. L. Wang, Q. Chen, J. Hu, H. Li, Y. F. Hu and L. M. Peng, *Chem. Phys. Lett.* **2005**, *406*, 95-100.

[17] X. Meng, D. Wang, J. Liu, B. Lin and Z. Fu, *Solid State Comm.* **2006**, *137*, 146-149.

[18] J. P. Jolivet, *De la solution à l'oxide*, CNRS Édition **1994**.

[19] K. Nakamoto, *Infrared and Raman Spectra of Inorganic and Coordination Compounds*, *Fourth Edition*, Wiley Interscience Publication **1986**.

[20] K. Nakamoto, J. Fujita, S. Tanaka and M. Kobayashi, *J. Am. Chem. Soc.* **1957**, *79*, 4904.

[21] J. Fujita, A. E. Martell and K. Nakamoto, *J. Chem. Phys.* **1962**, *36*, 339.